
Photon Emission in a Non-Equilibrium Quark-Gluon Plasma

Sigtryggur Hauksson

Department of Physics
McGill University
Montréal, Québec
April 2017

A thesis submitted to McGill University in partial fulfillment
of the requirements for the degree of Master of Science

© Sigtryggur Hauksson, 2017

CONTENTS

Abstract	v
Résumé	vi
Acknowledgments	vii
1 Introduction	1
1.1 The phase diagram of QCD	1
1.2 Heavy-ion collisions	4
1.3 Photon production in the QGP	7
1.4 Photons in heavy-ion collisions	11
1.5 This thesis	13
2 Theoretical foundations	15
2.1 The real time formalism in thermal equilibrium	15
2.2 Out-of-equilibrium propagators	25
2.3 Hard thermal loops	27
2.4 Resummed propagators	29
3 Bulk viscous corrections to two-to-two channels	35
3.1 Photon emission from two-to-two scattering	35
3.2 Evaluation of hard loop diagrams	39
3.3 Evaluation of soft loop diagrams	41
3.4 Bulk viscous corrections in heavy-ion collisions	43
4 The resummed occupation density of soft gluons	51
4.1 Heuristics of the LPM effect	51
4.2 Power counting of the LPM effect in thermal equilibrium	53
4.3 The non-equilibrium retarded polarization tensor	55
4.4 Evaluation of the non-equilibrium Π_{12}	57
4.5 The resummed rr propagator for soft gluons	63
4.6 A non-equilibrium sum rule	68

5	The resummed occupation density of hard quarks	75
5.1	Evaluation of $\Sigma_{<}$ and $\text{Im } \Sigma_{\text{ret}}$	75
5.2	The resummed rr fermion propagator	79
6	The LPM effect in a non-equilibrium isotropic QGP	83
6.1	Summing four-point functions	83
6.2	Summing ladder diagrams	92
6.3	Summary of results	97
7	Conclusion and next steps	101
	Appendices	103
A	The Feynman rules of QCD	103
B	Spinors	106
C	Final results from Chapter 3	109
C.1	Hard momentum loops	109
C.2	Soft momentum loops	111
	Bibliography	113

Abstract

A new state of matter called quark-gluon plasma (QGP) is produced in ultra-relativistic collisions of nuclei. Transport coefficients, such as shear viscosity and bulk viscosity, are fundamental properties of the QGP. Photons give access to these transport coefficients because they are emitted throughout the out-of-equilibrium evolution of the QGP medium. Previous work on non-equilibrium photons has dealt with the effect of shear viscosity on photons emitted in two-to-two scattering. In this thesis we evaluate the correction due to bulk viscosity and show that it has a sizable phenomenological effect. Furthermore, we present a first calculation of photons coming from quark bremsstrahlung and pair annihilation in a non-equilibrium QGP. These leading order processes in α_s are intricate because the emitting quark interacts with the medium during the photon emission. This is known as the LPM effect. We derive an integral equation describing all these processes for isotropic momentum distributions of quarks and gluons.

Résumé

Un nouvel état de la matière appelé le plasma de quarks et de gluons (QGP) est créé dans les collisions relativistes de noyaux atomiques. Les coefficients de transport, comme la viscosité de cisaillement et la viscosité de volume, sont des propriétés fondamentales du QGP. Les photons émis durant l'évolution hors d'équilibre du QGP donnent un accès direct à ces coefficients de transport. La recherche existante sur les photons émis hors-équilibre s'est penchée sur l'effet de la viscosité de cisaillement sur des photons venant de la diffusion élastique de deux particules. Dans cette thèse, nous évaluons la correction de la viscosité de volume et montrons qu'elle est importante pour la phénoménologie. En outre, nous présentons le premier calcul sur des photons venant du bremsstrahlung des quarks et de l'annihilation des paires dans un QGP non-équilibré. Ces processus, au premier ordre en α_s , sont plus complexes parce que le quark interagit avec le QGP lors de l'émission. Nous établissons une équation intégrale qui décrit tous ces processus pour une distribution statistique isotrope de quarks et de gluons.

Acknowledgments

Most importantly, I would like to thank my supervisor, Charles Gale, for his support and guidance on my research and life in academia. He has put me in a position to succeed. I would also like to express my gratitude to Sangyong Jeon for his valuable advice. I am indebted to Chun Shen for his help during the early stages of this work and for giving me access to his numerical programs. I thank Alina Czajka for clarifying discussions about thermal field theory. Finally, I thank all members of my research group for their companionship and intellectual stimulation.

I would furthermore like to express my gratitude to my friends and family. Ég vil sérstaklega þakka foreldrum mínum og systur fyrir ómetanlegan stuðning þeirra í gegnum árin. Ég þakka enn fremur Gabriel fyrir allar góðu stundirnar og fyrir að nenna að hlusta á mig tala um eðlisfræði. Ég tileinka foreldrum mínum þessa ritgerð.

Photon Emission in a Non-Equilibrium Quark-Gluon Plasma

Introduction

1.1 The phase diagram of QCD

One of the four fundamental forces in nature is the short-ranged strong nuclear force. It governs the structure of hadrons such as pions, protons and neutrons and underpins nuclear physics, describing the binding of protons and neutrons in atomic nuclei and processes such as alpha decay. The fundamental description of the strong force is given by quantum chromodynamics (QCD), a theory of quarks and gluons which carry colour charge. This colour charge comes in three types, often called red, green and blue. The strong force between quarks is mediated by gluons. Gluons are coloured particles and thus interact among themselves making the theory more complicated. See Appendix A for a brief review of QCD.

An interesting feature of QCD is how the strength of the force changes with energy scale. At very high energies the theory is weakly interacting and perturbative calculations can be used. This is called asymptotic freedom. At the lower energy scales of hadron structure the force is strong and less understood. In this regime it dictates confinement, meaning that coloured quarks cannot exist in isolation but must form colourless hadrons.

A major goal in physics today is to understand macroscopic matter made out of quarks and gluons. We want to understand the state of matter ruled by the strong force as temperature and net baryon density are varied. The simpler electromagnetic force offers a useful analogy here. It gives rise to a variety of interesting phases such as ferromagnets, superfluids, superconductors and strange metals. See Fig. 1.1 for

takes place at temperatures 150 – 200 MeV [3, 4]. Furthermore they have established the equation of state at vanishing net baryon density.

Finding the phases and equation of state of thermal QCD is interesting, but not the full story. Transport coefficients such as shear viscosity, bulk viscosity, electric charge conductivity and flavour diffusion are equally important. They describe how quickly the medium neutralizes small gradients in conserved quantities such as momentum, electric charge and flavour charge.

This thesis focuses on shear and bulk viscosity. Let's discuss them more closely. We consider a fluid in its rest frame that is perturbed from thermal equilibrium giving rise to a flow \mathbf{u} . For a radial expansion a diagonal component of the stress-energy tensor is

$$T_{ii} = P - \zeta \nabla \cdot \mathbf{u} \quad (1.1)$$

to first order in the velocity gradient. Here P is the thermodynamical pressure which comes from the fluid's equation of state, $P(\epsilon)$, where ϵ is the energy density. The pressure cannot keep up with the radial expansion so the radial momentum flow T_{ii} has an additional term, $\zeta \nabla \cdot \mathbf{u}$. The bulk viscosity, ζ , quantifies how far the medium is from equilibrium during radial expansion.

Let's now consider shear flow with $u_x \neq 0$ and $\partial_y u_x \neq 0$. To first order in the velocity gradient

$$T_{yx} = -\eta \partial_y u_x. \quad (1.2)$$

Thus the shear force needed to sustain the flow is proportional to the shear viscosity, η . A fluid with low η diffuses shear flow easily. To get intuition for shear viscosity it is helpful to consider a gas of hard, classical spheres. Using kinetic theory one shows that

$$\eta \sim \frac{mv}{\sigma} \quad (1.3)$$

where m is the mass of a sphere, v is their average velocity and σ is the cross section for scattering [5]. Interestingly the shear viscosity decreases as the interaction strength increases.

The shear viscosity of thermal QCD has received a great deal of attention. Unfortunately, as for other transport coefficients, it cannot be evaluated directly on the lattice for the time being. The problem boils down to lattice simulations using imaginary time to capture the effects of temperature. Dynamical quantities such as shear viscosity can then only be obtained by analytically continuing to real time. This turns out to be an ill-posed problem numerically. See e.g. [6] for ways to circumvent it.

At very high temperatures one can use perturbative QCD to find η . The shear viscosity of QCD was first evaluated at leading order in the coupling constant g in [7, 8]. These authors solved the Boltzmann equation numerically for a weakly perturbed medium. Finally, shear viscosity has been obtained using the gauge/gravity duality. This duality links observables in an infinitely strongly coupled conformal field theory with observables in a curved gravitational background of one additional dimension. There is no known dual to QCD, but η/s of maximally supersymmetric Yang-Mills theory has been shown to be $1/4\pi$ [9]. Here s is the entropy density. Unlike in the kinetic theory of hard spheres the shear viscosity does not vanish at infinite coupling strength but reaches a lower limit.

In conclusion the known theoretical tools are unsatisfactory when it comes to evaluating the shear viscosity of QGP at realistic coupling strength. Lattice studies cannot give a calculation from first principles, perturbation theory assumes very weak coupling and the gauge/gravity correspondence assumes very strong coupling and does not deal directly with QCD. One must turn to experiments.

1.2 Heavy-ion collisions

Many of the questions raised above can now be answered with experiments. Both the Relativistic Heavy-Ion Collider (RHIC) at the Brookhaven National Laboratory and the Large Hadron Collider (LHC) at the European Organization for Nuclear Research, CERN, perform ultra-relativistic collisions of heavy nuclei. There is convincing evidence that droplets of QGP are formed in these collisions. The droplets

cool and expand. Finally they transform into a soup of hadrons which fly off into the detectors. In these high energy collisions, pairs of quarks and antiquarks are created abundantly. Thus the medium formed has almost zero net baryon density, allowing us to explore the QCD phase diagram close to the temperature axis.

Simulations of heavy-ion collisions using relativistic hydrodynamics have been successful in explaining hadronic observables. This suggests that the QGP formed is close to thermal equilibrium and behaves collectively. A simulation starts with initial conditions which should be constrained by the underlying physics [10]. They are then typically evolved using hydrodynamics. Ideal hydrodynamics, which assumes local thermal equilibrium, is inadequate. Rather, one should use the non-equilibrium evolution of viscous hydrodynamics, preferably in 3+1 dimensions [11]. The equation of state, $P = P(\epsilon)$, comes from lattice QCD. As the medium cools into the hadronic phase hydrodynamics breaks down because of the rapid expansion. The continuous hydrodynamical fluid must be converted into hadrons. This is usually done by sampling hadrons from a momentum distribution that depends on the fluid's macroscopic observables [12]. Finally the hadrons scatter off each other [13] before being "measured" in the simulation.

A simple experimental observable that hydrodynamics explains successfully is the differential elliptic flow, $v_2(p_T)$, where p_T is the momentum component transverse to the beam axis, i.e. the component in the xy plane in Fig. 1.2. The coefficient v_2 is defined by Fourier expanding the hadronic yield, N , in the angle ϕ in the xy plane, i.e.

$$E \frac{d^3 N}{d^3 p} = \frac{1}{2\pi} \frac{dN}{p_T dp_T dy} \left[1 + 2 \sum_{n=1}^{\infty} v_n \cos n(\phi - \Psi_n) \right] \quad (1.4)$$

where y is the rapidity and Ψ_n are orientation angles.

The elliptic flow is an interesting observable because it can be used to constrain the shear viscosity of QGP. In heavy-ion collisions the nuclei collide at a finite impact parameter making the overlap region roughly almond-shaped, see Fig. 1.2. Assuming collective behaviour, the pressure gradient is larger on the short x-axis of the almond

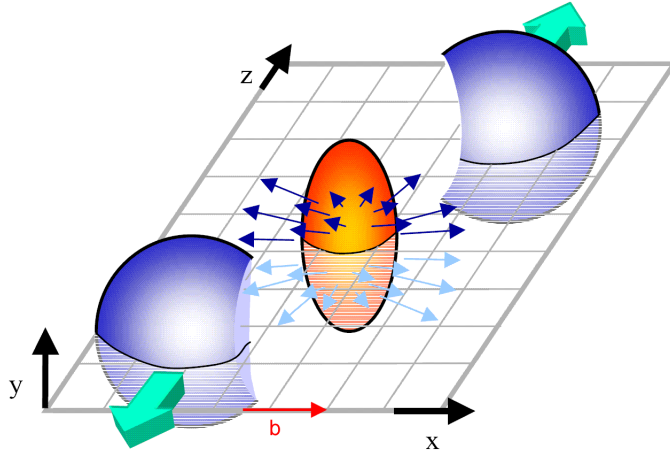


Figure 1.2: Cartoon of heavy-ion collisions at finite impact parameter. The QGP formed is roughly almond shaped which leads to an expansion in the xz plane. Figure from [14].

than on the long y -axis. The Euler equation of ideal hydrodynamics is

$$\frac{d\mathbf{u}}{dt} = -\frac{1}{\varepsilon + P}\nabla P, \quad (1.5)$$

to lowest order in velocity where P is pressure and ε is energy density. It shows that the difference in pressure gradient propels the medium to flow along the x -axis which leads to a finite v_2 .

Hydrodynamics can explain the shape of $v_2(p_T)$: An early paper varied the shear viscosity in a hydrodynamical simulation and found best agreement with experimental v_2 when using constant $\eta/s = 0.03$ [15], see Fig. 1.3. They did not include hadronic rescattering and used simple initial conditions.¹ Later and more sophisticated studies have found higher values of η/s but still only a few times the gauge/gravity limit of $1/4\pi$ [17, 18, 19]. This suggests that the QGP formed in experiments is strongly coupled. It has also been shown that including bulk viscosity is essential to fit the

¹There is a further problem that all hydrodynamical studies have in common. The value of shear viscosity affects not only the hydrodynamical evolution but also how the medium is converted into hadrons using a momentum distribution. Unfortunately these distributions are not unique and affect observables heavily. Changing the momentum distribution changes the shear viscosity extracted. There is a further problem for bulk viscosity because the momentum distributions used often violate the definition of the fluid's rest frame, see [16]. It is imperative to constrain these momentum distributions theoretically.

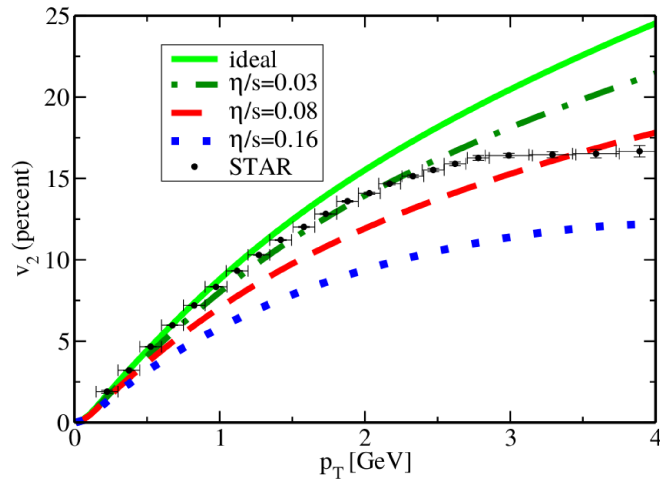


Figure 1.3: Results from an early hydrodynamical study of the effects of shear viscosity on elliptic flow [15]. The authors got best agreement with data with a very low value of shear viscosity, $\eta/s = 0.03$.

average p_T of different hadronic species [18].

Even more recent studies have used Bayesian analysis to constrain the viscosities of QGP [20]. The idea is to vary parameters of hydrodynamical simulations systematically. By using a random walk in parameter space with a drift towards values that fit experimental results better one gets a probability distribution for transport coefficients. The authors found the ratio of shear viscosity to entropy density to be close to $1/4\pi$ at $T \sim 150$ MeV and slowly increasing with temperature. They confirmed that bulk viscosity is necessary but could not constrain its value nor its temperature dependence.

1.3 Photon production in the QGP

We have described how we can learn about η/s and ζ/s from correlations of soft hadrons. It is important to obtain the transport coefficients from independent experimental observables, preferably ones that are more sensitive to the time evolution of the QGP medium. Photons are an ideal probe for this task because they are radiated from the QGP throughout its evolution. Furthermore they only feel the electromag-

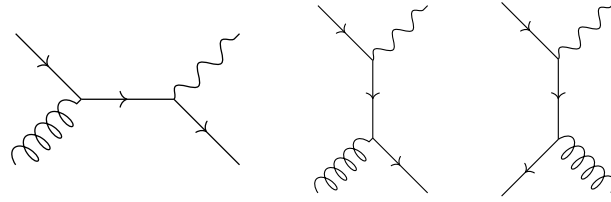


Figure 1.4: Two-to-two scattering in the QGP with a photon in the final state. Straight lines are quarks, wavy lines are photons and curly lines are gluons. Time runs from left to right.

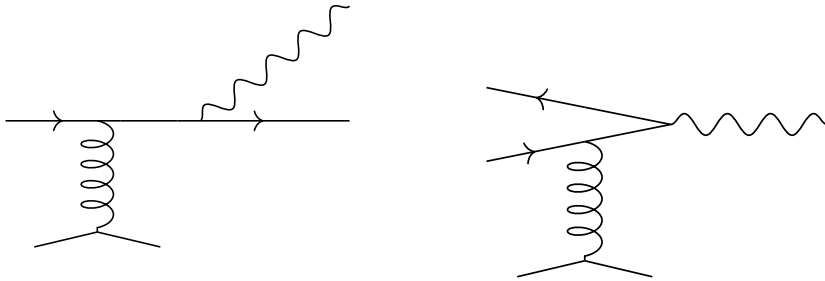


Figure 1.5: Photon production through bremsstrahlung off a quark and pair annihilation of a quark and antiquark. The quarks interact with the medium through a soft gluon exchange. These are leading order processes.

netic force: they escape the medium once they are created and give direct information about the QGP. This should be contrasted with final-state hadrons which are only sensitive to the final moments of the medium and which scatter off each other before being measured.

In order to understand photons in heavy-ion collisions we must understand photon production in the QGP. A convenient tool is perturbation theory. We focus on results at leading order in $\alpha_{EM} = e^2/4\pi$ and g . One of the leading-order channels is two-to-two scattering with a photon in the final state, see Fig. 1.4. They were evaluated for a QGP in thermal equilibrium over 25 years ago in [21] and [22]. When the exchanged particle is soft one must include its interaction with the thermal medium. We will discuss these matters at length in Chapter 3.

There are more leading order channels that are just as important. In [23] the authors evaluated the diagrams in Fig. 1.5. They are leading order when the quarks

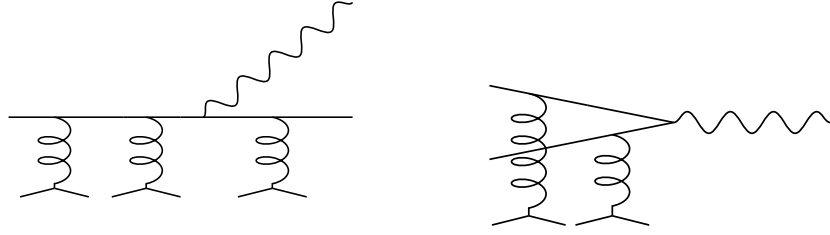


Figure 1.6: Examples of leading order diagrams for photon emission. The LPM effect says that at leading order hard quarks emitting a photon can interact arbitrarily often with the medium through soft gluon exchange.

are hard and almost on shell, the exchanged gluon is soft and the photon is almost collinear with the quarks. These diagrams correspond to a quark emitting a photon through bremsstrahlung and pair annihilation of a quark and antiquark. The quarks interact with the medium through a soft gluon exchange while producing the photon. Without this interaction the processes would be kinematically forbidden.

The fun does not end there. In [24] it was shown that at leading order the quarks in bremsstrahlung and pair annihilation can interact arbitrarily often with the medium through a soft gluon exchange, see Fig. 1.6. This is called the Landau-Pomeranchuk-Migdal (LPM) effect. It reduces the number of photons produced. We will discuss the physical meaning of the LPM effect in Chapter 4 and the chapters that follow. Finally Arnold, Moore and Yaffe cut the knot in [25, 26] by showing that the channels we have listed are the only ones that contribute at leading order. Furthermore they evaluated the suppression of photon production through the LPM effect for a QGP in thermal equilibrium.

Having the leading order result for photon production it is natural to ask whether these perturbative calculation correspond to the strongly interacting QGP formed in experiments. We can give two arguments in favour of using perturbation theory for photon production. Firstly, photons have been calculated at next-to-leading order in g . At realistic values of $\alpha_s = g^2/4\pi \approx 0.3$ the correction is a modest 20% [27].¹

¹One should however note that the correction entails a cancellation of a positive and a negative part each of which is 50 – 70% of the leading order result. This cancellation could be purely

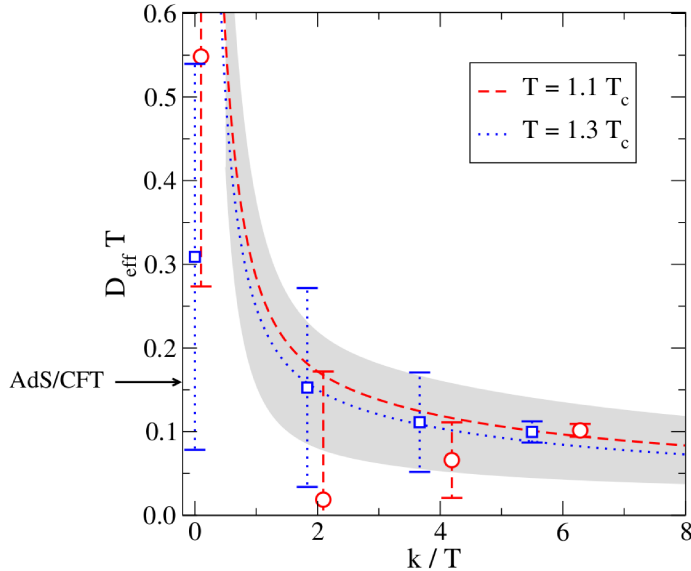


Figure 1.7: Lattice results on photon production in thermal QGP [30]. The grey band is the next-to-leading order result while the red and blue dots are lattice results at two temperatures. k is the photon energy. The plotted quantity is proportional to the photon production rate.

This should be contrasted with the poor convergence of heavy quark diffusion [28] and jet-medium interaction [29] at realistic α_s . Furthermore the next-to-leading order result has been compared with lattice calculations of photon production [30]. The agreement between lattice and perturbative results is surprisingly good at higher photon energies, see Fig. 1.7. At energies $k \lesssim T$ perturbative theory gives poor results as expected since perturbative analysis breaks down in that regime.

To extract the shear and bulk viscosity of QGP from photonic observables we must go beyond thermal equilibrium and consider photon emission from a non-equilibrium QGP. Microscopically this means using a more general momentum distribution for quarks and gluons than the equilibrium Fermi-Dirac or Bose-Einstein distributions. Schematically,

$$f_{\text{eq}} \longrightarrow f_{\text{eq}} + \delta f_{\text{shear}} + \delta f_{\text{bulk}} \quad (1.6)$$

where f_{eq} is the equilibrium part, δf_{shear} is the shear viscous part and δf_{bulk} is the

accidental.

bulk viscous part. The general distribution is derived from kinetic theory [31, 32]. δf_{shear} and δf_{bulk} contain η/s and ζ/s which explains how we can extract transport coefficients using photons. See Table 1.1 for an overview of previous work on photon production in a non-equilibrium QGP and new results in this thesis.

1.4 Photons in heavy-ion collisions

The final goal of calculating photon production in a non-equilibrium QGP is to extract transport coefficients from photon observables. This is not possible at present for two reasons: First, the QGP is not the only source of photons in heavy-ion collisions. Photons are emitted in initial collisions of nucleons and after hadronization when unstable hadrons decay. These sources are well understood. There are further sources that are less understood such as radiation from the medium before the onset of hydrodynamics [33, 34], during fragmentation of jets [35] and as quarks hadronize [36]. Experimentalists cannot distinguish these sources apart from subtracting the emission from some hadronic decays. Thus we must understand all the sources theoretically to isolate the interesting QGP photons.

The other obstacle is that phenomenological studies of photons in heavy-ion collisions do not fit experimental data. Specifically they underestimate both the total yield of photons and their elliptic flow. This is called the elliptic flow puzzle. It suggests that we are missing some major source of photons.¹

Let's look at a recent sophisticated photon study [38]. The authors model the time evolution of the QGP with hydrodynamics, the parameters of which are chosen to fit hadronic data. During the evolution each fluid cell emits photons according to rates that e.g. depend on the temperature and the velocity of the cell. In the QGP phase they use leading order perturbative results extrapolated to a realistic coupling strength. For the hadronic phase of the hydrodynamics they use phenomenological models. The rates include viscous corrections where they have been calculated. Radiation from the initial collisions of nucleons comes from perturbative vacuum QCD.

¹Tension also currently exists between the PHENIX and STAR photon data sets at RHIC [37].

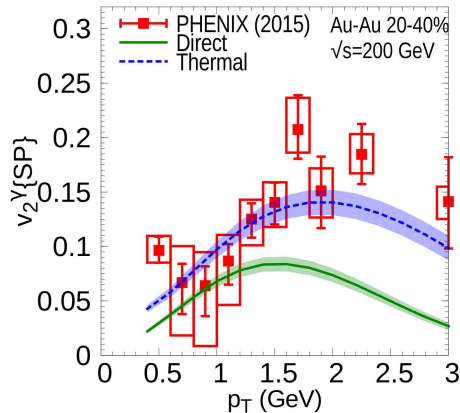


Figure 1.8: Differential elliptic flow of photons in Au-Au collisions in the 20-40% centrality bin (see Chapter 3). The green curve is the calculation of direct photons from [38]. Direct photons are all photons in heavy-ion collisions apart from those subtracted by experimentalists. The subtracted photons come from the decay of final-state hadrons. The theoretical prediction is significantly below the experimental data from PHENIX. The blue curve is the elliptic flow of photons emitted during the hydrodynamic phase only.

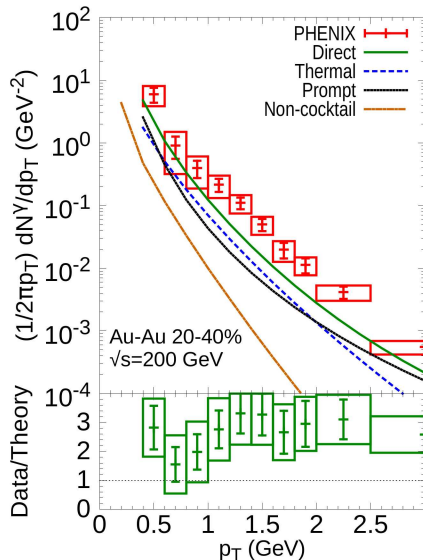


Figure 1.9: Photon yield as a function of p_T in Au-Au collisions in the 20-40% centrality bin. The green curve is the calculation from [38]. It is significantly below the experimental data from PHENIX. The other curves show photon sources separately. Thermal photons are emitted during the hydrodynamic evolution, prompt photons are emitted in the initial collision of nucleons and non-cocktail photons come from hadronic decays.

	Equilibrium	Shear correction	Bulk correction
2 to 2 scattering	[21, 22]	E.g. [39]	This thesis
Bremsstrahlung Pair annihilation	[23, 25]	Extension of thesis	This thesis
LPM effect	[25]	Extension of thesis	This thesis

Table 1.1: List of previous work on photon production in an equilibrium and non-equilibrium QGP.

The simulation also includes photons from hadronic decays after the hydrodynamic medium is converted into hadrons. Some of the results of this study can be seen in Fig. 1.8 and Fig. 1.9. They underestimate both the elliptic flow of photons and the photon yield indicating missing sources.

1.5 *This thesis*

Studying photon emission from a non-equilibrium QGP is important because it could enable the determination of transport coefficients. Such non-equilibrium QFT calculations are furthermore interesting in themselves. Table 1.1 summarizes previous work which has been limited to two-to-two scattering channels. Some of it is inconsistent in that it only includes viscous corrections to the incoming and outgoing particles but not the mediator [31, 40]. The first consistent calculations were performed in [41, 42, 43]. The authors of [38, 39] built on those calculations using a realistic f_{shear} . In this thesis we give a first calculation of the bulk viscous correction to two-to-two channels.

This thesis is also a first study of photon production through bremsstrahlung and pair-annihilation in a non-equilibrium QGP. We treat the LPM effect consistently. We focus on bulk viscous corrections in which case the momentum distribution is isotropic, i.e.

$$f(\mathbf{p}) = f(p) \tag{1.7}$$

Our derivation is valid for general isotropic f . Furthermore the ideas here can be generalized to allow for shear viscous corrections to bremsstrahlung and pair-annihilation.

The thesis is organized as follows: Chapter 2 is an introduction to the theoret-

ical tools needed. In Chapter 3 we calculate the bulk viscous correction to photon production through two-to-two scattering channels using a specific f_{bulk} . We explore the importance of this correction in phenomenological studies. The remainder of the thesis deals with bremsstrahlung, pair-annihilation and the LPM effect in a non-equilibrium QGP. Chapter 4 provides an overview of these channels. There we derive the resummed occupation density of soft gluons and extend an equilibrium sum rule. In Chapter 5 we derive the resummed occupation density of hard quarks. In Chapter 6 the Feynman diagrams are evaluated which gives a Boltzmann-like integral equation. We provide a new way of summing over the diagrams without using the equilibrium KMS condition. Finally in Chapter 7 we summarize the thesis. Standard material on QCD and spinors is relegated to appendices.

We use the $(+, -, -, -)$ metric. If P^μ is a four vector then p^0 is its time component, \mathbf{p} are its spatial components and $p = |\mathbf{p}|$. We use units where $\hbar = c = k_B = 1$ except for phenomenological results in Chapter 3.

2

Theoretical foundations

2.1 *The real time formalism in thermal equilibrium*

Most QFT calculations for high energy experiments use a perturbative expansion in the coupling constant, λ . One expands an n-point function of the full theory,

$$\langle 0 | \phi(x_1) \cdots \phi(x_n) | 0 \rangle, \quad (2.1)$$

in λ and evaluates each order in terms of two-point functions of the free theory ($\lambda = 0$). The scattering is assumed to take in place in vacuum so the particles are an excitation on top of the ground state of the theory, $|0\rangle$.

Processes in the QGP formed in heavy-ion collisions do not happen in vacuum but in a mostly thermalized medium. We need to evaluate n-point functions in the canonical ensemble which describes a system at fixed temperature. These n-point functions are given by

$$\langle \phi(x_1) \cdots \phi(x_n) \rangle_\beta := \frac{1}{Z} \sum_n e^{-\beta E_n} \langle n | \phi(x_1) \cdots \phi(x_n) | n \rangle \quad (2.2)$$

where

$$Z = \sum_n e^{-\beta E_n} \quad (2.3)$$

is the partition function. Here $|n\rangle$ are the eigenstates of the Hamiltonian H and

$\beta = 1/T$ where T is the temperature. This can be written more elegantly as

$$\langle \phi(x_1) \cdots \phi(x_n) \rangle_\beta := \text{Tr} [\rho \phi(x_1) \cdots \phi(x_n)]. \quad (2.4)$$

where $\rho = \exp(-\beta H)/Z$ is the density matrix for the canonical ensemble. To calculate these quantities perturbatively we need to derive Feynman rules at finite temperature.

The material on finite temperature field theory that follows is quite standard and is treated in numerous review articles and text books. For example [44] is a well known text book that covers the imaginary time formalism (see below) in depth and gives various applications. Furthermore [45] and [46] treat both the imaginary and the real time formalism and [45] also covers hard thermal loops (HTL) comprehensively. Finally [47] talks about the basics of out-of-equilibrium field theory. The treatment here is partially inspired by [45]. In what follows we assume the reader is familiar with the derivation of Feynman rules in vacuum using the path integral formalism. In this section we work exclusively in the canonical ensemble where all chemical potentials vanish.

In vacuum

$$\langle \phi_b(\mathbf{x}) | e^{-i\tau H} | \phi_a(\mathbf{x}) \rangle = \int_{\phi_a}^{\phi_b} \mathcal{D}\phi \exp \left[i \int_0^\tau d^4x \mathcal{L} \right] \quad (2.5)$$

(see chapter 9 in [48]). The left hand side is the transition amplitude from an initial field configuration, ϕ_a , to a final field configuration, ϕ_b , during time τ . The right hand side is a path integral from ϕ_a at $t = 0$ to ϕ_b at $t = \tau$. The weighting of the integral is determined by the Lagrangian \mathcal{L} .

The left hand side of eq. (2.5) has a striking resemblance with the partition function in the canonical ensemble

$$Z = \sum_n \langle n | e^{-\beta H} | n \rangle. \quad (2.6)$$

There are only two differences. Firstly, one must substitute τ by the complex number $-i\beta$. Secondly, we must sum over all initial states and demand that the evolution be

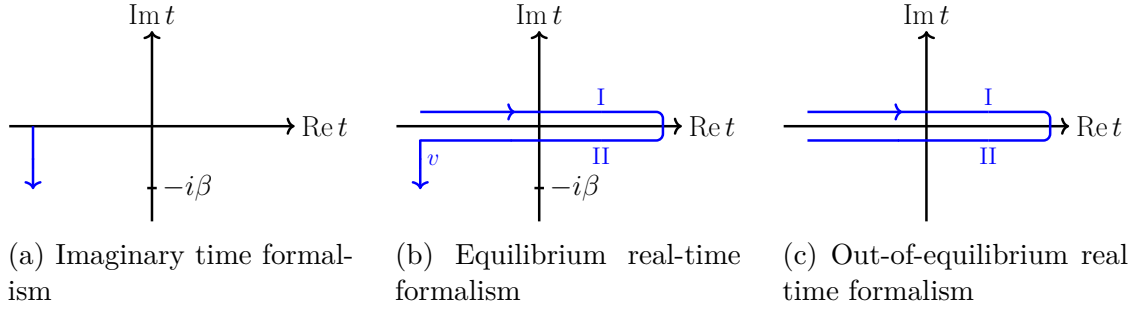


Figure 2.1: Time contours in different formalisms

periodic in $-i\beta$. In analogy with the vacuum result

$$Z = \int_{\text{periodic}} \mathcal{D}\phi \exp \left[- \int_0^\beta d^4x \mathcal{L}_{\text{Eucl.}} \right]. \quad (2.7)$$

The integral is over all possible paths that begin and end in the same field configuration.¹ We have analytically continued the Lagrangian to imaginary time giving the Euclidean Lagrangian.

From eq. (2.7) one derives finite temperature Feynman rules in the imaginary time formalism. In contrast to Euclidean vacuum theory time is confined to an interval $[0, \beta]$. Therefore one does not get continuous energy values under Fourier transformation but rather a discrete energy spectrum called Matsubara frequencies. We will not pursue the imaginary time formalism any further here. When using it one must do complicated sums in the discrete energies to evaluate diagrams with multiple loops. More seriously, we have analytically continued the physical time to obtain the temperature, leaving us with no real time variable. Thus we cannot calculate dynamical quantities, let alone out-of-equilibrium properties of systems.

In this thesis we use the real-time formalism, also known as the Keldysh-Schwinger or closed time path formalism. Above we captured the temperature by starting at time t_i and following a vertical path in the complex time plane to $t_i - i\beta$, \mathcal{C}_v , see Fig. 2.1a. We include real time by adding a horizontal path from t_i to t_f , \mathcal{C}_I , as well as a path from $t_f - i\epsilon$ to $t_i - i\epsilon$, \mathcal{C}_{II} which joins \mathcal{C}_v , see Fig. 2.1b. Taking the limits

¹This is true only for bosons. Fermionic fields obey antiperiodic boundary conditions [45].

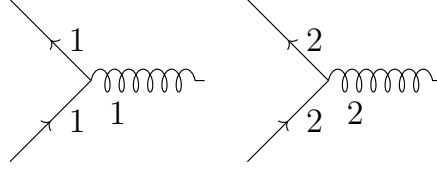


Figure 2.2: Vertices in the 1/2 basis in the real time formalism

$t_i \rightarrow -\infty, t_f \rightarrow \infty$ we get a contour \mathcal{C} . The partition function along it is

$$Z_{\mathcal{C}} = \int_{\text{periodic}} \mathcal{D}\phi \exp \left[i \int_{\mathcal{C}} d^4x \mathcal{L} \right]. \quad (2.8)$$

The Lagrangian is integrated along the contour. For a more rigorous justification, see [45].

We write $\mathcal{L} = \mathcal{L}_{\text{free}} - \mathcal{V}$ where \mathcal{V} is the interaction and add a source term, $j\phi$, so that

$$\begin{aligned} Z_{\mathcal{C}}(j) &= \int_{\text{periodic}} \mathcal{D}\phi \exp \left[i \int_{\mathcal{C}} d^4x (\mathcal{L}_{\text{free}} - \mathcal{V} + j\phi) \right] \\ &= \exp \left[-i \int_{\mathcal{C}} d^4x \mathcal{V} \left(\frac{\delta}{i\delta j(x)} \right) \right] \\ &\quad \times \int_{\text{periodic}} \mathcal{D}\phi \exp \left[i \int_{\mathcal{C}} d^4x (\mathcal{L}_{\text{free}} + j\phi) \right] \end{aligned} \quad (2.9)$$

We can evaluate the *free* path integral in the same way as in vacuum. The result is

$$Z_{\mathcal{C}}^0(j) \sim \exp \left[-\frac{1}{2} \int_{\mathcal{C}} d^4x \int_{\mathcal{C}} d^4y j(x) D_{\mathcal{C}}^0(x-y) j(y) \right] \quad (2.10)$$

where $D_{\mathcal{C}}^0$ is the free Feynman propagator generalized to our contour,

$$\begin{aligned} D_{\mathcal{C}}^0(x-y) &= \langle T_{\mathcal{C}} \phi(x) \phi(y) \rangle_{\beta} \\ &= \theta_{\mathcal{C}}(t_x, t_y) \langle \phi(x) \phi(y) \rangle_{\beta} + \theta_{\mathcal{C}}(t_y, t_x) \langle \phi(y) \phi(x) \rangle_{\beta}. \end{aligned} \quad (2.11)$$

The contour theta function $\theta_{\mathcal{C}}(t_x, t_y)$ is 1 if t_x is later on \mathcal{C} than t_y and 0 otherwise. The thermal propagators are defined as in eq. (2.4).

The vertical path, \mathcal{C}_v , only contributes through the periodic boundary condition in

ϕ .¹ As long as we remember that all propagators are thermal we can write $\mathcal{C} = \mathcal{C}_I \cup \mathcal{C}_{II}$. Then the full partition function is

$$Z_{\mathcal{C}}(j) = \exp \left[-i \int d^4x \left\{ \mathcal{V} \left(\frac{\delta}{i\delta j_1(x)} \right) - \mathcal{V} \left(\frac{\delta}{i\delta j_2(x)} \right) \right\} \right] \times \exp \left[-\frac{1}{2} \int d^4x \int d^4y j_a(x) D_{ab}^0(x-y) j_b(y) \right] \quad (2.12)$$

Here we have written the source as $j = j_1 + j_2$ where j_1 lives on \mathcal{C}_I and j_2 lives on \mathcal{C}_{II} . The indices a and b are summed over 1 and 2, and e.g.

$$D_{12}^0(x-y) = \langle T_{\mathcal{C}} \phi_1(x) \phi_2(y) \rangle_{\beta} \quad (2.13)$$

with ϕ_1 living on \mathcal{C}_I and ϕ_2 on \mathcal{C}_{II} . In this equation the time integral on \mathcal{C}_{II} goes from $-\infty$ to ∞ . To compensate we had to add a minus sign to the term $\mathcal{V} \left(\frac{\delta}{i\delta j_2(x)} \right)$.

We can finally state the Feynman rules. For each physical field there are two fields in the real-time formalism living on \mathcal{C}_I and \mathcal{C}_{II} . Thus there are four free propagators. Generalizing to complex scalar fields they can be written as

$$D_{11}(x) = \langle T \phi(x) \phi^\dagger(0) \rangle_{\beta} \quad (2.14)$$

$$D_{12}(x) = \langle \phi^\dagger(0) \phi(x) \rangle_{\beta} \quad (2.15)$$

$$D_{21}(x) = \langle \phi(x) \phi^\dagger(0) \rangle_{\beta} \quad (2.16)$$

$$D_{22}(x) = \langle \bar{T} \phi(x) \phi^\dagger(0) \rangle_{\beta} \quad (2.17)$$

where T is the usual time ordering and \bar{T} is anti-time ordering. We have assumed translational invariance so that $D(x, y) = D(x - y)$. An interaction vertex either has all fields of type 1 or all fields of type 2, see Fig. 2.2. In the second case we get a relative minus sign. We must sum over all possible assignments of 1 and 2 to vertices.

¹For a thorough discussion of the role of the vertical path see [49] and [50].

For ease of notation we define the following propagators:

$$D_{\text{ret}}(x) = \theta(x^0) \langle [\phi(x), \phi^\dagger(0)] \rangle \quad (2.18)$$

$$D_{\text{adv}}(x) = -\theta(-x^0) \langle [\phi(x), \phi^\dagger(0)] \rangle \quad (2.19)$$

$$D^>(x) = \langle \phi(x) \phi^\dagger(0) \rangle \quad (2.20)$$

$$D^<(x) = \langle \phi^\dagger(0) \phi(x) \rangle \quad (2.21)$$

Clearly $D^> = D_{21}$ and $D^< = D_{12}$. We also define the spectral function

$$\rho(x) = D^> - D^< = D_{\text{ret}} - D_{\text{adv}} = \langle [\phi(x), \phi(0)^\dagger] \rangle \quad (2.22)$$

We have derived the Feynman rules in the $1/2$ basis in the real-time formalism. The propagators have a simpler structure in the so-called r/a basis which lends itself more easily to power counting arguments [51]. We define

$$\phi_r := \frac{\phi_1 + \phi_2}{2}, \quad \phi_a := \phi_1 - \phi_2 \quad (2.23)$$

and similarly for other fields. Then it is easy to show that the four propagators are

$$\begin{aligned} D_{rr}(x) &= \frac{1}{2} \rho(x) + D^<(x) \\ D_{ra}(x) &= D_{\text{ret}}(x) \\ D_{ar}(x) &= D_{\text{adv}}(x) \\ D_{aa}(x) &= 0 \end{aligned} \quad (2.24)$$

Here e.g.

$$\begin{aligned} D_{ra}(x) = \langle T_C \phi_r(x) \phi_a^\dagger(0) \rangle &= \frac{1}{2} \left[\langle T_C \phi_1(x) \phi_1^\dagger(0) \rangle - \langle T_C \phi_1(x) \phi_2^\dagger(0) \rangle \right. \\ &\quad \left. + \langle T_C \phi_2(x) \phi_1^\dagger(0) \rangle - \langle T_C \phi_2(x) \phi_2^\dagger(0) \rangle \right] \end{aligned} \quad (2.25)$$

We will use both bases in this thesis.

The aa propagator vanishes identically. The number of independent propagators can be reduced further with general arguments. In translationally invariant systems we can relate the retarded and advanced propagators in momentum space:

$$\begin{aligned}
D_{\text{ret}}(P)^* &= \left(\int d^4x e^{iP \cdot x} \theta(x^0) \langle [\phi(x), \phi^\dagger(0)] \rangle \right)^* \\
&= \int d^4x e^{-iP \cdot x} \theta(x^0) \langle [\phi(0), \phi^\dagger(x)] \rangle \\
&= \int d^4x e^{iP \cdot x} \theta(-x^0) \langle [\phi(0), \phi^\dagger(-x)] \rangle \\
&= \int d^4x e^{iP \cdot x} \theta(-x^0) \langle [\phi(x), \phi^\dagger(0)] \rangle \\
&= -D_{\text{adv}}(P)
\end{aligned} \tag{2.26}$$

Here we did a change of variables $x \rightarrow -x$ and exploited translational invariance. Since $\rho = D_{\text{ret}} - D_{\text{adv}}$ there are only two independent propagators in eq. (2.24), D_{ret} and $D^<$.

In thermal equilibrium we can reduce the number of independent propagators to one using the Kubo-Martin-Schwinger (KMS) relation. It relies on the Hamiltonian generating time translations and describing the occupation of states in the canonical ensemble. Indeed

$$\begin{aligned}
D^<(t + i\beta, \mathbf{x}) &= \frac{1}{Z} \text{Tr}[e^{-\beta H} \phi^\dagger(0) \phi(t + i\beta, \mathbf{x})] \\
&= \frac{1}{Z} \text{Tr}[e^{-\beta H} \phi^\dagger(0) e^{-\beta H} \phi(t, \mathbf{x}) e^{\beta H}] \\
&= \frac{1}{Z} \text{Tr}[e^{-\beta H} \phi(t, \mathbf{x}) \phi^\dagger(0)] \\
&= D^>(t, \mathbf{x})
\end{aligned} \tag{2.27}$$

where we used the cyclic property of the trace. In momentum space this gives $D^<(K) = e^{-\beta k^0} D^>(K)$. One can then easily show that

$$D^>(K) = (1 + f_B(k^0)) \rho(K) \tag{2.28}$$

and

$$D^<(K) = f_B(k^0)\rho(K) \quad (2.29)$$

where

$$f_B(k^0) = \frac{1}{e^{\beta k^0} - 1} \quad (2.30)$$

is the Bose-Einstein distribution.

In thermal equilibrium we thus have

$$D_{rr}(K) = \left(\frac{1}{2} + f_B(k^0)\right) (D_{\text{ret}}(K) - D_{\text{adv}}(K)) \quad (2.31)$$

$$D_{ra}(K) = D_{\text{ret}}(K) \quad (2.32)$$

$$D_{ar}(K) = D_{\text{adv}}(K) \quad (2.33)$$

$$D_{aa}(K) = 0 \quad (2.34)$$

where $D_{\text{adv}} = -D_{\text{ret}}^*$. These relations are valid for the full propagators and are therefore true at every order in perturbation theory. The KMS relation has offered an immense simplification. Using their antiperiodicity one gets similar results for fermionic propagators in thermal equilibrium. The only difference is that

$$f_B(k^0) \longrightarrow -f_F(k^0) = -\frac{1}{e^{\beta k^0} + 1} \quad (2.35)$$

where f_F is the Fermi-Dirac distribution.

The only thing left is to find D_{ret}^0 , the free retarded propagator. It is the same as in vacuum as can easily be seen using canonical quantization. We show this for a real scalar field. For a free field we can always write [48]

$$\phi(x) = \int \frac{d^3p}{(2\pi)^3} \frac{1}{\sqrt{2E_{\mathbf{p}}}} \left(a_{\mathbf{p}} e^{-ip \cdot x} + a_{\mathbf{p}}^\dagger e^{ip \cdot x} \right) \Big|_{p^0=E_{\mathbf{p}}} \quad (2.36)$$

$a_{\mathbf{p}}^\dagger$ and $a_{\mathbf{p}}$ are raising and lowering operators. Then

$$[\phi(x), \phi(y)] = \int \frac{d^3p}{(2\pi)^3} \frac{1}{2E_{\mathbf{p}}} \left(e^{-ip \cdot (x-y)} - e^{ip \cdot (x-y)} \right) \Big|_{p^0=E_{\mathbf{p}}} \quad (2.37)$$

is just a number and evaluating the thermal expectation value is trivial. A calculation using

$$\theta(t) = i \int \frac{dk}{2\pi} \frac{e^{-ikt}}{k + i\epsilon} \quad (2.38)$$

then gives that

$$D_{\text{ret}}^0(P) = \frac{i}{P^2 - m^2 + i\epsilon p^0} \quad (2.39)$$

Using eq. (2.22) we see that

$$\rho(P) = 2\pi \operatorname{sgn}(p^0) \delta(P^2 - m^2) \quad (2.40)$$

We can finally write down the free propagators in the r/a basis. Using the identity

$$\operatorname{sgn}(p^0) \left(\frac{1}{2} + f_B(p^0) \right) = \frac{1}{2} + f_B(|p^0|) \quad (2.41)$$

we get that

$$D_{rr}^0(P) = \left(\frac{1}{2} + f_B(E_{\mathbf{p}}) \right) 2\pi \delta(P^2 - m^2) \quad (2.42)$$

$$D_{ra}^0(P) = \frac{i}{P^2 - m^2 + i\epsilon p^0} \quad (2.43)$$

$$D_{ar}^0(P) = \frac{i}{P^2 - m^2 - i\epsilon p^0} \quad (2.44)$$

$$D_{aa}^0(P) = 0 \quad (2.45)$$

where $E_{\mathbf{p}} = \sqrt{p^2 + m^2}$. All information about the thermal medium is contained in $f_B(E_{\mathbf{p}})$ in the rr propagator. The delta function and the absolute sign in f_B tell us that D_{rr} describes real particles that are on shell and have positive energy. Their momentum distribution is the Bose-Einstein function. The free propagators D_{ra}^0 and D_{ar}^0 describe fields that can be off shell and already exist in vacuum.

Later we will work with resummed rr propagators. They describe quasi-particles that have acquired a mass and a finite lifetime through their interaction with the thermal medium. The delta function is then replaced by a Breit-Wigner distribution

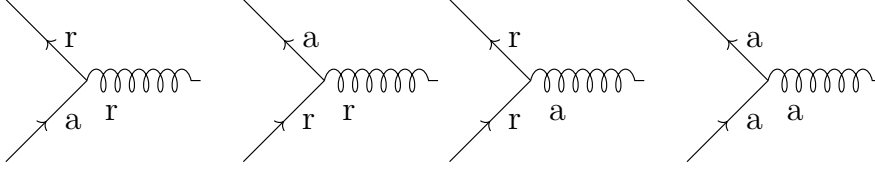


Figure 2.3: Vertices in the r/a basis in the real time formalism

with momentum dependent masses and lifetimes. Owing to the KMS condition the momentum distribution is still f_B in thermal equilibrium.

The propagators for vector bosons in the Feynman gauge are the same as in eq. (2.42)-(2.45) with an additional factor of $-g^{\mu\nu}$. The propagators for free spin 1/2 fermions are

$$S_{rr}^0(P) = \left(\frac{1}{2} - f_F(E_{\mathbf{p}}) \right) 2\pi \not{P} \delta(P^2 - m^2) \quad (2.46)$$

$$S_{ra}^0(P) = \frac{i \not{P}}{P^2 - m^2 + i\epsilon p^0} \quad (2.47)$$

$$S_{ar}^0(P) = \frac{i \not{P}}{P^2 - m^2 - i\epsilon p^0} \quad (2.48)$$

$$S_{aa}^0(P) = 0 \quad (2.49)$$

The only thing left before using the r/a basis is to check which vertices are possible. Let's consider a vertex with a gluon, a quark and an antiquark. Our knowledge of the 1/2 basis tells us that, schematically, the vertices are

$$\bar{\psi}_1 A_1 \psi_1 - \bar{\psi}_2 A_2 \psi_2 = \bar{\psi}_r A_r \psi_a + \bar{\psi}_r A_a \psi_r + \bar{\psi}_a A_r \psi_r + \frac{1}{4} \bar{\psi}_a A_a \psi_a. \quad (2.50)$$

They are summarized in Fig. 2.3. Each vertex has an odd number of a and the vertex with all indices a has an overall factor 1/4.

2.2 Out-of-equilibrium propagators

In this thesis we are interested in photon emission of systems that are not in thermal equilibrium. The relevant n-point functions are then

$$\langle \phi(x_1) \cdots \phi(x_n) \rangle := \text{Tr} [\rho \phi(x_1) \cdots \phi(x_n)] \quad (2.51)$$

where ρ is a general density operator at some initial time t_0 . Its time evolution can be absorbed in the fields [52]. We can still use the real time formalism but now the time contour is as in Fig. 2.1c. Instead of a vertical path denoting the system's state we have a weighting from ρ in the path-integral [53]. Intuitively, the time contour must begin and end at $t_0 \rightarrow -\infty$ where we know the density matrix.

The Feynman rules can be derived in the same way as in equilibrium. We get a doubling of the degrees of freedom and three non-trivial propagators in the r/a basis. In this thesis we assume throughout that our system is translationally invariant. This approximation is valid when the macroscopic length scale of the system is much longer than the microscopic scale on which quasi-particle interaction takes place. This assumption allows us to take Fourier-transforms of propagators and to relate the retarded and advanced propagator. In the same way as before we get that

$$D_{\text{ret}}^0(P) = \frac{i}{P^2 - m^2 + i\epsilon p^0} \quad (2.52)$$

The difficulty lies in finding an expression for D_{rr}^0 in out-of-equilibrium systems. The propagator is difficult to evaluate from first principles because of the dependence on the density operator. We cannot use the KMS condition either as we did in thermal equilibrium. Instead we rely on our understanding of the rr propagator as a sum of a vacuum contribution and medium contribution characterized by a momentum distribution of physical particles.

For scalar particles

$$D_{rr}^0(P) = \left(\frac{1}{2} + f(\mathbf{p}) \right) 2\pi\delta(P^2 - m^2) \quad (2.53)$$

where $f(\mathbf{p})$ is a general distribution function that characterizes the system we are interested in. It must be derived from kinetic theory. The quark and gluon propagators are analogous. For the convenience of the reader we have collected all quark and gluon propagators in the r/a and $1/2$ bases in non-equilibrium systems in Table 2.1 at the end of this chapter. We note that resummed propagators are much more complicated in non-equilibrium systems because one cannot use the KMS condition to simplify them as in eq. (2.31).

The non-equilibrium propagator in eq. (2.53) can be justified from first principles. In [53] Calzetta and Hu considered an out-of-equilibrium $\lambda\phi^4$ scalar field theory in the weak coupling limit. They used the real-time formalism assuming an initial density matrix of the form

$$\rho = C \exp \left[- \int d^3k \beta_{\mathbf{k}} a_{\mathbf{k}}^\dagger a_{\mathbf{k}} \right] \quad (2.54)$$

where a^\dagger (a) are raising (lowering) operator for the free fields and $\beta_{\mathbf{k}} \geq 0$ describe the initial occupation of each mode. The path integral depends on external sources $J^a(x)$ but also on non-local sources, K^{ab} , K^{abc} , ... The latter describe the initial state and are defined by expanding ρ in the ϕ , i.e.

$$\langle \phi_1, 0 | \rho | \phi_2, 0 \rangle = \exp \left[\frac{i}{2} \int d^4x d^4x' K_{ab}(x, x') \phi^a(x) \phi^b(x') + \dots \right] \quad (2.55)$$

Here a, b, c are indices in the 12 basis and the contraction is defined with metric $c^{ab} = \text{Diag}(1, -1)$.

Next we Legendre transform the path integral so that it depends not on the sources but on the mean field $\hat{\phi}$ and connected n-point functions, G^{ab}, G^{abc}, \dots . The relation defining the Legendre transformation gives rise to an infinite tower of equations which correspond to the BBGKY hierarchy in kinetic theory. For real calculations it must be truncated. We truncate at second order, assuming that G^{abc} and higher are dependent variables on $\hat{\phi}$ and G^{ab} . This is known as the 2PI formalism. Assuming vanishing background fields we get equations of motions for the propagators G^{ab} . At lowest order in the coupling λ the propagators in a translationally invariant system are



Figure 2.4: Vertices in scalar QED.

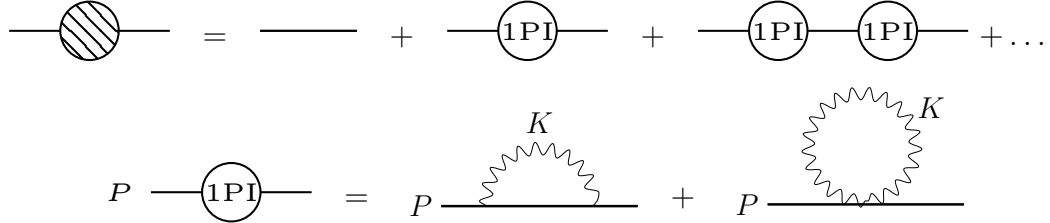


Figure 2.5: The resummed scalar propagator in scalar QED. 1PI stands for one-particle irreducible.

given by eq. (2.53) and corresponding equations. At this point f is some unknown function that can be shown to be real and positive.

Finally, Calzetta and Hu solved the equations of motion at next-to-leading order. We Wigner transform the propagators,

$$G^{ab}(X, k) = \int d^4(x - x') e^{ik \cdot (x - x')} G^{ab}(x, x') \quad (2.56)$$

where $X = (x + x')/2$. We need to assume that $G^{ab}(X, k)$ are slowly varying in X . This corresponds to the mean free path being much longer than the interaction time in kinetic theory. Then the equation of motion reduces to a Boltzmann equation in $f(X, p)$ with the collision kernel coming from the $\lambda\phi^4$ term in the Lagrangian. This shows that f should be interpreted as a momentum distribution, justifying our use of (2.53). Similar results have been obtained for weakly coupled gauge theories, see [54, 55].

2.3 Hard thermal loops

Finding out which diagrams contribute at a given order in the coupling constant is more involved in thermal field theory than in vacuum: it does not suffice to count the number of vertices to get the order of a diagram. Specifically, one runs into problems

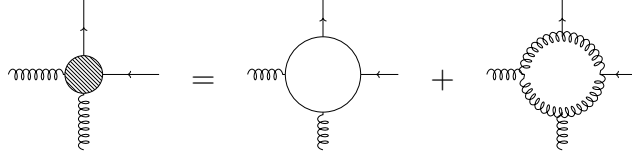


Figure 2.6: An effective vertex in the HTL scheme. The external momenta are soft and the internal momenta are hard.

for soft momenta, $P \sim gT$.

Let's take the simple example of scalar QED the vertices of which are shown in Fig. 2.4. The discussion will be schematic. A bare scalar propagator with soft momentum is

$$\frac{i}{P^2} \sim \frac{1}{e^2 T^2}. \quad (2.57)$$

We can imagine adding self-energy corrections as in Fig. 2.5. Each self-energy diagram turns out to be of order $\Pi \sim e^2 T^2$. When summing over all numbers of self-energy insertions we get a resummed propagator

$$\frac{i}{P^2 - \Pi}. \quad (2.58)$$

where Π is of the same order as P^2 . This suggests that it is inconsistent to use bare propagators for soft momenta.

A careful analysis shows that the part of Π with soft loop momentum is subleading. We can thus assume that the loop momentum is hard, $K \sim T$, when calculating Π . This whole procedure is called hard thermal loops (HTL). It entails using resummed propagators for soft momenta and restricting evaluation of the self-energy diagrams to hard loop momenta.

Let's now turn to the physically more relevant case of QCD. In [56] Braaten and Pisarski showed that one does not only need resummed soft propagators but also resummed vertices when all external momenta are soft. We get a correction to the usual vertex with a gluon, quark and antiquark but also new vertices with e.g. two gluons, a quark and an antiquark, see Fig. 2.6. The loop momenta can always be assumed to be hard. Crucially, the HTL reordering of the perturbative scheme

enables us to get gauge independent results at each order in g . This is because HTL self-energies and effective vertices are gauge independent, even when the external momenta are off shell [56, 57].

We will use HTL resummed propagators throughout this thesis. The power counting leading to the HTL scheme turns out to be the same in non-equilibrium systems that are not very far from equilibrium. As an example the assumption that soft loop momenta can be ignored holds as long as the density of soft gluons is not exceedingly high. In this thesis we assume that the momentum distribution functions are well behaved so that HTL works as in thermal equilibrium. See [58] for the constraints this puts on f .

2.4 Resummed propagators

In this thesis we use the HTL scheme in the r/a basis of the real time formalism. We need to derive the form of resummed propagators. For simplicity we consider scalar fields as in [59]. In later chapters we look at fermions and vector bosons.

The Dyson equation in the real time formalism is

$$D = D^0 + D^0 (-i\Pi) D \quad (2.59)$$

or more explicitly

$$\begin{bmatrix} D_{rr} & D_{ra} \\ D_{ar} & D_{aa} \end{bmatrix} = \begin{bmatrix} D_{rr}^0 & D_{ra}^0 \\ D_{ar}^0 & D_{aa}^0 \end{bmatrix} + \begin{bmatrix} D_{rr}^0 & D_{ra}^0 \\ D_{ar}^0 & D_{aa}^0 \end{bmatrix} (-i) \begin{bmatrix} \Pi_{rr} & \Pi_{ra} \\ \Pi_{ar} & \Pi_{aa} \end{bmatrix} \begin{bmatrix} D_{rr} & D_{ra} \\ D_{ar} & D_{aa} \end{bmatrix} \quad (2.60)$$

Here D are full propagators, D^0 are free propagators and Π are one-particle-irreducible self-energies. We define e.g. Π_{rr} as the self-energy diagram with both sources of type r , see Fig. 2.7 for clarification. The above equation is trivial as can be seen by writing

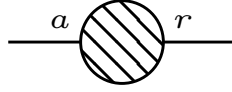


Figure 2.7: The ar component of the self-energy, Π_{ar} .

it component by component. Using that $D_{aa} = 0$ and $D_{aa}^0 = 0$ we find $\Pi_{rr} = 0$ so

$$\begin{bmatrix} D_{rr} & D_{ra} \\ D_{ar} & 0 \end{bmatrix} = \begin{bmatrix} D_{rr}^0 & D_{ra}^0 \\ D_{ar}^0 & 0 \end{bmatrix} + \begin{bmatrix} D_{rr}^0 & D_{ra}^0 \\ D_{ar}^0 & 0 \end{bmatrix} (-i) \begin{bmatrix} 0 & \Pi_{ra} \\ \Pi_{ar} & \Pi_{aa} \end{bmatrix} \begin{bmatrix} D_{rr} & D_{ra} \\ D_{ar} & 0 \end{bmatrix} \quad (2.61)$$

We get simple equations for the full retarded and advanced propagators

$$\begin{cases} D_{\text{ret}} = D_{\text{ret}}^0 + D_{\text{ret}}^0 (-i\Pi_{\text{ret}}) D_{\text{ret}} \\ D_{\text{adv}} = D_{\text{adv}}^0 + D_{\text{adv}}^0 (-i\Pi_{\text{adv}}) D_{\text{adv}} \end{cases} \quad (2.62)$$

where $\Pi_{ar} = \Pi_{\text{ret}}$ and $\Pi_{ra} = \Pi_{\text{adv}}$. Therefore

$$\begin{cases} D_{\text{ret}} = \frac{i}{P^2 - \Pi_{\text{ret}}} \\ D_{\text{adv}} = \frac{i}{P^2 - \Pi_{\text{adv}}} \end{cases} \quad (2.63)$$

since $i(D_{\text{ret}}^0)^{-1} = i(D_{\text{adv}}^0)^{-1} = P^2$ for massless particles. We can ignore the $i\epsilon p^0$ term in the free propagators assuming that $\text{Im}\Pi_{\text{ret}}$ is non-vanishing. $\text{Re}\Pi_{\text{ret}}$ is a thermal mass which the particle acquires by interacting with other particles in the medium. Similarly $\text{Im}\Pi_{\text{ret}}$ corresponds to the thermal decay width of the particle. In translationally invariant systems $D_{\text{ret}} = -D_{\text{adv}}^*$ so

$$\Pi_{\text{ret}} = \Pi_{\text{adv}}^* \quad (2.64)$$

The equation for the rr propagator is more complicated,

$$D_{rr} = D_{rr}^0 + D_{\text{ret}}^0 (-i\Pi_{\text{ret}}) D_{rr} + D_{rr}^0 (-i\Pi_{\text{adv}}) D_{\text{adv}} + D_{\text{ret}}^0 (-i\Pi_{aa}) D_{\text{adv}} \quad (2.65)$$

We could solve this equation directly but the result has no clear physical interpreta-

tion. Instead we write

$$D_{rr} = D_{<} + \frac{1}{2}(D_{\text{ret}} - D_{\text{adv}}) \quad (2.66)$$

where we need to evaluate $D_{<} = D_{12}$. Using equations (2.62) and (2.65) one gets that

$$D_{<} = D_{<}^0 + D_{\text{ret}}^0 (-i\Pi_{\text{ret}}) D_{<} + D_{<}^0 (-i\Pi_{\text{adv}}) D_{\text{adv}} + D_{\text{ret}}^0 (-i\Pi_{<}) D_{\text{adv}} \quad (2.67)$$

where we have defined

$$\Pi_{<} = \Pi_{aa} - \frac{1}{2}\Pi_{\text{ret}} + \frac{1}{2}\Pi_{\text{adv}} \quad (2.68)$$

Solving for $D_{<}$, using eq. (2.63), we get

$$D_{<} = \frac{(-iD_{\text{ret}}^0)^{-1} D_{<}^0 (-iD_{\text{adv}}^0)^{-1} + i\Pi_{<}}{\left[(-iD_{\text{ret}}^0)^{-1} - \Pi_{\text{ret}}\right] \left[(-iD_{\text{adv}}^0)^{-1} - \Pi_{\text{adv}}\right]} \quad (2.69)$$

Assuming the retarded self-energy is non-vanishing we can drop the first term because

$$D_{<}^0 (D_{\text{ret}}^0)^{-1} \propto P^2 \delta(P^2) = 0 \quad (2.70)$$

We are then left with

$$D_{<} = D_{\text{ret}} (-i\Pi_{<}) D_{\text{adv}}. \quad (2.71)$$

We have derived this simple equation for scalar fields. In the derivation we never had to reverse the order of propagators. Thus our argument generalizes to propagators of fermions and vector bosons which are matrix values in the the spinor or Lorentz indices. For $D_{>} = D_{21}$ one gets similarly that

$$D_{>} = D_{\text{ret}} (-i\Pi_{>}) D_{\text{adv}} \quad (2.72)$$

where

$$\Pi_{>} = \Pi_{aa} - \frac{1}{2}\Pi_{\text{adv}} + \frac{1}{2}\Pi_{\text{ret}}. \quad (2.73)$$

We can write

$$\Pi_{\text{ret}} - \Pi_{\text{adv}} = \Pi_{>} - \Pi_{<} \quad (2.74)$$

In translationally invariant systems this becomes

$$2i\text{Im} \Pi_{\text{ret}} = \Pi_{>} - \Pi_{<}. \quad (2.75)$$

which has an intuitive explanation. $\Pi_{>}$ describes the annihilation rate and $\Pi_{<}$ the creation rate of quasi-particles [45]. The equation tells us that the decay width of a single quasi-particle is related to the difference in annihilation and creation rates.

In order to use eq. (2.71) to do actual computations we need a simpler expression for $\Pi_{<}$. It turns out that going in the 1/2 basis gives

$$\Pi_{<} = -\Pi_{12} \quad (2.76)$$

and

$$\Pi_{>} = -\Pi_{21} \quad (2.77)$$

To show this we must relate self-energies in the r/a and the 1/2 bases. One can easily check that

$$\begin{bmatrix} D_{rr} & D_{ra} \\ D_{ar} & D_{aa} \end{bmatrix} = A \begin{bmatrix} D_{11} & D_{12} \\ D_{21} & D_{22} \end{bmatrix} B \quad (2.78)$$

with

$$A = \begin{bmatrix} 1/2 & 1/2 \\ 1 & -1 \end{bmatrix}, \quad B = \begin{bmatrix} 1/2 & 1 \\ 1/2 & -1 \end{bmatrix}. \quad (2.79)$$

The same equation is valid for the free propagators. Thus

$$\begin{bmatrix} \Pi_{11} & \Pi_{12} \\ \Pi_{21} & \Pi_{22} \end{bmatrix} = B^{-1} \begin{bmatrix} \Pi_{rr} & \Pi_{ra} \\ \Pi_{ar} & \Pi_{aa} \end{bmatrix} A^{-1} \quad (2.80)$$

which gives the expressions we want for $\Pi_{<}$ and $\Pi_{>}$.

We note that the number of independent self-energy components is the same as for

the propagators. In general $\Pi_{rr} = 0$ leaving us with three components. Translational invariance reduces them to two. Finally in equilibrium the KMS condition $D_{<} = e^{-\beta p^0} D_{>}$ along with eq. (2.71) and (2.72) gives

$$\Pi_{<} = e^{-\beta p^0} \Pi_{>} \quad (2.81)$$

which reduces the number to one. This equation is just a description of detailed balance. It tells us that the annihilation and creation rates must balance out so that the occupation of a state is fixed.

To conclude this chapter we rewrite our equation for D_{rr} . The derivation relies on the propagators commuting and is thus only valid for scalar particles. Using eq. (2.64) and (2.63) we see that

$$D_{\text{ret}} - D_{\text{adv}} = 2(\text{Im } \Pi_{\text{ret}}) D_{\text{ret}} D_{\text{adv}} \quad (2.82)$$

Thus we can write eq. (2.71) as

$$D_{<} = \frac{\Pi_{<}}{2i \text{Im } \Pi_{\text{ret}}} (D_{\text{ret}} - D_{\text{adv}}) \quad (2.83)$$

or if we prefer

$$D_{<} = \frac{\Pi_{<}}{\Pi_{>} - \Pi_{<}} (D_{\text{ret}} - D_{\text{adv}}). \quad (2.84)$$

We have therefore shown that

$$D_{rr} = \left[\frac{1}{2} + \frac{\Pi_{<}}{\Pi_{>} - \Pi_{<}} \right] (D_{\text{ret}} - D_{\text{adv}}) \quad (2.85)$$

Using the KMS condition

$$\frac{\Pi_{<}}{\Pi_{>} - \Pi_{<}} \quad (2.86)$$

reduces to the Bose-Einstein distribution in thermal equilibrium as expected. In a non-equilibrium system $\Pi_{<}/(\Pi_{>} - \Pi_{<})$ has the interpretation of a resummed momentum distribution function. This can be seen by comparing eq. (2.85) with the free rr

Bare propagator	Quarks ($i\not{K} \times$)	Gluons ($-ig^{\mu\nu} \times$)
11	$\frac{1}{K^2+i\epsilon} + 2\pi i\delta(K^2) f_q(\mathbf{k})$	$\frac{1}{K^2+i\epsilon} - 2\pi i\delta(K^2) f_g(\mathbf{k})$
12	$2\pi i\delta(K^2) [-\theta(-k^0) + f_q(\mathbf{k})]$	$-2\pi i\delta(K^2) [\theta(-k^0) + f_g(\mathbf{k})]$
21	$2\pi i\delta(K^2) [-\theta(k^0) + f_q(\mathbf{k})]$	$-2\pi i\delta(K^2) [\theta(k^0) + f_g(\mathbf{k})]$
22	$\frac{-1}{K^2-i\epsilon} + 2\pi i\delta(K^2) f_q(\mathbf{k})$	$\frac{-1}{K^2-i\epsilon} - 2\pi i\delta(K^2) f_g(\mathbf{k})$
rr	$\left[\frac{1}{2} - f_q(\mathbf{k})\right] (-2\pi i)\delta(K^2)$	$\left[\frac{1}{2} + f_g(\mathbf{k})\right] (-2\pi i)\delta(K^2)$
ra	$\frac{1}{K^2+i\epsilon k^0}$	$\frac{1}{K^2+i\epsilon k^0}$
ar	$\frac{1}{K^2-i\epsilon k^0}$	$\frac{1}{K^2-i\epsilon k^0}$
aa	0	0

Table 2.1: List of propagators for quarks and gluons in the real time formalism. The first half is in the 1/2 basis and the second half in the r/a basis. Gluon propagators are in the Feynman gauge.

propagator. We emphasize that we only derived eq. (2.85) for scalar bosons. A substantial part of this thesis is devoted to generalizing this expression for fermions and vector bosons. We will calculate the resummed occupation density for hard quarks and soft gluons.

Bulk viscous corrections to two-to-two channels

Two-to-two scattering with a photon in the final state is one of the leading order channels for photon production in the QGP. In this chapter we calculate corrections to it due to bulk viscosity and explore their phenomenological importance. Our calculation shares similarities with the evaluation of photon emission from QGP in thermal equilibrium [21, 22] and the shear viscous correction that was calculated recently [39].

3.1 Photon emission from two-to-two scattering

The rate of photon production, R , in a unit volume is given by [60]

$$k \frac{dR}{d^3k} = \frac{i}{2(2\pi)^3} (\Pi_{12}^\gamma)^\mu{}_\mu \quad (3.1)$$

where \mathbf{k} is the photon momentum and $\Pi_{12}^{\gamma\mu\nu}$ is one component of the photon polarization tensor. This equation remains valid in an out-of-equilibrium QGP [60].

The simplest diagram corresponding to Π_{12}^γ is a single quark loop as in Fig. 3.1. This corresponds to a quark and antiquark annihilating into a photon. For on-shell photons this diagram vanishes because of kinematic constraints. Specifically, the

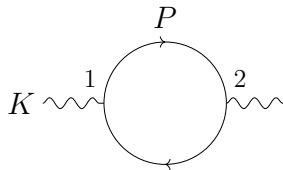


Figure 3.1: Hard quark loop. This diagram vanishes for on-shell photons.

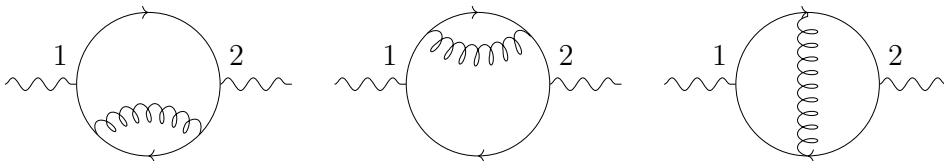


Figure 3.2: Leading order diagrams for photon production. The loop momentum is hard. The diagrams correspond to two-to-two scattering.

delta functions in the 12 propagators are such that $K^2 = P^2 = P \cdot K = 0$ which has vanishing phase space.

The leading order diagrams for on-shell photons have at least one gluon propagator and the rate is $\mathcal{O}(g^2 e^2)$. Some of these diagrams can be seen in Fig. 3.2. Using finite temperature cutting rules one can rewrite their contribution in terms of two-to-two scattering diagrams. This tedious calculation involves using the delta functions from propagators to change the integration variables [22, 61]. In the end one gets that

$$k \frac{dR}{d^3k} \Big|_{2\text{-to-}2} = \frac{1}{2(2\pi)^3} \sum_{\text{channels}} \int_P \int_{P'} \int_{K'} (2\pi)^4 \delta^{(4)}(P + P' - K - K') \quad (3.2)$$

$$\times |\mathcal{M}|^2 f(P) f(P') (1 \pm f(K')).$$

We use the short-hand $\int_P = \frac{1}{(2\pi)^3} \int \frac{d^3p}{2p^0}$ where $p^0 = p$ in the integral. \mathcal{M} is the amplitude for the two-to-two scattering diagrams in Fig. 3.3 evaluated in vacuum. f are momentum distribution functions that come from the original propagators. For the outgoing particle with momentum K' we must include Pauli blocking and Bose enhancement. Eq. (3.2) has the same form as the collision kernel in the Boltzmann equation for photons.

The t- and u-channel diagrams lead to infrared divergences in eq. (3.2). This can be traced back to our incorrect handling of the original loop diagrams. We assumed that the loop momentum was hard but the case of soft loop momentum is also leading order. In that case we must evaluate the loop diagrams in Fig. 3.4 directly using HTL resummed propagators for soft momenta. The infrared divergences are regulated because a quasi-particle acquires a mass through its interaction with the medium.

We must introduce a cut, q_{cut} , between the regimes with soft and hard quark loops.

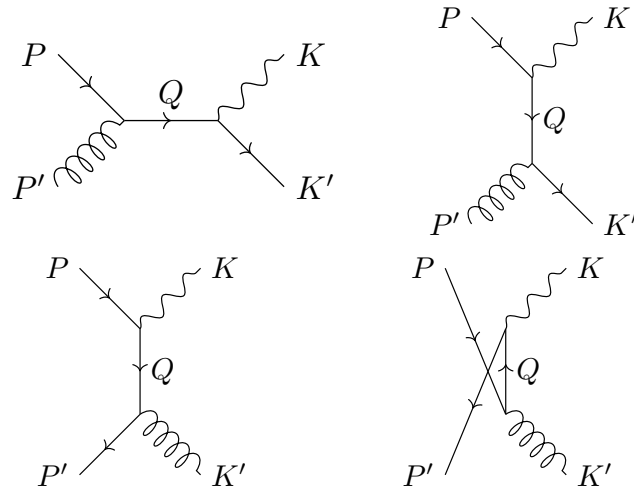


Figure 3.3: Two-to-two scattering diagrams that are obtained from cutting the loop diagrams in Fig. 3.2. The upper two are Coulomb scattering and the lower two are pair annihilation. In Coulomb scattering a gluon can scatter off a quark as shown here or off an antiquark (not shown).

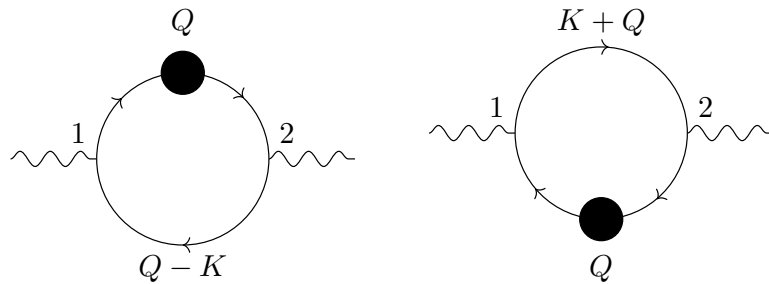


Figure 3.4: Leading order diagrams with soft loop momentum. Propagators with a soft momentum must be resummed.

The HTL approach in the soft regime is only valid for $q \sim gT \ll T$. To avoid infrared divergences in the hard regime we must have $q \sim T \gg gT$. Thus the cut must fulfill $gT \ll q_{\text{cut}} \ll T$. All final results should be independent of q_{cut} in that range.

Our calculation of the bulk viscous correction to these channels uses a momentum distribution that was derived in [38]. We explain the derivation briefly. Our starting point is the Boltzmann equation

$$k^\mu \partial_\mu f = \mathcal{C}[f]. \quad (3.3)$$

in which the left hand side corresponds to free streaming and the right hand side is the collision kernel. We write

$$f = f_{\text{eq}} + \delta f \quad (3.4)$$

where f_{eq} is an equilibrium distribution (Bose-Einstein or Fermi-Dirac) and $\delta f \ll f_{\text{eq}}$ is the non-equilibrium part. To lowest order

$$k^\mu \partial_\mu f_{\text{eq}} = \mathcal{C}[\delta f] \quad (3.5)$$

because $\mathcal{C}[f_{\text{eq}}]$ vanishes. The left hand side is evaluated explicitly and simplified using thermodynamic and hydrodynamic relations. In principle the collision kernel should be derived from QCD. Instead, we use the simpler relaxation time approximation

$$\mathcal{C}[\delta f] = -E \frac{\delta f}{\tau_R} \quad (3.6)$$

where τ_R characterizes how fast the system equilibrates. Assuming that all chemical potentials vanish one gets that δf is composed of a shear and a bulk viscous part.

One needs to be more careful about δf_{bulk} in QGP. For a conformal system where all masses are zero the bulk viscosity vanishes. Thus it is crucial to include particle masses. The physical masses quarks can be neglected but the thermal masses m_{th} of quarks and gluons are important. In [62] Jeon and Yaffe showed that the effective

kinetic theory for quasi-particles is

$$k^\mu \partial_\mu f - \frac{1}{2} \frac{\partial m_{\text{th}}^2}{\partial \mathbf{x}} \cdot \frac{\partial f}{\partial \mathbf{k}} = \mathcal{C}[f] \quad (3.7)$$

The thermal mass varies throughout the plasma with the temperature. These variations act as an external force.

Going through the same calculation using effective kinetic theory one finally gets that

$$\delta f_{\text{bulk}} = -f_{\text{eq}} (1 \pm f_{\text{eq}}) \left(\frac{m_{\text{th}}^2}{E} - E \right) \frac{\Pi}{15T(\epsilon + \mathcal{P})(\frac{1}{3} - c_s^2)} \quad (3.8)$$

where running of the coupling constant with temperature has been neglected. m_{th}^2 is a thermal mass of the quasi-particle and $E = \sqrt{p^2 + m_{\text{th}}^2}$. The bulk viscous pressure is $\Pi = -\zeta\theta$ and $\theta = \partial_\mu u^\mu$ is the expansion rate. Finally ϵ is energy density, \mathcal{P} is pressure and c_s is the speed of sound. The plus sign is for quarks and the minus sign for gluons.

Assuming that $\delta f_{\text{bulk}} \ll f_{\text{eq}}$ allows us to evaluate the correction to photon production to first order in δf . Then we can factor hydrodynamic variables out of integrals and separate the bulk and shear correction. In other words

$$k \frac{dR}{d^3k} = \Gamma_{\text{eq}} + \frac{\Pi}{15(\epsilon + \mathcal{P})(\frac{1}{3} - c_s^2)} \Gamma_{\text{bulk}} + \text{shear part.} \quad (3.9)$$

Our calculation amounts to evaluating Γ_{bulk} .

3.2 Evaluation of hard loop diagrams

Photon production through two-to-two in the hard loop momentum regime is given by eq. (3.2). We need to evaluate \mathcal{M} for the different channels in Fig. 3.3 and do the integrals numerically.

The first diagram in Fig. 3.3 with a quark or an antiquark contributes

$$\langle |\mathcal{M}|^2 \rangle = \mathcal{N} \frac{-u}{s}. \quad (3.10)$$

Similarly the second one gives

$$\langle |\mathcal{M}|^2 \rangle = \mathcal{N} \frac{-s}{t}. \quad (3.11)$$

and finally the last two pair annihilation channels give

$$\langle |\mathcal{M}|^2 \rangle = \mathcal{N} \frac{u}{t}. \quad (3.12)$$

Here we have summed over spin, flavour and colour of the initial and final particles.

We defined

$$\mathcal{N} = 16N_c C_F e^2 g^2 Q^2. \quad (3.13)$$

where $N_c = 3$ is the number of colours, $C_F = (N_c^2 - 1)/2N_c = 4/3$ is a colour factor (see Appendix A) and $Q^2 e^2 = \sum_s q_s^2$ where we sum the charge squared of quark flavours. Finally s , t and u are the usual Mandelstam variables defined as

$$\begin{aligned} s &= (P + P')^2 = (K + K')^2 \\ t &= (P - K)^2 = (P' - K')^2 \\ u &= (P' - K)^2 = (P - K')^2 \end{aligned} \quad (3.14)$$

They satisfy $s + t + u = 0$ assuming that all particles are massless and on shell [48, Chapter 5]. We can ignore the thermal masses to leading order in the hard loop diagrams.

We have to evaluate the integrals in eq. (3.2) numerically. Taking the delta function into account there are five independent integration variables. Choosing them cleverly we can do two of the integrals analytically, see [39, 7] for details. The integral over the t and u channels of eqs. (3.11) and (3.12) can then be written as

$$\begin{aligned} k \frac{dR}{d^3k} \Big|_{\text{hard}; t, u} &= \frac{\mathcal{N}}{16(2\pi)^7 k} \int_{q_{\text{cut}}}^{\infty} dq \int_{\max\{q-2k, -q\}}^q d\omega \int_{(q-\omega)/2}^{\infty} dp' \int_0^{2\pi} d\phi_{p'} \\ &\quad \times \frac{u-s}{t} f(\omega+k) f(p') (1 \pm f(\omega+p')) \end{aligned} \quad (3.15)$$

where the $\phi_{p'}$ integral can be performed analytically. Here ω is the time component of the exchanged momentum Q and $q = |\mathbf{q}|$. There is a cut in the q integral. $\phi_{p'}$ is the azimuthal angle of \mathbf{p}' in a coordinate frame where \mathbf{k} is in the z -direction and \mathbf{k} and \mathbf{q} span the xz plane. The Mandelstam variables in terms of these integration variables are

$$\begin{aligned} t &= \omega^2 - q^2 \\ u &= -2p'k(1 - \cos\theta_{kq}\cos\theta_{p'q} + \sin\theta_{kq}\sin\theta_{p'q}\cos\phi_{p'}) \\ s &= -t - u \end{aligned} \tag{3.16}$$

where

$$\cos\theta_{kq} = \frac{\omega^2 - q^2 + 2k\omega}{2kq} \tag{3.17}$$

and

$$\cos\theta_{p'q} = \frac{\omega^2 - q^2 + 2\omega p'}{2qp'}. \tag{3.18}$$

Eq. 3.15 can easily be expanded to first order in δf , see Appendix C. The final expression for the s channel which does not need a cutoff can also be seen there. The numerical integration was done using Gaussian quadrature.

3.3 Evaluation of soft loop diagrams

We now evaluate the diagrams in Fig. 3.4. They are

$$\begin{aligned} -i\Pi_{12\mu}^\mu \Big|_{\text{soft}} &= -e^2 Q^2 N_C \int \frac{d^4 Q}{(2\pi)^4} \text{Tr} \left[\gamma^\mu S_{21}(Q) \gamma_\mu S_{12}^0(Q+K) \right. \\ &\quad \left. + \gamma^\mu S_{21}^0(Q-K) \gamma_\mu S_{12}(Q) \right]. \end{aligned} \tag{3.19}$$

S^0 denotes a bare propagator and S is a HTL resummed propagator. When substituting in the bare propagators terms one gets

$$i\Pi_{12}^{\mu} \Big|_{\text{soft}} = -e^2 Q^2 N_C \frac{f_q(\mathbf{k})}{2k} \int \frac{d^4 Q}{(2\pi)^4} 2\pi \delta(q^0 - \mathbf{q} \cdot \hat{\mathbf{k}}) \times \text{Tr} \left[\gamma^{\mu} \{S_{12}(Q) - S_{21}(Q)\} \gamma_{\mu} \not{K} \right] \quad (3.20)$$

We have dropped terms with $\theta(q^0 - k^0)$ since $K \gg Q$. Furthermore we used that our momentum distribution is reflection symmetric, $f(-\mathbf{p}) = f(\mathbf{p})$, and that

$$\delta((Q - K)^2) \approx \delta((Q + K)^2) \approx \delta(2Q \cdot K) \approx \frac{1}{2k} \delta(q^0 - \mathbf{q} \cdot \hat{\mathbf{k}}) \quad (3.21)$$

We need to evaluate $S_{12} - S_{21}$. In Chapter 2 we showed that

$$S_{12} = S_{\text{ret}} (-i\Sigma_{<}) S_{\text{adv}}, \quad (3.22)$$

$$S_{21} = S_{\text{ret}} (-i\Sigma_{>}) S_{\text{adv}}, \quad (3.23)$$

and that in translationally invariant systems

$$\Sigma_{>} - \Sigma_{<} = 2i \text{Im} \Sigma_{\text{ret}}. \quad (3.24)$$

Thus

$$S_{21} - S_{12} = S_{\text{ret}} 2\text{Im} \Sigma_{\text{ret}} S_{\text{adv}} \quad (3.25)$$

This is a very convenient expression. The right hand side is entirely in terms of Σ_{ret} because $S_{\text{adv}} = -S_{\text{ret}}^*$ so we do not need to evaluate $\Sigma_{<}$ and $\Sigma_{>}$. The retarded HTL self-energy has been evaluated in non-equilibrium QGP in [63].

The trace in eq. (3.20) can now be written as

$$\begin{aligned} & \text{Tr} \left[\gamma^{\mu} S_{\text{ret}}(Q) \text{Im} \Sigma_{\text{ret}}(Q) S_{\text{adv}}(Q) \gamma_{\mu} \not{K} \right] \\ &= -\text{Tr} \left[\gamma^{\mu} \frac{1}{Q - \Sigma_{\text{ret}}} \text{Im} \Sigma_{\text{ret}}(Q) \frac{1}{Q - \Sigma_{\text{ret}}^*} \gamma_{\mu} \not{K} \right] \end{aligned} \quad (3.26)$$

A tedious exercise in γ algebra shows that this can be simplified considerably. Our final expression is

$$k \frac{dR}{d^3k} \Big|_{\text{soft}} = -\frac{8e^2 Q^2 N_C}{2(2\pi)^3} \frac{f_q(\mathbf{k})}{k} \int^{q_{\text{cut}}} \frac{d^3q}{(2\pi)^3} \text{Im} \frac{K \cdot (Q - \Sigma_{\text{ret}}(Q))}{(Q - \Sigma_{\text{ret}}(Q))^2} \Big|_{q^0=\mathbf{q}\cdot\hat{\mathbf{k}}} \quad (3.27)$$

Here

$$\Sigma_{\text{ret}}^\mu(Q) = C_F g^2 \int \frac{pdp}{2\pi^2} \frac{d\Omega_p}{4\pi} (f_q(\mathbf{p}) + f_g(\mathbf{p})) \frac{P^\mu}{P \cdot Q + i\epsilon} \Big|_{p^0=p}. \quad (3.28)$$

Inserting our momentum distribution and expanding up to first order gives some rather complicated expressions for $\Gamma_{\text{bulk}} \Big|_{\text{soft}}$ which must be evaluated numerically. See Appendix C for details.

3.4 Bulk viscous corrections in heavy-ion collisions

Γ_{bulk} only depends on the coupling constant g and k/T . We evaluated it numerically using the equations in Appendix C, including up, down and strange quarks which thermalize in heavy-ion collisions. The physical mass of these quarks is assumed to vanish.

We must first check that Γ_{bulk} is independent of the cut between hard and soft loops q_{cut} when $gT \ll q_{\text{cut}} \ll T$. For weak coupling there is indeed a wide range of values of q_{cut} that give nearly identical results, see Fig. 3.5. At realistic coupling strength, $g = 2$, Γ_{bulk} is highly dependent on q_{cut} . This was to be expected as $gT > T$ for such strong coupling. We chose the value of q_{cut} that minimizes Γ_{bulk} in analogy with the weak coupling result. This is roughly at $q_{\text{cut}} \approx \sqrt{g}$. In Fig. 3.6 we show how the bulk viscous correction at realistic coupling strength varies with k/T . The correction is exponentially suppressed at high photon energy like the thermal rate.

Our consistent calculation of Γ_{bulk} was rather involved. It is interesting to see whether one can make some approximations and still get a reasonably correct value. In [31] Dusling evaluated shear viscous corrections, making a number of simplifying assumptions. The paper assumes that the exchanged momentum in two-to-two scattering is soft so that the incoming particles are not deflected. It only uses equilibrium

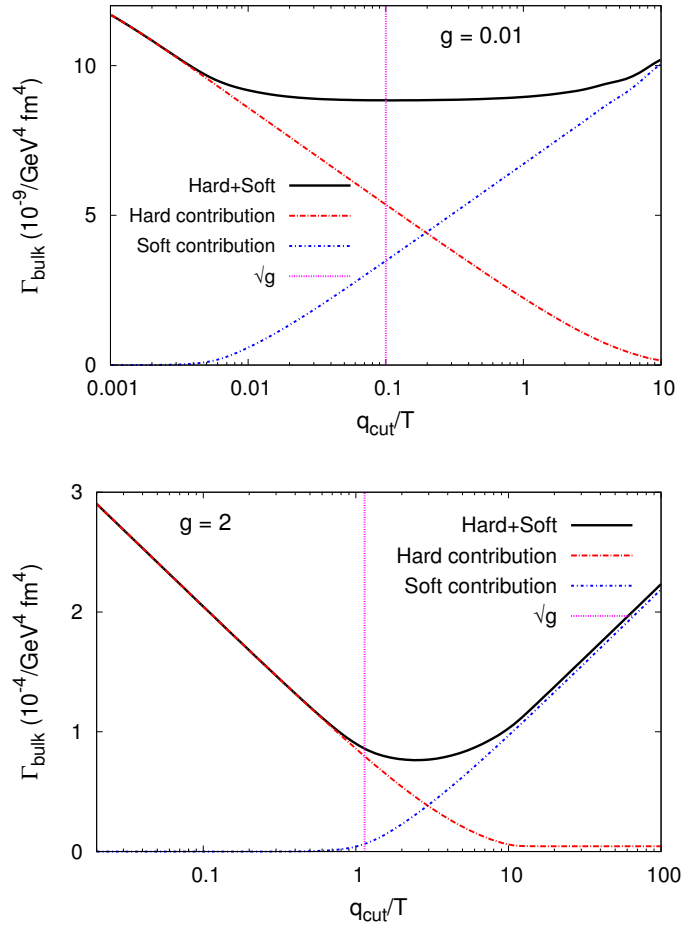


Figure 3.5: Dependence of Γ_{bulk} on q_{cut} at $k/T = 10$. q_{cut} is the cut between hard and soft momentum loops. The upper diagram is for $g = 0.01$. For such weak coupling there is a wide range of values of q_{cut} that give identical results. At realistic coupling strength, $g = 2$, like in the lower diagram the results are highly dependent on q_{cut} .

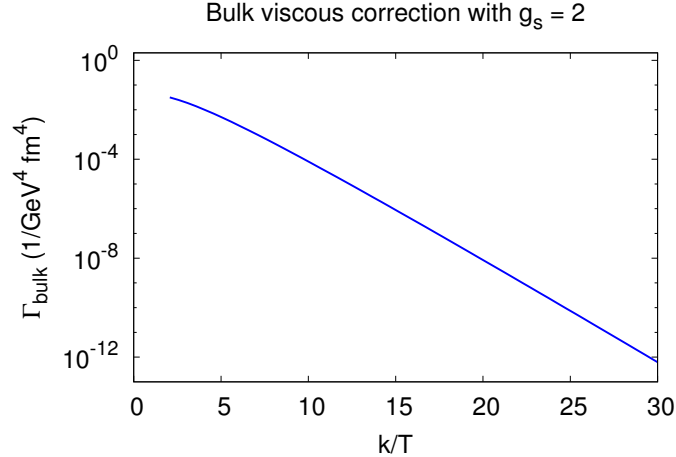


Figure 3.6: Γ_{bulk} at realistic coupling strength, $g = 2$, as a function of k/T .

HTL resummation for the soft mediator, neglecting δf corrections. Finally is neglects the δf correction to the outgoing particle. This gives a closed-form expression for the shear viscous correction. A similar calculation, which we refer to as the forward scattering approximation, can be made for the bulk viscosity.

In Fig. 3.7 we compare our full calculation and the forward scattering approximation. There is a big difference at low photon energies where the assumption of non-deflecting incoming particles breaks down. Even at higher energies there is a 20% difference suggesting that viscous corrections are important in the HTL scheme. In conclusion our consistent calculation is necessary for an accurate evaluation of Γ_{bulk} .

On its own Γ_{bulk} gives limited information about the importance of bulk viscous corrections in heavy-ion collisions. Since

$$k \frac{dR}{d^3k} = \Gamma_{\text{eq}} - \frac{\Pi}{15(\epsilon + \mathcal{P})(\frac{1}{3} - c_s^2)} \Gamma_{\text{bulk}} + \text{shear part.} \quad (3.29)$$

one needs to know hydrodynamical factors like Π and ϵ to ascertain the size of these corrections. In this aim we combined our calculation with hydrodynamical simulations of heavy-ion collisions.

We explain the hydrodynamical simulations used only briefly, see Chapter 1.2 for some background information. The initial conditions are provided by IP-Glasma [10].

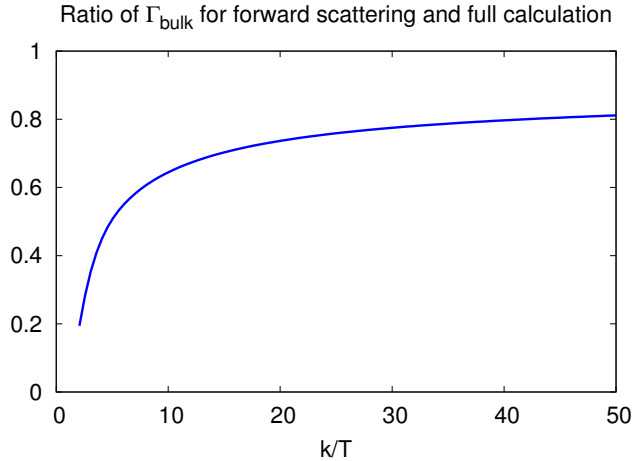


Figure 3.7: Ratio of Γ_{bulk} in the forward scattering approximation and our full calculation. Forward scattering refers to the approximations made in [31]. At low photon momentum the forward scattering approximation underestimates Γ_{bulk} severely. At higher momenta there is a 20% difference.

The initial medium is formed by soft gluons at high density that are sourced by hard particles in the nuclei. The gluonic fields are evolved according to the sourceless, classical Yang-Mills equation until the medium approaches thermodynamic equilibrium. At that point one switches to a hydrodynamic description. As the plasma expands it is driven away from equilibrium. At a temperature of $T = 105$ MeV we switch to a hadronic transport model [13].¹

For the hydrodynamic evolution we used MUSIC [11], a viscous hydrodynamic code in 3+1 dimensions. The shear viscosity is $\eta/s = 0.095$ and independent of temperature. This value was determined by fitting measurements of hadron correlations [18]. The bulk viscosity is temperature dependent and peaks around the crossover between the QGP and the hadronic phase, see Fig. 3.8. The form of $\zeta/s(T)$ was obtained by matching lattice data in the QGP phase [64] and from a hadronic resonance gas model in the hadronic phase [65]. Second order transport coefficients were determined in [66].

¹This switching temperature from hydrodynamics to transport models is lower than in most studies. It is chosen to include photons produced at low temperature in the hadronic phase [38]. A better approach might be to switch earlier to a hadronic transport model and include photon production through hadronic scattering. Unfortunately, the available codes for hadronic transport do not take electromagnetic probes into account.

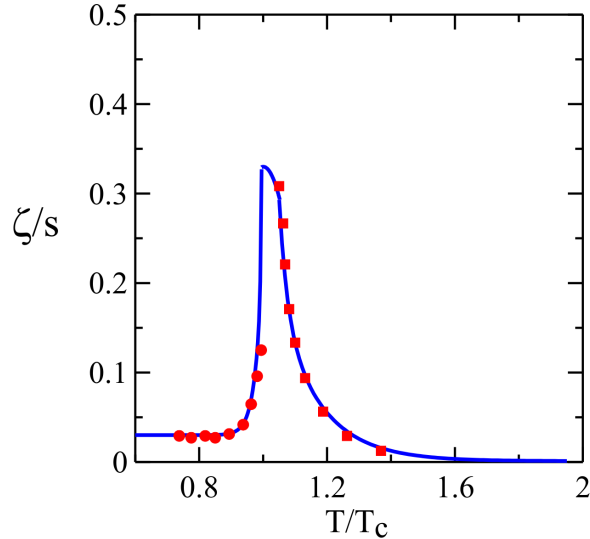


Figure 3.8: The temperature dependence of bulk viscosity used in our simulations. It peaks at the crossover between the hadronic and QGP phase at $T_c = 180$ MeV. The points come from [64] and [65].

All hydrodynamical events we present in this thesis are for Au-Au collisions at a center-of-mass energy 200 GeV per nucleon. The events are in the 0 – 40% centrality class.¹

We add photon production on top of the hydrodynamic evolution. Each fluid cell emits radiation by a rate R that depends on its hydrodynamic variables. Furthermore the flow of the cell, u^μ , can redshift or blueshift the radiation. The total number of photons emitted with momentum \mathbf{k} is

$$k \frac{dN_{\text{thermal}}}{d^3k} = \int d^4x \left[k \frac{dR}{d^3k} (T(x), E_k) \Big|_{k=K \cdot u(x)} \right]. \quad (3.30)$$

where the integral is over the space-time evolution of the hydrodynamic medium. Our calculation of kdR/d^3k was for an infinite medium with constant hydrodynamic variables. Eq. 3.30 is nevertheless a very good approximation because photon pro-

¹Centrality classes are a convenient way of binning collisions by the impact parameter. 0 – 40% refers to the 40% of events with the lowest impact parameter. This can be experimentally determined by measuring the hadronic yield of collisions.

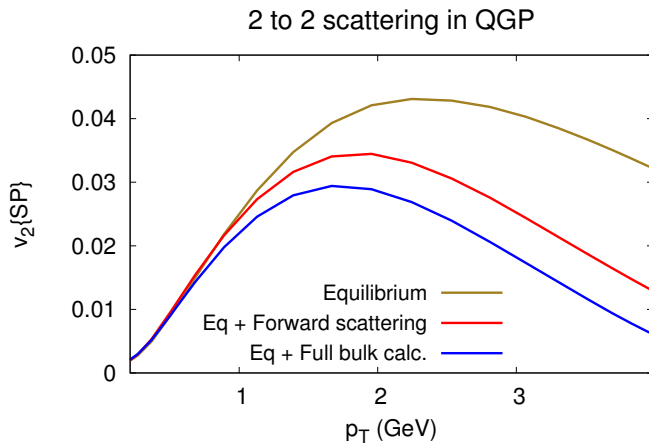


Figure 3.9: Elliptic flow of photons coming from two-to-two scattering in the QGP phase. The curves differ in how the bulk viscous correction is treated, whether it is absent (equilibrium) or evaluated using our full calculation or the forward scattering approximation. Shear viscous corrections are not included in this figure.

duction takes place on a scale that is much smaller than the macroscopic scale over which hydrodynamic quantities change.

The hydrodynamic evolution goes through both the QGP and the hadronic phase. In the QGP phase we use perturbative rates at $g = 2$. In the two-to-two scattering channels we include a shear viscous correction and our bulk correction. For quark bremsstrahlung, pair annihilation and the LPM effect we only have the equilibrium rate. Photon production in the hadronic phase is calculated using effective Lagrangians, see [38] for further details. We use QGP rates for $T > 180$ MeV and hadronic phase rates for $T < 180$ MeV. The results are only mildly dependent on the switching temperature between the phases. In addition we include radiation from the initial collisions of nuclei [38].

Let's first consider only photons coming from two-to-two scattering in the QGP phase. The differential yield of these photons, dN/dp_T , varies by many orders of magnitude while the bulk viscous correction only reduces it by 10 – 20%. The photon elliptic flow, $v_2(p_T)$,¹ is more sensitive to the correction as can be seen in Fig. 3.9 we

¹In experiments there are not enough statistics to calculate correlations of photons with photons so one calculates correlations of photons with hadrons. We do the same thing here using the scalar product method, see [38] for further details.

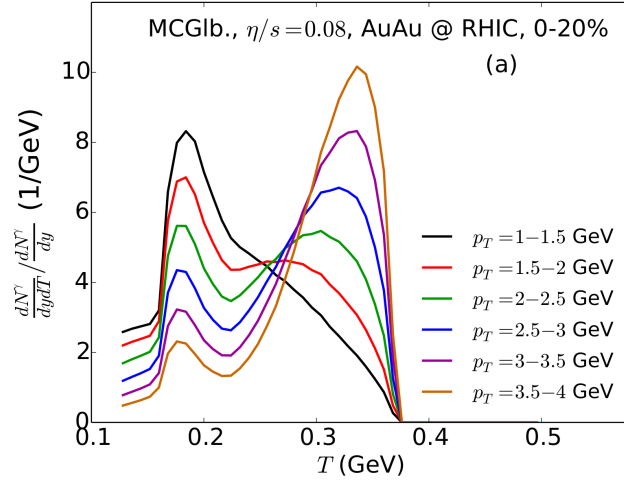


Figure 3.10: Yield of photons in different p_T bins by the temperature of the emitting cell. The figure is from a closely related study [67].

show $v_2(p_T)$ for photons from the two-to-two scattering channels. All the calculations are for the same underlying hydrodynamic events. We compare equilibrium radiation from two-to-two scattering to the case when bulk viscous correction are taken into account. The difference is small at low p_T but at higher p_T it is significant.

The bulk viscous correction to $v_2(p_T)$ can be understood intuitively. In Fig. 3.10 we show at which temperature photons with different p_T are emitted in a closely related study [67]. Photons at higher transverse momentum, $p_T \sim 3$ GeV, come from high temperature cells which have low flow but also from low temperature cells with high flow. Since bulk viscosity peaks at low temperature the bulk correction mostly affects these latter cells. Looking at eq. 3.9 we see that for an expanding medium, $\Pi = -\zeta\theta < 0$, the correction reduces the number of photons from these low temperature cells with high flow. This explains why the elliptic flow of photons is reduced. Our argument hinges on Γ_{bulk} being positive which is true because $\delta f_{\text{bulk}} < 0$ for an expanding medium.

We finally consider the effect of our bulk viscous correction to direct photons, i.e. photons in heavy-ion collisions that are not subtracted by experimentalists. In Fig. 3.11 we compare the elliptic flow of direct photons with and without our bulk

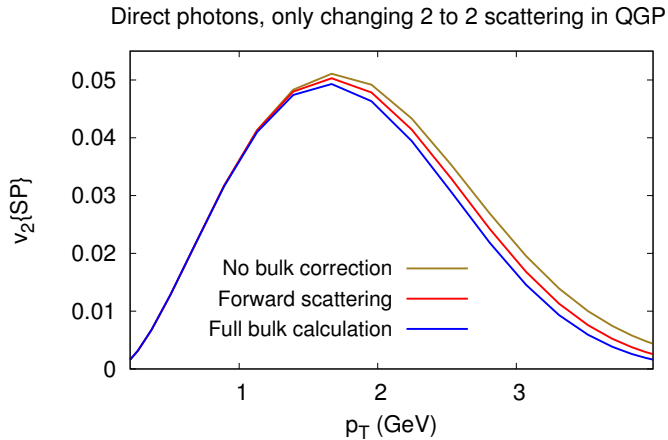


Figure 3.11: Elliptic flow of direct photons. The curves only differ in the treatment of the bulk viscous corrections to two-to-two scattering in the QGP phase.

viscous correction to two-to-two scattering in QGP. All other photon channels and all hydrodynamical events are kept the same in the comparison. The bulk correction of course reduces the elliptic flow. The reduction is substantial when bearing in mind that we are only changing one channel out of many.

We have seen that the bulk correction reduces both the yield and the elliptic flow of photons coming from two-to-two scattering in the QGP phase. Previous studies have shown that the shear correction to the same channel also reduces v_2 [38]. One would expect viscous corrections to other channels to reduce the elliptic flow even further. All of this suggest that the elliptic flow puzzle might be more serious than previously believed. Viscous corrections clearly do not solve the elliptic flow puzzle. However, once it is solved they will allow for the extraction of transport coefficients of the QGP from photonic observables, a worthy reward.

The resummed occupation density of soft gluons

In the next few chapters we will analyze photon production through bremsstrahlung and pair-annihilation in non-equilibrium QGP treating the LPM effect consistently. In this chapter we first review why these channels contribute at leading order in thermal equilibrium. We provide both a heuristic explanation and a more rigorous argument in the real-time formalism. We then evaluate the polarization tensor of soft gluons and show that they give the same enhancement in g in non-equilibrium QGP as in thermal equilibrium. Finally we derive a sum rule which facilitates the evaluation of the LPM effect in non-equilibrium QGP.

4.1 *Heuristics of the LPM effect*

Let's first see why the bremsstrahlung and pair-annihilation channels in Fig. 1.5 contribute at leading order. We focus on bremsstrahlung, following [25] and [23]. The momenta are defined as in Fig. 4.1. Naively the rate seems to go like $\mathcal{O}(e^2g^4)$ which is subdominant to the leading order $\mathcal{O}(e^2g^2)$. However, this does not apply in the leading order momentum regime where the gluon is soft, $Q \sim gT$, and the quarks are nearly on-shell, $P_1^2 = P_2^2 = L_1^2 = L_2^2 \sim g^2T^2$. Furthermore the photon is collinear to the quark emitting it, $\hat{\mathbf{k}} \cdot \hat{\mathbf{p}}_2 = 1 - \mathcal{O}(g)$. This is equivalent to $K \cdot P_2 \sim g^2T^2$ since the quark and photon are on shell.

Let's consider scalar QED and scalar QCD for simplicity. The square of the gluon propagator is $1/Q^4 \sim 1/g^4$. The square of the scalar quark propagator is

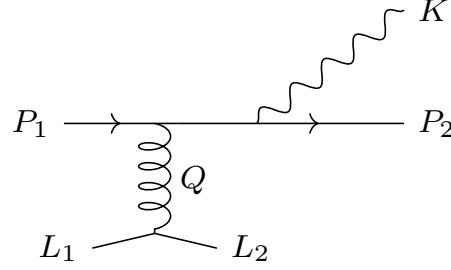


Figure 4.1: Definition of momenta in our analysis of bremsstrahlung.

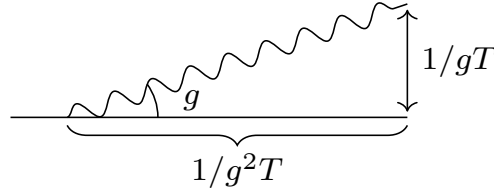


Figure 4.2: Length scales in the LPM effect.

$1/(P_2 + K)^4 \sim 1/g^4$. The photon vertex in scalar QED is

$$\epsilon \cdot (P_2 + K + P_2). \quad (4.1)$$

Choosing ϵ to be the physical polarization that has only spatial components orthogonal to \mathbf{k} we see that the vertex squared gives $\mathcal{O}(g^2 e^2)$. The gluon vertices squared are $\mathcal{O}(g^4)$. Finally there is a phase space suppression. To obtain the rate in thermal QGP we must integrate over $\mathbf{p}_1, \mathbf{p}_2, \mathbf{l}_1, \mathbf{l}_2$ with the correct momentum distribution. Only a part of the phase space complies with our kinematic restraints. Specifically $\mathbf{q} \sim g$ gives $\mathcal{O}(g^3)$ suppression and $\hat{\mathbf{k}} \cdot \hat{\mathbf{p}}_2 = 1 - \mathcal{O}(g)$ gives a $\mathcal{O}(g)$ suppression. Putting everything together we see that the rate goes like

$$\frac{1}{g^4} \times \frac{1}{g^4} \times g^2 e^2 \times g^4 \times g^4 = e^2 g^2 \quad (4.2)$$

which is leading order.

Let's now see why the LPM effect in bremsstrahlung matters at leading order, see Fig. 1.6. The creation of the photon is over when the wavepackets of the photon

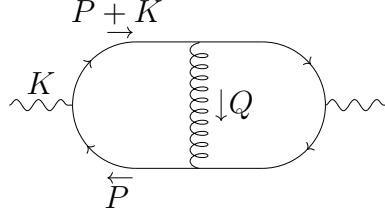


Figure 4.3: Definition of momenta in the argument for bremsstrahlung and pair annihilation contribution at leading order.

and the emitting quark are separated. The photon has momentum $\mathcal{O}(gT)$ transverse to the quark momentum. Thus its spatial extent in the transverse direction is $1/gT$. Furthermore the opening angle between the quark and photon is $\mathcal{O}(g)$. Simple trigonometry then shows that the quark and photon travel distance $1/g^2T$ before separating, see Fig. 4.2. During this time of $1/g^2T$ the quark can scatter arbitrarily often because the mean free time between soft scattering is $\mathcal{O}(1/g^2T)$ [58]. This repeated soft scattering must be taken into account at leading order.

4.2 Power counting of the LPM effect in thermal equilibrium

For actual calculations of photon production rate, R , one uses that

$$k \frac{dR}{d^3k} = \frac{i}{2(2\pi)^3} (\Pi_{12}^\gamma)^\mu{}_\mu \quad (4.3)$$

where \mathbf{k} is the photon momentum and $\Pi_{12}^{\gamma\mu\nu}$ is a component of the photon polarization tensor. The diagram corresponding to bremsstrahlung and pair annihilation is in Fig. 4.3. To include the LPM effect one must sum over all number of gluon rungs in the quark loop, see Fig. 4.4. Fig. 4.5 explains why this corresponds to the LPM effect.

Let's analyse the power counting in thermal equilibrium again but now using the actual diagrams that contribute to Π_{12}^γ . This will lay ground for our evaluation of them in Chapter 6. Furthermore we will see how to generalize the argument for a non-equilibrium QGP. Our discussion is based on [25].

We first consider Fig. 4.4. We have on-shell quarks, $P^2 \sim g^2T^2$, collinear emission of photons, $P \cdot K \sim g^2T^2$, and a soft gluon exchange, $Q \sim gT$. We do the analysis in

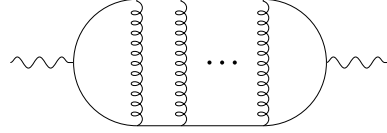


Figure 4.4: The diagrams for the LPM effect.

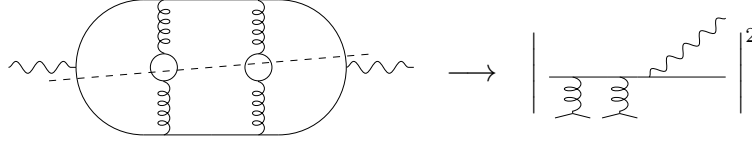


Figure 4.5: Explanation of why the diagram in Fig. 4.4 gives the rate for bremsstrahlung and the pair annihilation including the LPM effect. The gluon propagators are resummed explaining the quark loops. Cutting the diagram gives the amplitude squared.

the r/a basis in the real time formalism. For a soft gluon the rr propagator is

$$G_{rr} = \left(\frac{1}{2} + f_B(q^0) \right) [G_{\text{ret}} - G_{\text{adv}}] \sim \frac{1}{g^3} \quad (4.4)$$

where we get g^{-1} from the Bose-Einstein distribution, $f_B(q^0) \sim T/q^0$, and g^{-2} from the retarded and advanced propagators that go like $1/Q^2$. Since the gluon self-energy is also of order g^2 we must use resummed gluon propagators.

There is a pinching pole enhancement from the quark propagators. The distance between the poles of the two propagators in the complex p^0 plane is $\mathcal{O}(g^2T)$ giving a factor $1/g^2$. Let's for simplicity consider bare scalar propagators. The residue theorem gives that

$$\begin{aligned} & \int dp^0 S_{ar}(K+P)S_{ra}(P) \\ &= \int dp^0 \frac{1}{[(p^0 + i\epsilon)^2 - p^2][(p^0 + k - i\epsilon)^2 - |\mathbf{p} + \mathbf{k}|^2]} \\ &\sim \frac{1}{T^2} \times \frac{1}{p+k - |\mathbf{p} + \mathbf{k}|} \sim \frac{1}{g^2 T^3} \end{aligned} \quad (4.5)$$

when $\hat{\mathbf{p}} \cdot \hat{\mathbf{k}} = 1 - \mathcal{O}(g)$. The two pairs of quark propagators thus give a factor $1/g^4$. A correct calculation includes thermal masses and decay widths in the propagators because they are $\mathcal{O}(g^2)$. In other words, we must use resummed quark propagators.

The gluon vertices contribute g^2 and as we argued above the photon vertices give a factor g^2 when the quarks and photon are almost collinear. There is a g^3 phase space suppression from demanding that \mathbf{q} be soft, this forces q^0 to be soft as well. Furthermore there is a g^2 phase space suppression since \mathbf{p} is collinear to \mathbf{k} . P is automatically on shell because of the pinching poles. Bringing everything together we see that the diagram is of order $e^2 g^2$ as we expected.

Adding an additional gluon rung as in Fig. 4.4 gives a factor g^3 from the phase space suppression of the gluon momentum, g^{-3} from the gluon propagator, g^{-2} from the additional pinching poles and g^2 from the new vertices. Thus we can add arbitrarily many gluon rungs to the diagram at leading order. This gives rise to the LPM effect.

Most of the argument above hinges on kinematics and is thus equally valid in a non-equilibrium QGP. We used the properties of propagators in two crucial places. Firstly we must use resummed quark propagators when evaluating the pinching poles. We discuss resummed quark propagators in non-equilibrium QGP in Chapters 5 and 6. Secondly we need the resummed G_{rr} propagator for gluons which we derive in this chapter. The equilibrium argument above relied on an enhancement from the Bose-Einstein distribution in the resummed G_{rr} . It comes from the KMS condition which is only valid in equilibrium. In this chapter we show that one gets a similar enhancement in a non-equilibrium QGP.

4.3 The non-equilibrium retarded polarization tensor

We need to evaluate the resummed rr propagator in a non-equilibrium QGP. Using our results for scalar fields from Chapter 2 we expect it to be of the form

$$G_{rr} = \left[\frac{1}{2} + \frac{\Pi_{<}}{2i \text{Im} \Pi_{\text{ret}}} \right] (G_{\text{ret}} - G_{\text{adv}}). \quad (4.6)$$

However, the polarization tensors $\Pi_{<}^{\mu\nu}$ and $\text{Im} \Pi_{\text{ret}}^{\mu\nu}$ are matrices in the Lorentz indices making eq. (4.6) ambiguous. In the next few sections we derive the rr propagator for soft gluons. We show that the occupation number, which we can write schematically

as $\Pi_{<}/2i\text{Im}\Pi_{\text{ret}}$ is indeed of order $\mathcal{O}(g^{-1})$. This means that the LPM effect is also leading order in non-equilibrium systems.

To begin with we need to evaluate $\Pi_{<}^{\mu\nu}$ and $\text{Im}\Pi_{\text{ret}}$ using the hard thermal loop (HTL) scheme. In [63] Mrowczynski and Thoma showed that for reflection symmetric distribution functions, $f(-\mathbf{p}) = f(\mathbf{p})$,

$$\begin{aligned} \Pi_{\text{ret}}^{\mu\nu}(Q) = & -g^2 \int \frac{d^3p}{(2\pi)^3} \frac{f_{\text{tot}}(\mathbf{p})}{p} \\ & \times \frac{-(P^\mu Q^\nu + P^\nu Q^\mu)P \cdot Q + P^\mu P^\nu Q^2 + g^{\mu\nu}(P \cdot Q)^2}{(P \cdot Q + i\epsilon)^2} \Bigg|_{p^0=p} \end{aligned} \quad (4.7)$$

where

$$f_{\text{tot}} = 2N_f f_q + 2N_c f_g. \quad (4.8)$$

f_q and f_g are general quark and gluon momentum distributions. N_f is the number of flavours and N_c the number of colours.

There are two important things to note about eq. (4.7). Firstly $\Pi_{\text{ret}} = \mathcal{O}(g^2 T^2)$ and the leading contribution from the integral is when $P \sim T$. This confirms that the HTL scheme is valid for reasonable f_{tot} . Secondly it is easy to verify that the polarization tensor satisfies a Ward identity

$$Q_\mu \Pi_{\text{ret}}^{\mu\nu}(Q) = 0. \quad (4.9)$$

This is true even when the gluon is off shell.¹ This is different from vacuum where the Ward identity is only satisfied for on-shell gluons. The vacuum contribution after renormalization is suppressed relative to the thermal contribution and can be ignored. The Ward identity in eq. (4.9) will play a crucial role in our derivation of G_{rr} .

Before proceeding to $\Pi_{<}^{\mu\nu}$ we write eq. (4.7) in a more convenient form. For any

¹In the HTL scheme in thermal equilibrium there are in fact multiple Ward identities connecting an n-point function with the difference of two (n-1) point functions, see [56].

function $F(P)$

$$\int \frac{d^3 p}{(2\pi)^3} \frac{F(P)}{2p} \Big|_{p^0=p} = \int \frac{d^4 P}{(2\pi)^4} 2\pi\delta(P^2) \theta(p^0) F(P). \quad (4.10)$$

Thus

$$\begin{aligned} \Pi_{\text{ret}}^{\mu\nu}(Q) &= -2g^2 \int \frac{d^4 P}{(2\pi)^4} 2\pi\delta(P^2) \theta(p^0) f_{\text{tot}}(\mathbf{p}) \\ &\quad \times \frac{\partial}{\partial P^\omega} \left[P^\mu g^{\omega\nu} - \frac{Q^\omega P^\mu P^\nu}{P \cdot Q + i\epsilon} \right]. \end{aligned} \quad (4.11)$$

Integrating by parts leaves us with¹

$$\begin{aligned} \Pi_{\text{ret}}^{\mu\nu}(Q) &= -2g^2 \int \frac{d^4 P}{(2\pi)^4} 2\pi\delta(P^2) \theta(p^0) \left(\frac{\partial f_{\text{tot}}(\mathbf{p})}{\partial P^\omega} \right) \\ &\quad \times \left[-P^\mu g^{\omega\nu} + \frac{Q^\omega P^\mu P^\nu}{P \cdot Q + i\epsilon} \right] \end{aligned} \quad (4.12)$$

We interpret $\partial f_{\text{tot}}(\mathbf{p})/\partial P^0 = 0$ so that the sum over ω only needs to go over spatial indices. Then

$$2i \text{Im} \Pi_{\text{ret}}^{\mu\nu}(Q) = ig^2 \int \frac{d^3 p}{(2\pi)^3} \frac{P^\mu P^\nu}{p} q^i \left(\frac{\partial f_{\text{tot}}(\mathbf{p})}{\partial p^i} \right) 2\pi\delta(P \cdot Q) \Big|_{p^0=p} \quad (4.13)$$

4.4 Evaluation of the non-equilibrium Π_{12}

We now turn our attention to $\Pi_{<}^{\mu\nu} = -\Pi_{12}^{\mu\nu}$ for soft gluons. To entertain the reader we present a derivation in the Feynman gauge. The relevant Feynman diagrams can

¹One can see that the derivative of the delta function does not contribute after contracting it with the square bracket. The derivative of the theta function vanishes as long as for small p $f_{\text{tot}}(\mathbf{p}) \sim p^A$ with $A > -2$. This is true for all relevant momentum distributions we are aware of.

be seen in Fig. 4.6. The quark loop is

$$\begin{aligned}
& -i\Pi_{12\ AB}^{\mu\nu}(Q) \Big|_{\text{quark loop}} \\
&= -N_f \int \frac{d^4 P}{(2\pi)^4} \text{Tr} \left[(ig\gamma^\mu) t_{cd}^A S_{12}(P) (-ig\gamma^\nu) t_{dc}^B S_{21}(K) \right] \\
&= g^2 \delta^{AB} \frac{N_f}{2} \int \frac{d^4 P}{(2\pi)^4} \text{Tr} \left[\gamma^\mu \not{P} \gamma^\nu \not{K} \right] \tilde{\Delta}_{12}(P) \tilde{\Delta}_{21}(K) \\
&= 2g^2 \delta^{AB} N_f \int \frac{d^4 P}{(2\pi)^4} (P^\mu K^\nu + K^\mu P^\mu - g^{\mu\nu} P \cdot K) \tilde{\Delta}_{12}(P) \tilde{\Delta}_{21}(K)
\end{aligned} \tag{4.14}$$

Here $K = P - Q$. A and B are colour indices of the gluon and a and b are colour indices of the quark. See Appendix A for evaluation of colour factors and [48] for traces of gamma matrices. There is an overall minus sign because of the fermion loop. For convenience we have defined $\tilde{\Delta}_{12}$ by

$$S_{12}(P) = i\not{P} \tilde{\Delta}_{12}(P). \tag{4.15}$$

Substituting $\tilde{\Delta}_{12}$ and $\tilde{\Delta}_{21}$ we get

$$\begin{aligned}
\Pi_{12}^{\mu\nu}(Q) \Big|_{\text{quark loop}} &= 2iN_f g^2 \int \frac{d^4 P}{(2\pi)^4} (P^\mu K^\nu + K^\mu P^\mu - g^{\mu\nu} P \cdot K) \\
&\quad \times 2\pi i \delta(P^2) \left[f_q(\mathbf{p}) \theta(p^0) + (f_q(\mathbf{p}) - 1) \theta(-p^0) \right] \\
&\quad \times 2\pi i \delta(K^2) \left[(f_q(\mathbf{k}) - 1) \theta(k^0) + f_q(\mathbf{k}) \theta(-k^0) \right]
\end{aligned} \tag{4.16}$$

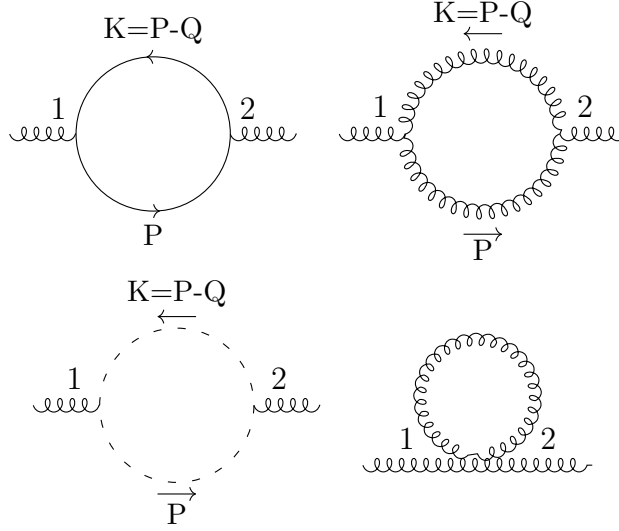
where we have omitted the colour factors.

In Chapter 6 we'll discover that we only need spacelike gluon momenta. In that case some terms can be dropped. Specifically

$$\delta(P^2) \theta(p^0) \delta(K^2) \theta(-k^0) \sim \delta(p^0 - p) \delta(k^0 + k) \tag{4.17}$$

and by using the triangular inequality we see that this only contributes when

$$q^0 = p^0 - k^0 = |\mathbf{p}| + |\mathbf{p} - \mathbf{q}| = |\mathbf{p}| + |\mathbf{q} - \mathbf{p}| \geq |\mathbf{q}|, \tag{4.18}$$

Figure 4.6: Diagrams contributing to Π_{12} .

Similarly the term with $\theta(-p^0)\theta(k^0)$ does not contribute. By doing the change of variables $P \rightarrow Q - P = -K$ in the term with $\theta(-p^0)\theta(-k^0)$ we get

$$\begin{aligned} \Pi_{12}^{\mu\nu}(Q) \Big|_{\text{quark loop}} &= 2ig^2 N_f \int \frac{d^4 P}{(2\pi)^2} \frac{P^\mu K^\nu + K^\mu P^\nu - g^{\mu\nu} P \cdot K}{4|\mathbf{p}| |\mathbf{k}|} \\ &\quad \times 2f_q(\mathbf{p}) (1 - f_q(\mathbf{k})) \delta(p^0 - |\mathbf{p}|) \delta(k^0 - |\mathbf{k}|) \end{aligned} \quad (4.19)$$

where we used that $f_q(\mathbf{p}) = f_q(-\mathbf{p})$.

We now use the assumption that Q is soft. Then $Q \ll P$ allowing us to approximate $K \approx P$ everywhere except in $\delta(k^0 - |\mathbf{k}|)$. Expanding to lowest order in Q it's easy to see that

$$\delta(k^0 - |\mathbf{k}|) = \delta\left(\frac{\mathbf{p} \cdot \mathbf{q}}{p} - q^0\right) = p \delta(P \cdot Q) \quad (4.20)$$

where $p^0 = p$. Our final expression for the quark loop is

$$\begin{aligned} \Pi_{12}^{\mu\nu}(Q) \Big|_{\text{quark loop}} &= ig^2 N_f \int \frac{d^3 p}{(2\pi)^3} \frac{P^\mu P^\nu}{p} 2\pi \delta(P \cdot K) 2f_q(\mathbf{p}) (1 - f_q(\mathbf{p})) \Big|_{p^0=p} \end{aligned} \quad (4.21)$$

We now turn to the other diagrams. The tadpole diagram vanishes because the

vertex must be both of type 1 and 2. The gluon loop diagram gives

$$\begin{aligned}
-i\Pi_{12\ AD}^{\mu\omega}(Q) \Big|_{\text{gluon loop}} &= \frac{1}{2} \int \frac{d^4P}{(2\pi)^4} (-i\Delta_{12}(P)) (-i\Delta_{21}(K)) (-g^2) \\
&\times [g^{\mu\nu} (Q - K)^\rho + g^{\nu\rho} (K + P)^\mu + g^{\rho\mu} (-P - Q)^\nu] f^{ABC} \\
&\times [g^{\omega\nu} (-Q + K)^\rho + g^{\nu\rho} (-K - P)^\omega + g^{\rho\omega} (P + Q)^\nu] f^{DBC}
\end{aligned} \tag{4.22}$$

Here Δ_{12} and Δ_{21} are defined by

$$G_{12}^{\mu\nu} = -ig^{\mu\nu} \Delta_{12}. \tag{4.23}$$

See Appendix A for the colour factors.

The ghost loop diagram is

$$\begin{aligned}
-i\Pi_{12\ AB}^{\mu\nu}(Q) \Big|_{\text{ghost loop}} &= - \int \frac{d^4P}{(2\pi)^4} (-gf^{CAD} P^\mu) i\Delta_{12}(P) (gf^{DBC} K^\nu) i\Delta_{21}(K)
\end{aligned} \tag{4.24}$$

There is an overall minus sign because of the ghost loop. We have used that the ghost propagators are

$$i\Delta(P) \tag{4.25}$$

where Δ is the same as for gluons. In other words the momentum distribution of the unphysical ghosts is the same as that of gluons, see [68] for a derivation. Making the change of variables $P \rightarrow Q - P = -K$ and using that $\Delta_{12}(-P) = \Delta_{21}(P)$ one gets

$$\begin{aligned}
\Pi_{12\ AB}^{\mu\nu}(Q) \Big|_{\text{ghost loop}} &= \frac{iN_c g^2}{2} \int \frac{d^4P}{(2\pi)^4} (P^\mu K^\nu + K^\mu P^\nu) \Delta_{12}(P) \Delta_{21}(K)
\end{aligned} \tag{4.26}$$

which is explicitly symmetric in the Lorentz indices.

The integrals in eqs. (4.22) and (4.26) can be evaluated in the same way as the

quark loop integral. The final result for the full gluon polarization tensor is

$$\begin{aligned} \Pi_{<}^{\mu\nu}(Q) &= -ig^2 \int \frac{d^3p}{(2\pi)^3} \frac{P^\mu P^\nu}{p} 2\pi\delta(P \cdot Q) \Big|_{p^0=p} \\ &\times [2N_f f_q(\mathbf{p})(1 - f_q(\mathbf{p})) + 2N_c f_g(\mathbf{p})(1 + f_g(\mathbf{p}))]. \end{aligned} \quad (4.27)$$

This equation can also be seen in [58] but the authors do not provide a derivation. We remind the reader that this equation is valid for soft, spacelike gluons and reflection symmetric momentum distributions. This component of the polarization tensor also obeys a Ward identity, $Q_\mu \Pi_{<}^{\mu\nu}(Q) = 0$.

Eq. (4.27) has an intuitive explanation. $\Pi_{<} = -\Pi_{12}$ corresponds to the creation of soft gluons. They are sourced by hard quarks and gluons with momentum P . The delta function forces the soft gluon to be spacelike. The factor $f_q(1 - f_q)$ corresponds to the momentum distribution of the incoming and outgoing hard quark. It includes Pauli blocking. Similarly $f_g(1 + f_g)$ corresponds to the hard gluon emitting the soft gluon.

A crucial thing to note is that $\Pi_{<}^{\mu\nu} \sim \mathcal{O}(gT^2)$ because of enhancement from $\delta(P \cdot Q)$ while $\Pi_{\text{ret}}^{\mu\nu} \sim \mathcal{O}(g^2T^2)$. Thus

$$\frac{\Pi_{<}}{2i\text{Im} \Pi_{\text{ret}}} \sim g^{-1}. \quad (4.28)$$

showing that soft gluons give the same enhancement in the LPM effect in non-equilibrium QGP as in thermal equilibrium. We will elaborate this point in the next section.

A critical reader might question the different power structure of $\Pi_{<}$ and Π_{ret} . The Feynman diagrams are the same in both cases, as is the power structure of vertices. The propagators are of course different but it's easy to see that they lead to the same enhancement in g . Why should the final result then be different for $\Pi_{<}$ and Π_{ret} ?

The answer is as follows: Let Q be the soft external momentum and P the hard loop momentum. The vertices lead to factors

$$P^\mu P^\nu \quad (4.29)$$

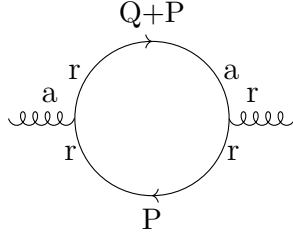


Figure 4.7: One of the diagrams contributing to $\Pi_{\text{ret}} = \Pi_{ar}$

which give $\mathcal{O}(gT^2)$ contributions to Π and factors

$$P^\mu Q^\nu + Q^\mu P^\nu, \quad g^{\mu\nu} P \cdot Q \quad (4.30)$$

which give $\mathcal{O}(g^2T^2)$ contributions. It turns out that all factors of the first kind cancel when evaluating Π_{ret} making the leading order contribution $\mathcal{O}(g^2T^2)$. This cancellation does not take place for $\Pi_{<}$ so the leading order is $\mathcal{O}(gT^2)$.

Let's look more closely at why this cancellation takes place for Π_{ret} . One of the Feynman diagrams can be seen in Fig. 4.7. The leading order part of the integral goes like

$$\begin{aligned} & \int d^4P \frac{P^\mu P^\nu \delta(P^2)}{(Q+P)^2 + i\epsilon(q^0 + p^0)} \\ & \sim \int d^3p \frac{P^\mu P^\nu}{2q^0 p^0 - 2\mathbf{p} \cdot \mathbf{q} + i\epsilon p^0} \Big|_{p^0=p} \\ & + \int d^3p \frac{P^\mu P^\nu}{2q^0 p^0 - 2\mathbf{p} \cdot \mathbf{q} + i\epsilon p^0} \Big|_{p^0=-p} \end{aligned} \quad (4.31)$$

The delta function comes from the rr propagator and the denominator comes from the ra propagator. By making the change of variables $\mathbf{p} \rightarrow -\mathbf{p}$ in the last integral it's easy to see that the two terms cancel. This cancellation does not take place if $P^\mu P^\nu$ is replaced by $P^\mu Q^\nu + Q^\mu P^\nu$ or $g^{\mu\nu} P \cdot Q$.

4.5 The resummed rr propagator for soft gluons

We now evaluate the resummed rr propagator for soft gluons. Just as in the case of scalar fields we have that

$$G_{rr} = \frac{1}{2} (G_{\text{ret}} - G_{\text{adv}}) + G_{<} \quad (4.32)$$

where

$$G_{<} = G_{\text{ret}} (-i\Pi_{<}) G_{\text{adv}}. \quad (4.33)$$

The propagators and self-energies are all matrices in the Lorentz indices. We want to derive an expression of the form $G_{<} \sim G_{\text{ret}} - G_{\text{adv}}$ which boils down to interchanging the order of G_{ret} and $\Pi_{<}$ in eq. (4.33). We must analyze their tensor structure more closely.

Let's first consider the polarization tensors, $\Pi^{\mu\nu}(Q)$. The material that follows is quite standard, see e.g. [44, chapter 5.4]. In vacuum $\Pi^{\mu\nu}(Q)$ can only depend on two tensors, Q^μ and the flat metric tensor $g^{\mu\nu}$. In thermal equilibrium we also have the four-velocity of the thermal medium, u^μ . In this thesis we consider a general isotropic momentum distribution, $f(p)$. Then $f(q)$ does not contain any factors of the form $\mathbf{q} \cdot \mathbf{A}$ so the only tensors in $\Pi(Q)$ are u^μ , Q^μ and $g^{\mu\nu}$. Having more tensors only introduce technical complications. (See [69] for retarded propagators in an anisotropic plasma.)

Let $\Pi^{\mu\nu}$ be any of the components of the polarization tensor for soft gluons. Since Π is symmetric in its Lorentz indices it can only depend on

$$g^{\mu\nu}, \quad u^\mu u^\nu, \quad Q^\mu Q^\nu, \quad u^\mu Q^\nu + Q^\mu u^\nu \quad (4.34)$$

We have shown that in the HTL scheme we have a Ward identity

$$Q_\mu \Pi^{\mu\nu}(Q) = 0. \quad (4.35)$$

Contracting the tensors above with Q_μ gives

$$Q^\nu, \quad Q \cdot u u^\nu, \quad Q^2 Q^\mu, \quad Q \cdot u Q^\nu + Q^2 u^\nu \quad (4.36)$$

The Ward identity gives us two constraints on the tensor structure of Π . We are then left with two tensors that Π can depend on. It is convenient to write

$$\Pi^{\mu\nu} = \Pi_T P_T^{\mu\nu} + \Pi_L P_L^{\mu\nu}, \quad (4.37)$$

where Π_T and Π_L are scalars. In the frame where $u = (1, 0, 0, 0)$

$$\begin{aligned} P_T^{00} &= P_T^{0i} = P_T^{i0} = 0 \\ P_T^{ij} &= \delta^{ij} - \frac{q^i q^j}{\mathbf{q}^2} \\ P_L^{\mu\nu} &= \frac{Q^\mu Q^\nu}{Q^2} - g^{\mu\nu} - P_T^{\mu\nu} \end{aligned} \quad (4.38)$$

It's easy to check that

$$\begin{aligned} P_L^2 &= -P_L \\ P_T^2 &= -P_T \\ P_L P_T &= P_T P_L = 0 \\ Q_\mu P_T^{\mu\nu} &= Q_\mu P_L^{\mu\nu} = 0 \end{aligned} \quad (4.39)$$

As an example the first equation means that $P_T^{\mu\nu} P_{T\nu\omega} = -P_{T\omega}^\mu$. The equation $P_T^{ij} q_j = 0$ shows that P_T corresponds to transversely polarized degrees of freedom relative to the three-momentum \mathbf{q} . On the other hand $P_L^{ij} q_j \sim q^i$ so P_L describes longitudinal degrees of freedom.

Let's derive the resummed retarded propagator in the Feynman gauge. To simplify the notation we write $\Pi = \Pi_{\text{ret}}$ from now on. We can write the bare propagator as

$G_{\text{ret}}^0 = \tilde{G}_{\text{ret}}^0 g$ where g is the metric. From

$$(1 - G_{\text{ret}}^0 (-i\Pi)) G_{\text{ret}} = G_{\text{ret}}^0 \quad (4.40)$$

we see that

$$\begin{aligned} G_{\text{ret}} &= \tilde{G}_{\text{ret}}^0 \left[1 - \tilde{G}_{\text{ret}}^0 g (-i\Pi_T P_T - i\Pi_L P_L) \right]^{-1} g \\ &= \tilde{G}_{\text{ret}}^0 \sum_{n=0}^{\infty} \left(\tilde{G}_{\text{ret}}^0 \right)^n (-i\Pi_T P_T - i\Pi_L P_L)^n g \\ &= \tilde{G}_{\text{ret}}^0 \left[g - \sum_{n=1}^{\infty} \left(i\Pi_T \tilde{G}_{\text{ret}}^0 \right)^n P_T - \sum_{n=1}^{\infty} \left(i\Pi_L \tilde{G}_{\text{ret}}^0 \right)^n P_L \right] \\ &= \tilde{G}_{\text{ret}}^0 \left[g + P_T + P_L - \frac{P_T}{1 - i\Pi_T \tilde{G}_{\text{ret}}^0} - \frac{P_L}{1 - i\Pi_L \tilde{G}_{\text{ret}}^0} \right] \\ &= \frac{-iQ^\mu Q^\nu}{Q^2 Q^2} + \frac{iP_T}{Q^2 - \Pi_T} + \frac{iP_L}{Q^2 - \Pi_L}. \end{aligned} \quad (4.41)$$

Here we used that $\tilde{G}_{\text{ret}}^0 = -i/Q^2$. The propagator is a sum of transversal and longitudinal propagators with different self-energies. There is also a term corresponding to our choice of gauges. We have omitted the $i\epsilon$ prescription in \tilde{G}_{ret}^0 because we assume that the quasi-particles have a finite life-time, $\text{Im } \Pi_T \neq 0$, $\text{Im } \Pi_L \neq 0$.

We can now move from these well known considerations to our calculation of the resummed rr propagator. Using eq. (4.33) and $G_{\text{adv}} = -G_{\text{ret}}^*$ we get that

$$\begin{aligned} G_{<} &= \left[\frac{-iQ^\mu Q^\nu}{Q^2 Q^2} + \frac{iP_T}{Q^2 - \Pi_T} + \frac{iP_L}{Q^2 - \Pi_L} \right] [-i\Pi_T^< P_T - i\Pi_L^< P_L] \\ &\quad \times \left[\frac{-iQ^\mu Q^\nu}{Q^2 Q^2} + \frac{iP_T}{Q^2 - \Pi_T^*} + \frac{iP_L}{Q^2 - \Pi_L^*} \right] \\ &= \frac{i\Pi_T^< P_T}{(Q^2 - \text{Re } \Pi_T)^2 + (\text{Im } \Pi_T)^2} + \frac{i\Pi_L^< P_L}{(Q^2 - \text{Re } \Pi_L)^2 + (\text{Im } \Pi_L)^2} \end{aligned} \quad (4.42)$$

Similarly

$$\begin{aligned} G_{\text{ret}} - G_{\text{adv}} &= \\ &= \frac{-2\text{Im } \Pi_T P_T}{(Q^2 - \text{Re } \Pi_T)^2 + (\text{Im } \Pi_T)^2} + \frac{-2\text{Im } \Pi_L P_L}{(Q^2 - \text{Re } \Pi_L)^2 + (\text{Im } \Pi_L)^2}. \end{aligned} \quad (4.43)$$

Therefore

$$G_{rr} = \left[\frac{1}{2} - \frac{\Pi_T^<}{2i\text{Im } \Pi_T} P_T - \frac{\Pi_L^<}{2i\text{Im } \Pi_L} P_L \right] (G_{\text{ret}} - G_{\text{adv}}) \quad (4.44)$$

This is similar to the scalar field case except we must consider transversal and longitudinal modes separately.

To finish the derivation we calculate

$$\frac{\Pi_{<}^T}{2i\text{Im } \Pi_{\text{ret}}^T}, \quad \frac{\Pi_{<}^L}{2i\text{Im } \Pi_{\text{ret}}^L} \quad (4.45)$$

from eqs. (4.13) and (4.27). To get Π_L one uses that $\Pi^{00} = \frac{\mathbf{q}^2}{Q^2} \Pi_L$. In our case $\Pi_{<}^\mu{}_\mu = 0$ and $\text{Im } \Pi_{<}^\mu{}_\mu = 0$ so $\Pi_{<}^\mu{}_\mu = -2\Pi_T - \Pi_L$ gives that $\Pi_T^< = -\frac{1}{2}\Pi_L^<$ and similarly for $\text{Im } \Pi_{\text{ret}}$. Thus we only need to evaluate Π^{00} . We have

$$\begin{aligned} & 2i \text{Im } \Pi_{\text{ret}}^{00}(Q) \\ &= ig^2 \int \frac{d^3p}{(2\pi)^3} pq^i \left(\frac{\partial f_{\text{tot}}}{\partial p^i} \right) 2\pi \delta(P \cdot Q) \Big|_{p^0=p} \\ &= ig^2 \int \frac{d^3p}{(2\pi)^3} \mathbf{p} \cdot \mathbf{q} \left(\frac{\partial f_{\text{tot}}}{\partial p} \right) 2\pi \delta(pq^0 - \mathbf{p} \cdot \mathbf{q}) \\ &= ig^2 q^0 \int_{-1}^1 \frac{d(\cos \theta)}{2\pi} \int_0^\infty dp p^3 \left(\frac{\partial f_{\text{tot}}}{\partial p} \right) \delta(pq^0 - pq \cos \theta) \\ &= ig^2 q^0 \frac{1}{2\pi} \int_0^\infty dp p^2 \left(\frac{\partial f_{\text{tot}}}{\partial p} \right) \end{aligned} \quad (4.46)$$

θ is the angle between \mathbf{q} and \mathbf{p} . We are only interested in spacelike gluons so the delta function always contributes. Similarly

$$\Pi_{<}^{00}(Q) = -ig^2 \frac{1}{2\pi} \int_0^\infty dp p^2 [2N_f f_q(1 - f_q) + 2N_c f_g(1 + f_g)] \quad (4.47)$$

Bringing all our calculations together and defining $y = p/T$ we get that

$$\frac{\Pi_T^<}{2i\text{Im } \Pi_T} = \frac{\Pi_L^<}{2i\text{Im } \Pi_L} = \Omega \frac{T}{q^0} \quad (4.48)$$

where

$$\Omega = \frac{-\int_0^\infty dy y^2 \frac{d}{dy} [2N_f f_q + 2N_c f_g]}{\int_0^\infty dy y^2 [2N_f f_q(1 - f_q) + 2N_c f_g(1 + f_g)]} \quad (4.49)$$

Finally we can write a simple expression for the rr propagator. We drop the factor $1/2$ which does not contribute at leading order. We are then left with

$$\begin{aligned} G_{rr}^{\mu\nu} &\approx \Omega \frac{T}{q^0} (-P_T - P_L)^{\mu\chi} (G_{\text{ret}} - G_{\text{adv}})^{\chi\nu} \\ &= \Omega \frac{T}{q^0} \left(g^{\mu\chi} - \frac{Q^\mu Q^\chi}{Q^2} \right) (G_{\text{ret}} - G_{\text{adv}})^{\chi\nu} \\ &= \Omega \frac{T}{q^0} (G_{\text{ret}} - G_{\text{adv}})^{\mu\nu} \end{aligned} \quad (4.50)$$

i.e.

$$G_{rr} \approx \Omega \frac{T}{q^0} (G_{\text{ret}} - G_{\text{adv}}) \quad (4.51)$$

Here we used that $Q_\mu P^{\mu\nu} = 0$.

There are a number of things to note about this expression. Most importantly we get $1/g$ from the factor T/q^0 so the LPM effect matters at leading order, irrespective of whether the system is in or out of equilibrium. This is interesting because the bare momentum distribution, f_g , need not go like $1/g$ for soft momenta. Ω describes the occupation density of soft gluons that are sourced by hard particles in the medium. The occupation density is the same for longitudinal and transversal modes. This is not too surprising; when $\mathbf{q} = 0$ there is no axis to define longitudinal and transversal with respect to so the modes must be the same. For soft three-momenta we expect the modes to be similar.

Finally we must check that eq. (4.51) reduces to

$$\begin{aligned} G_{rr} &= \left[\frac{1}{2} + f_B(q^0) \right] (G_{\text{ret}} - G_{\text{adv}}) \\ &\approx \frac{T}{q^0} (G_{\text{ret}} - G_{\text{adv}}) \end{aligned} \quad (4.52)$$

in thermal equilibrium where f_B is the Bose-Einstein distribution. We derived this expression in Chapter 2 using the KMS relation. We only need to show that $\Omega = 1$

in equilibrium. That's clear from eq. (4.49) and the fact that

$$\begin{aligned}\frac{df_F(x)}{dx} &= -f_F(x)(1 - f_F(x)) \\ \frac{df_B(x)}{dx} &= -f_B(x)(1 + f_B(x))\end{aligned}\tag{4.53}$$

where f_F is the Fermi-Dirac distribution. Thus we are guaranteed to have $\Omega > 0$ if the system is close enough to equilibrium so our interpretation of Ω as an occupation density makes sense. More generally we have $\Omega > 0$ as long as $f_q, f_g > 0$, $f_q < 1$ (Pauli blocking) and f_g and f_q are monotonically decreasing with momentum.

4.6 A non-equilibrium sum rule

We end this chapter by evaluating an integral over rr gluon rungs that figures prominently in the LPM effect. We get an exceedingly simple result even though the resummed propagator is quite complicated. Our derivation is an extension of the derivation given in [70] for the equilibrium case.

In Chapter 6 we shows that the collision integral in the LPM effect is

$$\mathcal{C}(\mathbf{q}_\perp) = g^2 C_F \int \frac{dq_0 dq_z}{(2\pi)^2} 2\pi\delta(q_0 - q_z) G_{rr}(Q)^{\mu\nu} \hat{K}_\mu \hat{K}_\nu\tag{4.54}$$

where G_{rr} is the resummed rr gluon propagator. At leading order only soft gluons contribute so we can safely extend the integral to all of momentum space. We orient our coordinate system so that $\hat{K}^\mu = (1, 0, 0, 1)$ is the scaled photon momentum. We work in the rest frame of the plasma, $u^\mu = (1, 0, 0, 0)$. \mathbf{q}_\perp is the component of \mathbf{q} that is orthogonal to the photon momentum.

Using eq. (4.43) and (4.51) we see that

$$\begin{aligned}\mathcal{C}(\mathbf{q}_\perp) &= g^2 C_F \int \frac{dq_0 dq_z}{(2\pi)^2} 2\pi\delta(q_0 - q_z) \Omega \frac{T}{q^0} \\ &\times \sum_{\alpha=T,L} \frac{-2 \text{Im} \Pi_\alpha(Q)}{(Q^2 - \text{Re} \Pi_\alpha(Q))^2 + (\text{Im} \Pi_\alpha(Q))^2} P_\alpha(Q)^{\mu\nu} \hat{K}_\mu \hat{K}_\nu\end{aligned}\tag{4.55}$$

To simplify the notation we write $\Pi = \Pi_{\text{ret}}$. After contracting the Lorentz indices

using $K^2 = 0$ and $Q \cdot K = 0$ we get that

$$\begin{aligned} \mathcal{C}(\mathbf{q}_\perp) = g^2 C_F \int \frac{dq_0 dq_z}{(2\pi)^2} 2\pi \delta(q_0 - q_z) \Omega \frac{T}{q^0} \left(1 - \frac{q_z^2}{q^2}\right) \\ \times \left[\frac{2 \operatorname{Im} \Pi_L(Q)}{(Q^2 - \operatorname{Re} \Pi_L(Q))^2 + (\operatorname{Im} \Pi_L(Q))^2} \right. \\ \left. - \frac{2 \operatorname{Im} \Pi_T(Q)}{(Q^2 - \operatorname{Re} \Pi_T(Q))^2 + (\operatorname{Im} \Pi_T(Q))^2} \right] \end{aligned} \quad (4.56)$$

To evaluate this integral we use the following properties of Π_L and Π_T :

1. Π is only dependent on $x = q^0/q$
2. $\operatorname{Re} \Pi(-x) = \operatorname{Re} \Pi(x)$ and $\operatorname{Im} \Pi(-x) = -\operatorname{Im} \Pi(x)$
3. $\operatorname{Im} \Pi(x = 0) = 0$
4. $\operatorname{Im} \Pi(x) = 0$ if $x \geq 1$
5. $\operatorname{Re} \Pi(x) \geq 0$ if $x \geq 1$
6. $\Pi(x)$ can be extended to an analytic function in the upper half complex plane.
7. $|\Pi(z)| = \mathcal{O}(1)$ as $|z| \rightarrow \infty$.
8. $\Pi(z) = -a^2$ has no solutions in the upper half complex plane for $a > 0$.

Some of these conditions have a clear physical meaning. Linear response theory shows that the Debye mass $m_D^2 = \operatorname{Re} \Pi_L(0)$ describes the screening of static chromoelectric fields by the plasma [45]. Specifically the potential due to a static colour charge is

$$V(r) \sim \frac{\exp(-m_D r)}{r} \quad (4.57)$$

Similarly $\operatorname{Re} \Pi_T(0)$ describes the screening of static chromomagnetic fields. It vanishes in an isotropic plasma. Therefore property (3) means that static colour fields in the plasma do not decay with time. Property (4) means that spacelike gluon modes in the plasma do not decay. Property (5) guarantees that these stable modes have a real mass and are not tachyonic.

In the isotropic case, $f(\mathbf{p}) = f(p)$, properties (1) to (7) can be seen by evaluating Π_L and Π_T explicitly. We omit the details of the derivation because it is the same as in thermal equilibrium [71, 45]. One gets that

$$\Pi_L(x) = m_D^2(1 - x^2) \left(1 - \frac{x}{2} \log \frac{x + 1 + i\epsilon}{x - 1 + i\epsilon} \right) \quad (4.58)$$

and

$$\Pi_T(x) = \frac{m_D^2}{2} \left[x^2 + \frac{x}{2}(1 - x^2) \log \frac{x + 1 + i\epsilon}{x - 1 + i\epsilon} \right] \quad (4.59)$$

where

$$m_D^2 = \frac{g^2}{\pi^2} \int_0^\infty dp p [2N_f f_q(p) + 2N_c f_g(p)] \quad (4.60)$$

is the non-equilibrium Debye mass. We choose the branch cut of the logarithm to be along the negative real axis. Then

$$\log \frac{x + 1 + i\epsilon}{x - 1 + i\epsilon} = \log \left| \frac{x + 1}{x - 1} \right| - i\pi\theta(1 - x^2). \quad (4.61)$$

When $\Pi(x)$ is analytically continued to $\Pi(z)$ the branch cut is in the lower half complex plane. We have checked property (8) numerically.

We now proceed with our evaluation of eq. (4.56). Integrating q_z out and changing to the variable

$$x = \frac{q_0}{q} = \frac{q_0}{\sqrt{q_0^2 + q_\perp^2}} \quad (4.62)$$

one gets

$$\mathcal{C}(\mathbf{q}_\perp) = g^2 C_F \frac{2\Omega T}{\pi} \int_0^1 \frac{dx}{x} \left[\frac{\text{Im } \Pi_L(x)}{(\mathbf{q}_\perp^2 + \text{Re } \Pi_L(x))^2 + (\text{Im } \Pi_L(x))^2} - \frac{\text{Im } \Pi_T(x)}{(\mathbf{q}_\perp^2 + \text{Re } \Pi_T(x))^2 + (\text{Im } \Pi_T(x))^2} \right]. \quad (4.63)$$

Here we used property (2) to reduce the integration domain from $-1 \leq x \leq 1$ to $0 \leq x \leq 1$.

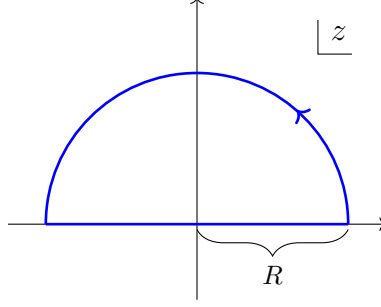


Figure 4.8: The contour used in the derivation of the Kramers-Kronig relations.

We define a function χ in the upper half complex plane by

$$\chi(z) = \frac{1}{(\mathbf{q}_\perp^2 + \Pi(z))(z^2 - 1) + iz\epsilon} \quad (4.64)$$

$\Pi(z)$ is the analytic continuation of either $\Pi_T(x)$ or $\Pi_L(x)$. Note that χ has no simple poles in the upper half plane: Since $\text{Im} \Pi(x = \pm 1) = 0$ and $\text{Re} \Pi(x = \pm 1) \geq 0$ (see (2), (4) and (5)) the term $iz\epsilon$ pushes the poles at $z = \pm 1$ into the lower half plane. Furthermore property (8) tells us that the factor $(\mathbf{q}_\perp^2 + \Pi(z))$ will not give a pole for $\mathbf{q}_\perp^2 > 0$.¹

We want to relate the real and imaginary part of χ using the Kramers-Kronig relations. Let's recall the standard derivation. We define a contour, γ , in the complex plane as in Fig. 4.8. Letting $R \rightarrow \infty$ and using that the integral over the semicircle vanishes (property (7)) we get

$$2\pi i \chi(y) = \oint_\gamma dz \frac{\chi(z)}{z - y - i\epsilon} = \int_{-\infty}^{\infty} dx \frac{\chi(x)}{x - y - i\epsilon} \quad (4.65)$$

Taking the imaginary part on both sides gives

$$\begin{aligned} \text{Re} \chi(y) &= \frac{1}{\pi} \int_{-\infty}^{\infty} dx \frac{\text{Im} \chi(x)}{x - y} \\ &= \frac{1}{\pi} \int_{-\infty}^{\infty} dx \frac{x \text{Im} \chi(x)}{x^2 - y^2} + \frac{1}{\pi} \int_{-\infty}^{\infty} \frac{y \text{Im} \chi(x)}{x^2 - y^2} = \frac{2}{\pi} \int_0^{\infty} dx \frac{x \text{Im} \chi(x)}{x^2 - y^2} \end{aligned} \quad (4.66)$$

¹When $\mathbf{q}_\perp^2 = 0$ there is a pole for $\Pi_T(z)$ at $z = 0$, however this single point is of no importance in the LPM effect where one integrates over \mathbf{q}_\perp . We will ignore the case of $\mathbf{q}_\perp^2 = 0$ from now on.

where we used that $\text{Im } \chi(-x) = -\text{Im } \chi(x)$. Therefore

$$\frac{2}{\pi} \int_0^\infty dx \frac{x}{x^2 - y^2} \text{Im } \chi(x) = \frac{1}{y^2 - 1} \frac{\mathbf{q}_\perp^2 + \text{Re } \Pi(y)}{(\mathbf{q}_\perp^2 + \text{Re } \Pi(y))^2 + (\text{Im } \Pi(y))^2} \quad (4.67)$$

Multiplying both sides with y^2 and taking the limit $y \rightarrow \infty$ gives

$$\frac{2}{\pi} \int_0^\infty dx x \text{Im } \chi(x) = -\frac{1}{\mathbf{q}_\perp^2 + \text{Re } \Pi(\infty)} \quad (4.68)$$

because $\text{Im } \Pi(x) = 0$ if $x \geq 1$. Setting $y = 0$ in eq. (4.67) and using $\text{Im } \Pi(x = 0) = 0$ we get that

$$\frac{2}{\pi} \int_0^\infty \frac{dx}{x} \text{Im } \chi(x) = -\frac{1}{\mathbf{q}_\perp^2 + \text{Re } \Pi(0)} \quad (4.69)$$

Taking the difference gives

$$\begin{aligned} & \int_0^\infty \frac{dx}{x} \frac{\text{Im } \Pi(x)}{(\mathbf{q}_\perp^2 + \text{Re } \Pi(x))^2 + (\text{Im } \Pi(x))^2} \\ &= \frac{\pi}{2} \left[\frac{1}{q^2 + \text{Re } \Pi(\infty)} - \frac{1}{q^2 + \text{Re } \Pi(0)} \right] \end{aligned} \quad (4.70)$$

We are only interested in spacelike gluons, i.e. the integration region $[0, 1]$. Since $\text{Im } \Pi$ vanishes for $x \geq 1$ we must do the substitution $(x^2 - 1)\text{Im } \Pi(x) \rightarrow \epsilon$ in that integration range. Then it's easy to show that

$$\begin{aligned} & \int_1^\infty \frac{dx}{x} \frac{\text{Im } \Pi(x)}{(\mathbf{q}_\perp^2 + \text{Re } \Pi(x))^2 + (\text{Im } \Pi(x))^2} \\ &= \int_1^\infty \frac{dx}{x} (x^2 - 1) \pi \delta \left(\left[\mathbf{q}_\perp^2 + \text{Re } \Pi(x) \right] \left[x^2 - 1 \right] \right) = 0 \end{aligned} \quad (4.71)$$

because $\text{Re } \Pi \geq 0$ for $x \geq 1$.

We can now summarize our result:

$$\begin{aligned} \mathcal{C}(\mathbf{q}_\perp) = g^2 C_F \Omega T & \left[\frac{1}{\mathbf{q}_\perp^2 + \text{Re } \Pi_L(\infty)} - \frac{1}{\mathbf{q}_\perp^2 + \text{Re } \Pi_L(0)} \right. \\ & \left. - \frac{1}{\mathbf{q}_\perp^2 + \text{Re } \Pi_T(\infty)} + \frac{1}{\mathbf{q}_\perp^2 + \text{Re } \Pi_T(0)} \right] \end{aligned} \quad (4.72)$$

Quite surprisingly the collision kernel, $\mathcal{C}(\mathbf{q}_\perp)$, only depends on four constants. An easy calculation using eq. (4.58) and (4.59) gives that on the real axis

$$\Pi_L(\infty) = \Pi_T(\infty) = \frac{m_D^2}{3}. \quad (4.73)$$

This is the plasma frequency which describes the energy of a spatially uniform oscillating mode in the plasma. It is the same for Π_L and Π_T because one cannot decompose a spatially uniform mode into a longitudinal and transversal part. Furthermore $\Pi_T(0) = 0$ showing that chromomagnetic sources are not screened. Thus our final result is

$$\mathcal{C}(\mathbf{q}_\perp) = g^2 C_F \Omega T \left[\frac{1}{\mathbf{q}_\perp^2} - \frac{1}{\mathbf{q}_\perp^2 + m_D^2} \right] \quad (4.74)$$

The collision kernel only depends on the occupation density of soft gluons, Ω , and the Debye mass, m_D^2 .

The resummed occupation density of hard quarks

In order to evaluate the LPM effect we will need the resummed rr propagator, $S_{rr}(P)$, for hard and almost on-shell quarks, $P \sim T$ and $P^2 \sim g^2 T^2$. Schematically we can write

$$S_{rr} = \left[\frac{1}{2} + \frac{\Sigma_{<}}{2i\text{Im}\Sigma_{\text{ret}}} \right] (S_{\text{ret}} - S_{\text{adv}}). \quad (5.1)$$

as for scalar fields. Σ is the quark self-energy. In this chapter we will give a rigorous derivation of this equation and evaluate $\Sigma_{<}$ and $\text{Im}\Sigma_{\text{ret}}$ for the momentum regime we are interested in.

5.1 Evaluation of $\Sigma_{<}$ and $\text{Im}\Sigma_{\text{ret}}$

Let's examine the power counting structure of $\text{Im}\Sigma_{\text{ret}} = \text{Im}\Sigma_{ar}$ for hard, on-shell quarks. The relevant diagrams are in Fig. 5.1. The r/a indices cannot be placed differently because the aa propagator vanishes.

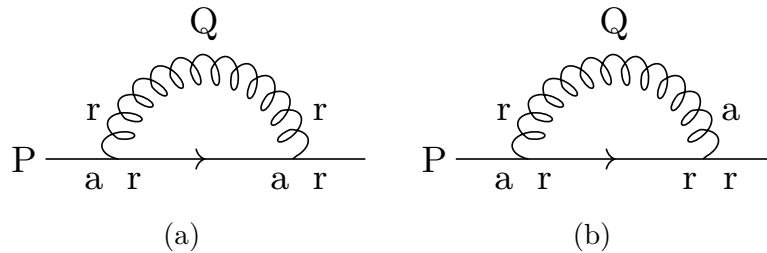


Figure 5.1: Diagrams contributing to Σ_{ret} at leading order in g .

Let's first look at the Feynman diagram in Fig. 5.1a. It is

$$-i\Sigma_{\text{ret}}(P)\Big|_{(a)} = (ig)^2 C_F \int \frac{d^4 Q}{(2\pi)^4} G_{rr}^{\mu\nu}(Q) \gamma_\mu S_{\text{ret}}(P-Q) \gamma_\nu. \quad (5.2)$$

We must use free propagators for hard momenta but HTL resummed propagators for soft momenta. For the colour factor, see Appendix A. Then

$$\text{Im } \Sigma_{\text{ret}}(P)\Big|_{(a)} = (ig)^2 C_F \int \frac{d^4 Q}{(2\pi)^4} G_{rr}^{\mu\nu}(Q) \gamma_\mu \text{Im } iS_{\text{ret}}(P-Q) \gamma_\nu. \quad (5.3)$$

This expression relies on G_{rr} being real. That is clear for the bare propagator and we showed it for the resummed one in last chapter.

There are three separate momentum regimes in the above integral when P is hard. First Q can be soft. The gluon propagator then gives a g^3 enhancement, g coming from the factor $\Pi_{<}/2i\text{Im } \Pi$ and g^2 coming from $G_{\text{ret}} - G_{\text{adv}}$. The quark propagator is

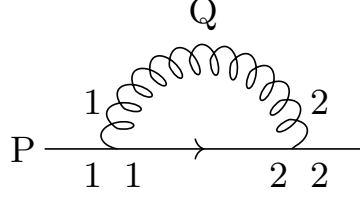
$$\text{Im } iS_{\text{ret}}(P-Q) \sim (\not{P} - \not{Q}) \delta((P-Q)^2) \approx \not{P} \delta(2P \cdot Q) \quad (5.4)$$

and thus goes like $\frac{1}{g}$. We used explicitly that P is on shell. Finally there is a g^4 phase space suppression and a factor g^2 from the vertices. Thus the diagram goes like $g^{-3} \times g^{-1} \times g^4 \times g^2 = g^2$ in this momentum regime.

The second momentum regime is when the internal quark is soft and the gluon is hard. There is no g^{-1} enhancement from the gluon occupation density so this regime is suppressed. Finally both internal particles can be hard. Then both propagators are bare and the integral goes like

$$\int d^4 Q \delta(Q^2) \delta((P-Q)^2) \sim \int d^4 Q \delta(Q^2) \delta(2P \cdot Q + \mathcal{O}(g^2 T^2)) \quad (5.5)$$

Q and P are on shell within $\mathcal{O}(g^2 T^2)$ and they must be orthogonal to each other within $\mathcal{O}(g^2 T^2)$. This leads to a g^2 phase space suppression. To see this, integrate q^0 out and express the remaining integral in terms of the angle between \mathbf{p} and \mathbf{q} .

Figure 5.2: The diagram contributing to $\Sigma_{<}$ at leading order in g

Schematically,

$$d^3q \sim dq q^2 d\theta \sin \theta \sim g^2 \quad (5.6)$$

when $\theta \sim g$. There is no compensating enhancement.

One can analyze the diagram in Fig. 5.1b in a similar way. The regimes with a hard internal quark and a hard gluon or a soft quark and a hard gluon have the same power structure as before. The regime with a soft gluon and a hard quark now only contributes at order g^3 because there is no Bose enhancement. We have thus shown that at leading order

$$\text{Im } \Sigma_{\text{ret}}(P) = -g^2 C_F \int^{gT} \frac{d^4 Q}{(2\pi)^4} G_{rr}^{\mu\nu}(Q) \gamma_\mu \text{Im } iS_{\text{ret}}^0(P-Q) \gamma_\nu. \quad (5.7)$$

The gluon propagator is resummed and the fermion propagator is bare.¹ Note that our derivation is only valid for the imaginary part of Σ_{ret} and relied on that $P \sim T$, $P^2 \sim g^2 T^2$.

Let's now find $\Sigma_{<} = -\Sigma_{12}$ for hard, on-shell quarks. This is easiest to do in the $1/2$ basis. The relevant diagram can be seen in Fig. 5.2. We can write

$$-i\Sigma_{<}(P) = (ig)^2 C_F \int \frac{d^4 Q}{(2\pi)^4} G_{<}^{\mu\nu}(Q) \gamma_\mu S_{<}(P-Q) \gamma_\nu. \quad (5.8)$$

where $G_{<} = G_{12}$ and $S_{<} = S_{12}$ can be either bare or resummed as before. The bare gluon and quark propagators both contain a delta function. Furthermore $G_{<}$ has a

¹A discerning reader might object that the quark propagator in eq. (5.7) is hard and almost on-shell and should thus be resummed. This would bring about great complications since the equation for $\text{Im } \Sigma_{\text{ret}}$ would then include a factor of $\text{Im } \Sigma_{\text{ret}}$, i.e. we would get an integral equation that would have to be solved self-consistently. Fortunately $(P-Q)^2 \sim 2P \cdot Q \sim gT^2 \gg g^2 T^2$ so the internal quark is not sufficiently on shell to warrant resummation.

Bose enhancement at soft momenta because schematically

$$G_{<} = \frac{\Pi_{<}}{2i\text{Im}\Pi_{\text{ret}}} (G_{\text{ret}} - G_{\text{adv}}) \quad (5.9)$$

The power counting argument is thus the same as for $\text{Im}\Pi_{\text{ret}}$. In the end we get that

$$\Sigma_{<}(P) = (-i)g^2 C_F \int^{gT} \frac{d^4 Q}{(2\pi)^4} G_{rr}^{\mu\nu}(Q) \gamma_\mu S_{<}^0(P-Q) \gamma_\nu. \quad (5.10)$$

where $S_{<}^0$ is a bare propagator. We have used that at leading order $G_{<} = G_{rr}$ for soft momenta.

We are now ready to calculate the resummed occupation density for hard, on-shell quarks

$$\frac{\Sigma_{<}}{2i\text{Im}\Sigma_{\text{ret}}}. \quad (5.11)$$

Inserting $\text{Im}iS_{\text{ret}}^0(K) = \pi\text{sgn}(K^0)\not{K}\delta(K^2)$, in eq. (5.7) and using $P \gg Q$ we get

$$\text{Im}\Sigma_{\text{ret}}(P) = -\pi g^2 C_F \text{sgn}(p^0) \gamma_\mu \not{P} \gamma_\nu \int^{gT} \frac{d^4 Q}{(2\pi)^4} G_{rr}^{\mu\nu}(Q) \delta(2P \cdot Q). \quad (5.12)$$

Note how all spinor indices can be taken out of the integral. Similarly inserting $S_{<}^0$ in eq. (5.10) we get

$$\begin{aligned} \Sigma_{<}(P) &= 2\pi i g^2 C_F [f_q(\mathbf{p})\theta(p^0) + (f_q(\mathbf{p}) - 1)\theta(-p^0)] \gamma_\mu \not{P} \gamma_\nu \\ &\times \int^{gT} \frac{d^4 Q}{(2\pi)^4} G_{rr}^{\mu\nu}(Q) \delta(2P \cdot Q). \end{aligned} \quad (5.13)$$

$\text{Im}\Sigma_{\text{ret}}$ and $\Sigma_{<}$ have the same matrix structure so we can take their ratio. We finally get a very simple result for the resummed occupation number

$$F(P) := -\frac{\Sigma_{<}}{2i\text{Im}\Sigma_{\text{ret}}} = f_q(\mathbf{p})\theta(p^0) + (1 - f_q(\mathbf{p}))\theta(-p^0) \quad (5.14)$$

This makes perfect sense. The KMS condition tells us that $F(P)$ should reduce to the Fermi-Dirac distribution $f_F(p^0)$ in thermal equilibrium. Going from equilibrium to non-equilibrium we made the correspondence $f_F(|p^0|) \rightarrow f_q(\mathbf{p})$. Thus F must be a

function in $f_q(\mathbf{p})$ that reduces to $f_F(p^0)$ when we substitute $f_q(\mathbf{p})$ by $f_F(|p^0|)$. Using the identity

$$1 - f_F(-x) = f_F(x) \quad (5.15)$$

it is easy to see that eq. (5.14) fulfills this condition.

We can also give a more physical explanation of eq. (5.14). $p^0 > 0$ corresponds to initial state quarks while $p^0 < 0$ corresponds to final state quarks. The occupation numbers are then exactly what we would expect from kinetic theory. Here $1 - f_q(\mathbf{p})$ is Pauli blocking which means that a fermion is less likely to be produced because of the Pauli exclusion principle. Apart from this, the resummed momentum distribution is the same as the bare momentum distribution.

5.2 The resummed rr fermion propagator

We have derived the resummed occupation number $\Sigma_{<}/2i\text{Im}\Sigma_{\text{ret}}$ for hard, on-shell quarks. However, we have not yet shown that one can actually write

$$S_{rr} = \left[\frac{1}{2} + \frac{\Sigma_{<}}{2i\text{Im}\Sigma_{\text{ret}}} \right] (S_{\text{ret}} - S_{\text{adv}}). \quad (5.16)$$

or equivalently

$$S_{<} = \frac{\Sigma_{<}}{2i\text{Im}\Sigma_{\text{ret}}} (S_{\text{ret}} - S_{\text{adv}}) \quad (5.17)$$

We will remedy that in this section. We assume throughout that $f(\mathbf{p}) = f(p)$. Our argument is partially based on [25] and [72].

We have that

$$S_{<} = S_{\text{ret}} (-i\Sigma_{<}) S_{\text{adv}} \quad (5.18)$$

where

$$S_{\text{ret}} = \frac{i}{\not{p} - \Sigma_{\text{ret}}}, \quad S_{\text{adv}} = \frac{i}{\not{p} - \Sigma_{\text{adv}}} \quad (5.19)$$

and $\Sigma_{\text{adv}} = \Sigma_{\text{ret}}^*$. These identities can be derived in the same way as for scalar fields in Chapter 2.

The physical (vacuum) mass of the light quarks is much smaller than the tem-

perature of weakly interacting QGP and can thus be neglected. The free quark propagators are then

$$\frac{i}{\not{P} - m} \approx \frac{i}{\not{P}}. \quad (5.20)$$

The mass term in the propagator is fundamentally different from the \not{P} term because it does not contain a gamma matrix. This corresponds to mass term in the Lagrangian breaking the chiral symmetry of the theory, $\psi \rightarrow e^{i\alpha\gamma^5}\psi$. Using massless propagators, the thermal self energy is $\Sigma = \Sigma_\mu\gamma^\mu$. Interestingly, the quarks acquire a thermal mass but chiral invariance is intact [73].¹ We will use this fact throughout our analysis.

Assuming that $f(\mathbf{p}) = f(p)$ there are only two relevant four-vectors, the four-velocity of the system, u^μ , and the momentum of the quark, P^μ . In the Lorentz frame where $u^\mu = (1, 0, 0, 0)$ we therefore have

$$\Sigma \sim \mathbf{p}. \quad (5.21)$$

for all components of the self energy.

In order to show eq. (5.17) we will decompose the propagator into quark and antiquark components of left- and right-handed helicity. See Appendix B for further information on spinor indices. We write the Dirac matrices as

$$\gamma^\mu = \begin{bmatrix} 0 & \sigma^\mu \\ \bar{\sigma}^\mu & 0 \end{bmatrix} \quad (5.22)$$

where $\sigma^\mu = (1, \boldsymbol{\sigma})$ and $\bar{\sigma}^\mu = (1, -\boldsymbol{\sigma})$. $\boldsymbol{\sigma}$ are the usual Pauli matrices. The left- and right-handed components of the retarded propagator are defined as

$$S_{\text{ret}} = \begin{bmatrix} 0 & S_{\text{ret}}^L \\ S_{\text{ret}}^R & 0 \end{bmatrix} \quad (5.23)$$

¹In an QCD-like theory with n_f flavours of massless quarks there is a $SU(n_f)_V \times SU(n_f)_A \times U(1)_V \times U(1)_A$ chiral symmetry of the Lagrangian. The $SU(n_f)_A$ symmetry is spontaneously broken at low temperatures but our perturbative formalism applies to high temperatures where the symmetry is intact. Furthermore there is a $U(1)_A$ anomaly (see Chapter 30 of [74]) but that is a non-perturbative effect that does not concern us.

where

$$S_{\text{ret}}^L = \frac{i(p - \Sigma_{\text{ret}}) \cdot \sigma}{(p - \Sigma_{\text{ret}})^2}, \quad S_{\text{ret}}^R = \frac{i(p - \Sigma_{\text{ret}}) \cdot \bar{\sigma}}{(p - \Sigma_{\text{ret}})^2} \quad (5.24)$$

and similarly for S_{adv} and S_{rr} . Let's focus on the right-handed component. Using $\Sigma \sim \mathbf{p}$ we can write

$$\begin{aligned} S_{\text{ret}}^R &= \frac{i}{(p - \Sigma_{\text{ret}})^2} \left[p^0 - \Sigma^0 + (p - \Sigma \cdot \hat{\mathbf{p}}) \boldsymbol{\sigma} \cdot \hat{\mathbf{p}} \right] \\ &= \frac{i}{2} \left[\frac{1 - \boldsymbol{\sigma} \cdot \hat{\mathbf{p}}}{p^0 - \Sigma^0 + p - \Sigma \cdot \hat{\mathbf{p}}} + \frac{1 + \boldsymbol{\sigma} \cdot \hat{\mathbf{p}}}{p^0 - \Sigma^0 - p + \Sigma \cdot \hat{\mathbf{p}}} \right] \end{aligned} \quad (5.25)$$

where $\hat{\mathbf{p}} = \mathbf{p}/p$. Here Σ denotes Σ_{ret} . We define $u(\mathbf{p})$ and $v(\mathbf{p})$ as the eigenvalues of $\boldsymbol{\sigma} \cdot \hat{\mathbf{p}}$ with positive and negative eigenvalues respectively. The normalization is $u^\dagger u = v^\dagger v = 2p$. Then

$$S_{\text{ret}}^R = \frac{i}{2p} \left[\frac{vv^\dagger}{p^0 + p - \Sigma \cdot p^-/p} + \frac{uu^\dagger}{p^0 - p - \Sigma \cdot p^+/p} \right]. \quad (5.26)$$

See Appendix B for a derivation of the factors vv^\dagger and uu^\dagger . Here $p^{+\mu} = (|\mathbf{p}|, \mathbf{p})$ and $p^{-\mu} = (|\mathbf{p}|, -\mathbf{p})$. u corresponds to a right-handed quark because the pole of the propagator has $\text{Re } p^0 > 0$ and v is a left-handed antiquark. Similarly

$$S_{\text{ret}}^L = \frac{i}{2p} \left[\frac{uu^\dagger}{p^0 + p - \Sigma \cdot p^-/p} + \frac{vv^\dagger}{p^0 - p - \Sigma \cdot p^+/p} \right]. \quad (5.27)$$

where now u is a right-handed antiquark and v is a left-handed quark.

In matrix form $S_{<}$ is given by

$$S_{<} = \begin{bmatrix} 0 & S_{\text{ret}}^L (-i\Sigma_{<} \cdot \bar{\sigma}) S_{\text{adv}}^L \\ S_{\text{ret}}^R (-i\Sigma_{<} \cdot \sigma) S_{\text{adv}}^R & 0 \end{bmatrix} \quad (5.28)$$

In Appendix B we show that

$$\begin{aligned} u^\dagger \sigma_\mu u &= 2p_\mu^+, & u^\dagger \bar{\sigma}_\mu u &= 2p_\mu^-, \\ v^\dagger \sigma_\mu v &= 2p_\mu^-, & v^\dagger \bar{\sigma}_\mu v &= 2p_\mu^+. \end{aligned} \quad (5.29)$$

Furthermore all combinations with one u and one v vanish. Using eq. (5.26) - (5.29) and that $S_{\text{adv}} = -S_{\text{ret}}^*$ it is straightforward to show that

$$\begin{aligned}
S_{<}^R \Big|_v &= \frac{p^- \cdot \Sigma_{<}}{2i p^- \cdot \text{Im} \Sigma_{\text{ret}}} (S_{\text{ret}}^R - S_{\text{adv}}^R) \Big|_v \\
S_{<}^R \Big|_u &= \frac{p^+ \cdot \Sigma_{<}}{2i p^+ \cdot \text{Im} \Sigma_{\text{ret}}} (S_{\text{ret}}^R - S_{\text{adv}}^R) \Big|_u \\
S_{<}^L \Big|_v &= \frac{p^+ \cdot \Sigma_{<}}{2i p^+ \cdot \text{Im} \Sigma_{\text{ret}}} (S_{\text{ret}}^L - S_{\text{adv}}^L) \Big|_v \\
S_{<}^L \Big|_u &= \frac{p^- \cdot \Sigma_{<}}{2i p^- \cdot \text{Im} \Sigma_{\text{ret}}} (S_{\text{ret}}^L - S_{\text{adv}}^L) \Big|_u
\end{aligned} \tag{5.30}$$

Here $S_{<}^R \Big|_v$ refers to the v component of $S_{<}^R$.

We have derived an expression relating $S_{<}$ and $S_{\text{ret}} - S_{\text{adv}}$ for all four components of the quark field. These components do not interact with each other at photon or gluon vertices. Therefore the LPM Feynman diagram decomposes into four diagrams with the different components in the quark loop.

We have shown by an explicit calculation that $\Sigma_{<}$ and $\text{Im} \Sigma_{\text{adv}}$ have the same matrix structure. This means that

$$\frac{p^- \cdot \Sigma_{<}}{2i p^- \cdot \text{Im} \Sigma_{\text{ret}}} = \frac{p^+ \cdot \Sigma_{<}}{2i p^+ \cdot \text{Im} \Sigma_{\text{ret}}} = -F(P) \tag{5.31}$$

Thus all four components have the same occupation density as expected in an isotropic plasma at vanishing baryon chemical potential. We can thus write an elegant equation for the full, resummed rr propagator for hard, on-shell quarks,

$$S_{rr} = \left[\frac{1}{2} - F(P) \right] (S_{\text{ret}} - S_{\text{adv}}) \tag{5.32}$$

where

$$F(P) = f_q(\mathbf{p})\theta(p^0) + (1 - f_q(\mathbf{p}))\theta(-p^0). \tag{5.33}$$

The LPM effect in a non-equilibrium isotropic QGP

6.1 *Summing four-point functions*

In previous chapters we derived all the ingredients for evaluating the LPM effect in an isotropic non-equilibrium QGP. Specifically we showed that the resummed occupation number of soft gluons gives a $\mathcal{O}(g)$ enhancement as in equilibrium. We extended a sum rule for integrals over gluon rungs. Furthermore we derived the resummed occupation number of hard quarks. In this chapter our work culminates in finding an integral equation that describes bremsstrahlung, pair-annihilation and the LPM effect in a non-equilibrium QGP.

As we have discussed the rate of photon production, R , in a unit volume is

$$k \frac{dR}{d^3k} = \frac{i}{2(2\pi)^3} (\Pi_{12}^\gamma)^\mu{}_\mu \quad (6.1)$$

where $\Pi_{12}^{\gamma\mu\nu}$ is a component of the photon self-energy and \mathbf{k} is the photon momentum. The external photons must link a quark and an antiquark. Thus we must evaluate the four-point function

$$S_{1122}(x_1, x_2; y_1, y_2) = \langle T_C \{ \bar{\psi}_1(x_1) \psi_1(x_2) \bar{\psi}_2(y_1) \psi_2(y_2) \} \rangle. \quad (6.2)$$

See Fig. 6.1a for clarification of the indices. When going to momentum space we can approximate the momentum in a quark rail as constant because it only changes slightly through soft gluon exchange. We thus need to evaluate the diagram in Fig.

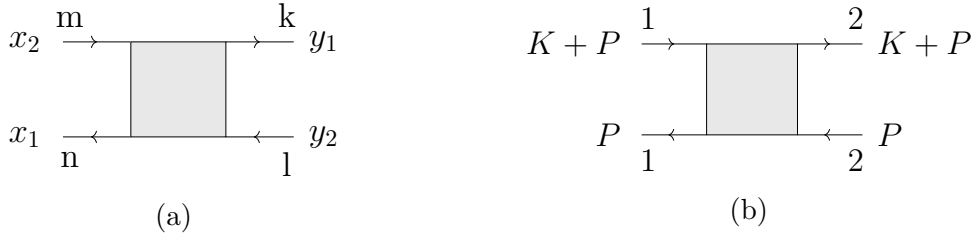


Figure 6.1: Definition of the four-point function $S_{nmkl}(x_1, x_2; y_1, y_2)$ in position space. n, m, k, l are either 1 or 2. Also shown is the diagram we need to evaluate, i.e. S_{1122} in momentum space.

6.1b.¹ K is the photon momentum and P is the loop momentum.

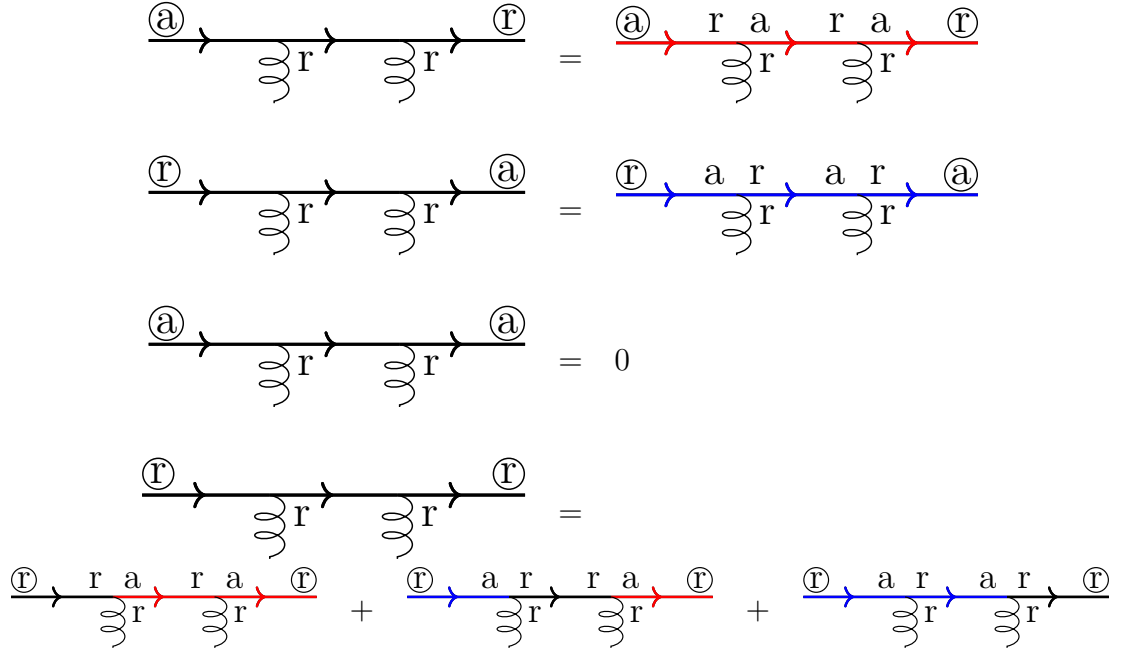
Our analysis has all been done in the r/a basis in which power counting is much simpler. To evaluate S_{1122} we have to express it in terms of four-point functions in the r/a basis. Using that $\psi_1 = \psi_r + \psi_a/2$ and $\psi_2 = \psi_r - \psi_a/2$ it is easy to show that

$$\begin{aligned}
 S_{1122} = & \\
 & S_{rrrr} + \frac{1}{2}S_{arrr} + \frac{1}{2}S_{rarr} - \frac{1}{2}S_{rrar} - \frac{1}{2}S_{rrra} \\
 & + \frac{1}{4}S_{aarr} - \frac{1}{4}S_{arar} - \frac{1}{4}S_{arra} - \frac{1}{4}S_{raar} - \frac{1}{4}S_{rara} + \frac{1}{4}S_{rraa} \\
 & + \frac{1}{8}S_{raaa} + \frac{1}{8}S_{araa} - \frac{1}{8}S_{aara} - \frac{1}{8}S_{aaar} + \frac{1}{16}S_{aaaa}.
 \end{aligned} \tag{6.3}$$

At first sight our task seems daunting. We need to evaluate all these different four-point functions. They correspond to Feynman diagrams with an arbitrary number of gluon rungs. If there is no simple rule for the placement of r and a indices in internal vertices in a four-point function we cannot sum up the diagrams with a different number of gluon rungs.

For a QGP in thermal equilibrium Arnold, Moore and Yaffe used a KMS relation to simplify the task [25]. Specifically, they used an identity from [75] that relates

¹See [25] for further justification. They e.g. show why the diagram with a quark rail from x_1 to x_2 and another one from y_1 to y_2 does not contribute at leading order. They also show why diagrams with crossed gluon rungs are not leading order.

Figure 6.2: Analysis of quark rails with begin and end with indices in the r/a basis.

$$\frac{r \ a}{\text{wavy } r} \quad \frac{a \ r}{\text{wavy } r}$$

Figure 6.3: Vertices that contribute at leading order.

four-point functions in equilibrium. At zero chemical potential

$$S_{1122} = \alpha_1 S_{aarr} + \alpha_2 S_{aaar} + \alpha_3 S_{aara} + \alpha_4 S_{araa} \\ + \alpha_5 S_{raaa} + \alpha_6 S_{arra} + \alpha_7 S_{arar} + c.c. \quad (6.4)$$

where the coefficients depend on the incoming momenta. As an example $\alpha_1 = f_F(p^0 + k^0)(1 - f_F(p^0))$. The derivation is similar to the one we gave of a KMS relation for two-point functions in Chapter 2. We show below that S_{aarr} is the only four-point function in eq. (6.4) that contributes at leading order. Thus one gets that

$$S_{1122} = 2f_F(p^0 + k^0)(1 - f_F(p^0)) \text{Re } S_{aarr}. \quad (6.5)$$

The KMS condition is not valid in non-equilibrium systems. We will therefore take a different route to evaluate S_{1122} , using the power counting scheme explicitly. Let's

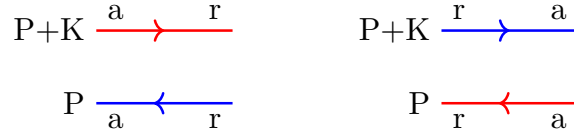


Figure 6.4: The pairs of propagators that give pinching poles.

first analyze quark rails as in Fig. 6.2. At leading order all gluon rungs must be rr propagators to get the $1/g$ enhancement. Furthermore there is always an odd number of a indices at a vertex as we showed in Chapter 2. Thus one quark propagator ends in a and the other one in r at each vertex, see Fig. 6.3. Finally, we will use that aa propagators vanish identically.

We first consider a quark rail that starts with a and ends with r . (To help the reader we colour S_{ra} blue and S_{ar} red in Fig. 6.2.) The first propagator must be S_{ar} because S_{aa} vanishes. The next propagator must start with a and thus it is also S_{ar} . Continuing like this we see that the rail must end with r and that all quark propagators are S_{ar} . Similarly, a quark rail that starts with r and ends in a can only have S_{ra} propagators. Finally, a quark rail that starts and ends with a vanishes at leading order in our momentum regime. Thus we can ignore S_{araa} , S_{aara} , S_{arra} , S_{raar} , S_{aaar} , S_{raaa} and S_{aaaa} . (In fact S_{aaaa} vanishes at all orders [75].)

Quark rails that start and end with r are slightly more involved. A straightforward analysis shows that they always consist of zero or more S_{ra} propagators, then one S_{rr} and finally zero or more S_{ar} propagators. For a rr quark rail with n propagators there are therefore n possibilities depending on where the S_{rr} propagator is. See Fig. 6.2 for the case of a rail with two gluon rungs.

We now analyze the remaining nine four-point functions. At leading order each pair of propagators must give pinching poles. By a pair we mean propagators from the two quark rails that are between the same gluon rungs. $S_{ra} = S_{\text{ret}}$ and $S_{ar} = S_{\text{adv}}$ have poles on each side of the real axis so we need one of each in a pair, see Fig. 6.4. The pole structure of S_{rr} can be seen from

$$S_{rr} = \left[\frac{1}{2} - F(P) \right] (S_{\text{ret}} - S_{\text{adv}}). \quad (6.6)$$

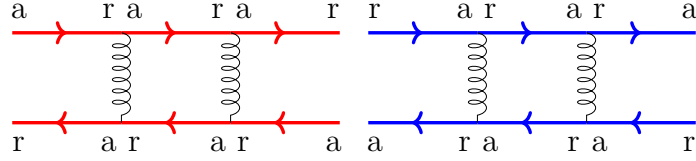


Figure 6.5: S_{rara} and S_{arar} . There are no pinching poles so these diagrams do not contribute at leading order.

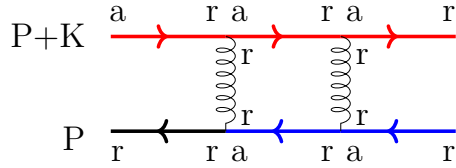


Figure 6.6: The only way of placing r/a indices in S_{rarr} at leading order. In a general diagram with arbitrarily many gluon rungs S_{rr} must still be on the far left.

where

$$F(P) = f_q(\mathbf{p})\theta(p^0) + (1 - f_q(\mathbf{p}))\theta(-p^0) \quad (6.7)$$

as we showed in last chapter. S_{rr} has poles on both sides of the real axis, the term that does not give pinching poles can be dropped.

Our knowledge of quark rails tells us that S_{rara} and S_{arar} have no pinching poles and can thus be discarded, see Fig. 6.5. Then there are seven four-point functions left which we will express in terms of S_{rraa} and S_{aarr} . To get pinching poles from all pairs in S_{rarr} we must place the indices as in Fig. 6.6 with S_{rr} on the far left. Eq. (6.6) then gives that at leading order

$$S_{rarr} = \left(\frac{1}{2} - F(P)\right) S_{aarr}. \quad (6.8)$$

The leading order diagram for S_{aarr} is in Fig. 6.7. Similarly one can show that

$$S_{rrar} = -\left(\frac{1}{2} - F(P)\right) S_{rraa} \quad (6.9)$$

$$S_{arrr} = -\left(\frac{1}{2} - F(P + K)\right) S_{aarr} \quad (6.10)$$

$$S_{rrra} = \left(\frac{1}{2} - F(P + K)\right) S_{rraa}. \quad (6.11)$$

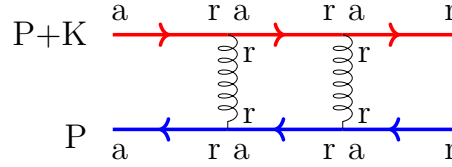


Figure 6.7: The only way of placing r/a indices in S_{aarr} at leading order.

The only four-point function left is S_{rrrr} , the analysis of which is more involved. There is exactly one rr propagator on each quark rail. The S_{rr} propagators must be either on top of each other or immediately diagonal to each other, see Fig. 6.8 for how we will miss a pinching pole pair otherwise.

For specificity we consider the case of two gluon rungs. Then there are three possibilities of having the rr propagators on top of each other. In Fig. 6.9 we rewrite them at leading order using eq. (6.6). In Fig. 6.10 we rewrite the remaining leading order contributions. Summing all the contributions we see that most terms cancel and only terms corresponding to S_{rraa} and S_{aarr} remain, see Fig. 6.11. It is easy to see that a similar cancellation takes place for an arbitrary number of gluon rungs. Specifically four-point functions with S_{rr} immediately diagonal to each other cancel out with four-point functions with S_{rr} on top of each other. We are then left with

$$S_{rrrr} = - \left(\frac{1}{2} - F(P) \right) \left(\frac{1}{2} - F(P + K) \right) [S_{rraa} + S_{aarr}] \quad (6.12)$$

Eq. (6.12) can be viewed as an expression of unitarity, i.e. the fact that probability is conserved in quantum theory. The S -matrix is the time evolution operator from the distant past to the distant future. Unitarity implies

$$\mathcal{S}^\dagger \mathcal{S} = 1. \quad (6.13)$$

It is convenient to define the transfer matrix \mathcal{T} by $\mathcal{S} = 1 + i\mathcal{T}$. It describes the probability of scattering and must satisfy

$$\mathcal{T}^\dagger \mathcal{T} = i (\mathcal{T}^\dagger - \mathcal{T}). \quad (6.14)$$

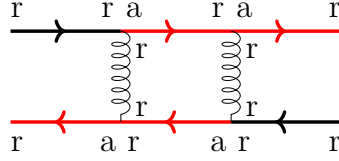


Figure 6.8: An example of a diagram that does not contribute to S_{rrrr} at leading order because the S_{rr} propagators are placed too far apart. The propagators in the middle do not give pinching poles.

S_{rraa} is composed of retarded propagators for quarks and antiquarks. It describes their propagation in the medium as can be seen from the factor $\theta(t)$ in configuration space. Thus it corresponds to $i\mathcal{T}$.¹ Similarly S_{aarr} is composed of advanced propagators describing propagation backwards in time and therefore it corresponds to $-i\mathcal{T}^\dagger$. Finally, S_{rrrr} is a completely symmetric four-point function without time ordering. It can be viewed as composed of S_{rraa} and S_{aarr} four-point functions so it corresponds to $\mathcal{T}^\dagger\mathcal{T}$. The factors with $F(P)$ and $F(P+K)$ in eq. (6.12) denote Pauli blocking because of other quarks in the medium.

We have evaluated all the terms in eq. (6.3) at leading order. Summing them up using eq. (6.8) to (6.12) gives

$$S_{1122} = F(P+K)(1-F(P))[S_{rraa} + S_{aarr}] \quad (6.15)$$

It is easy to see that $S_{rraa} = S_{aarr}^*$, either from their definition or from the fact that $S_{ra}^* = -S_{ar}$. We have thus derived that

$$S_{1122} = 2F(P+K)(1-F(P))\text{Re} S_{aarr} \quad (6.16)$$

without using the KMS condition. This expression is convenient because S_{aarr} has a simple structure, see Fig. 6.12. Of course this reduces to eq. (6.5) in thermal equilibrium because $F(P)$ reduces to $f_F(p^0)$.

¹Even the diagram without a gluon rung includes scattering because the quark propagators are resummed.

$$\begin{aligned}
& \begin{array}{c} \text{r} \rightarrow \text{r a} \rightarrow \text{r a} \rightarrow \text{r} \\ \text{r} \leftarrow \text{r a} \leftarrow \text{r a} \leftarrow \text{r} \end{array} \\
& \begin{array}{c} \text{r} \rightarrow \text{a a} \rightarrow \text{r a} \rightarrow \text{r} \\ \text{r} \leftarrow \text{a a} \leftarrow \text{r a} \leftarrow \text{r} \end{array} \\
& \begin{array}{c} \text{a} \rightarrow \text{r a} \rightarrow \text{r a} \rightarrow \text{r} \\ \text{a} \leftarrow \text{r a} \leftarrow \text{r a} \leftarrow \text{r} \end{array} \\
& = - \left(\frac{1}{2} - F(P) \right) \left(\frac{1}{2} - F(P + K) \right) \\
& \times \left[\begin{array}{c} \text{r} \rightarrow \text{a a} \rightarrow \text{r a} \rightarrow \text{r} \\ \text{r} \leftarrow \text{a a} \leftarrow \text{r a} \leftarrow \text{r} \end{array} + \begin{array}{c} \text{a} \rightarrow \text{r a} \rightarrow \text{r a} \rightarrow \text{r} \\ \text{a} \leftarrow \text{r a} \leftarrow \text{r a} \leftarrow \text{r} \end{array} \right] \\
\\
& \begin{array}{c} \text{r} \rightarrow \text{a r} \rightarrow \text{r a} \rightarrow \text{r} \\ \text{r} \leftarrow \text{a r} \leftarrow \text{r a} \leftarrow \text{r} \end{array} \\
& \begin{array}{c} \text{r} \rightarrow \text{a r} \rightarrow \text{a a} \rightarrow \text{r} \\ \text{r} \leftarrow \text{a r} \leftarrow \text{a a} \leftarrow \text{r} \end{array} \\
& \begin{array}{c} \text{r} \rightarrow \text{a a} \rightarrow \text{r a} \rightarrow \text{r} \\ \text{r} \leftarrow \text{a a} \leftarrow \text{r a} \leftarrow \text{r} \end{array} \\
& = - \left(\frac{1}{2} - F(P) \right) \left(\frac{1}{2} - F(P + K) \right) \\
& \times \left[\begin{array}{c} \text{r} \rightarrow \text{a r} \rightarrow \text{a a} \rightarrow \text{r} \\ \text{r} \leftarrow \text{a r} \leftarrow \text{a a} \leftarrow \text{r} \end{array} + \begin{array}{c} \text{r} \rightarrow \text{a a} \rightarrow \text{r a} \rightarrow \text{r} \\ \text{r} \leftarrow \text{a a} \leftarrow \text{r a} \leftarrow \text{r} \end{array} \right] \\
\\
& \begin{array}{c} \text{r} \rightarrow \text{a r} \rightarrow \text{a r} \rightarrow \text{r} \\ \text{r} \leftarrow \text{a r} \leftarrow \text{a r} \leftarrow \text{r} \end{array} \\
& \begin{array}{c} \text{r} \rightarrow \text{a r} \rightarrow \text{a a} \rightarrow \text{r} \\ \text{r} \leftarrow \text{a r} \leftarrow \text{a a} \leftarrow \text{r} \end{array} \\
& \begin{array}{c} \text{r} \rightarrow \text{a r} \rightarrow \text{a r} \rightarrow \text{a} \\ \text{r} \leftarrow \text{a r} \leftarrow \text{a r} \leftarrow \text{a} \end{array} \\
& = - \left(\frac{1}{2} - F(P) \right) \left(\frac{1}{2} - F(P + K) \right) \\
& \times \left[\begin{array}{c} \text{r} \rightarrow \text{a r} \rightarrow \text{a a} \rightarrow \text{r} \\ \text{r} \leftarrow \text{a r} \leftarrow \text{a a} \leftarrow \text{r} \end{array} + \begin{array}{c} \text{r} \rightarrow \text{a r} \rightarrow \text{a r} \rightarrow \text{a} \\ \text{r} \leftarrow \text{a r} \leftarrow \text{a r} \leftarrow \text{a} \end{array} \right]
\end{aligned}$$

Figure 6.9: Leading order contributions to S_{rrrr} where the S_{rr} propagators are on top of each other.

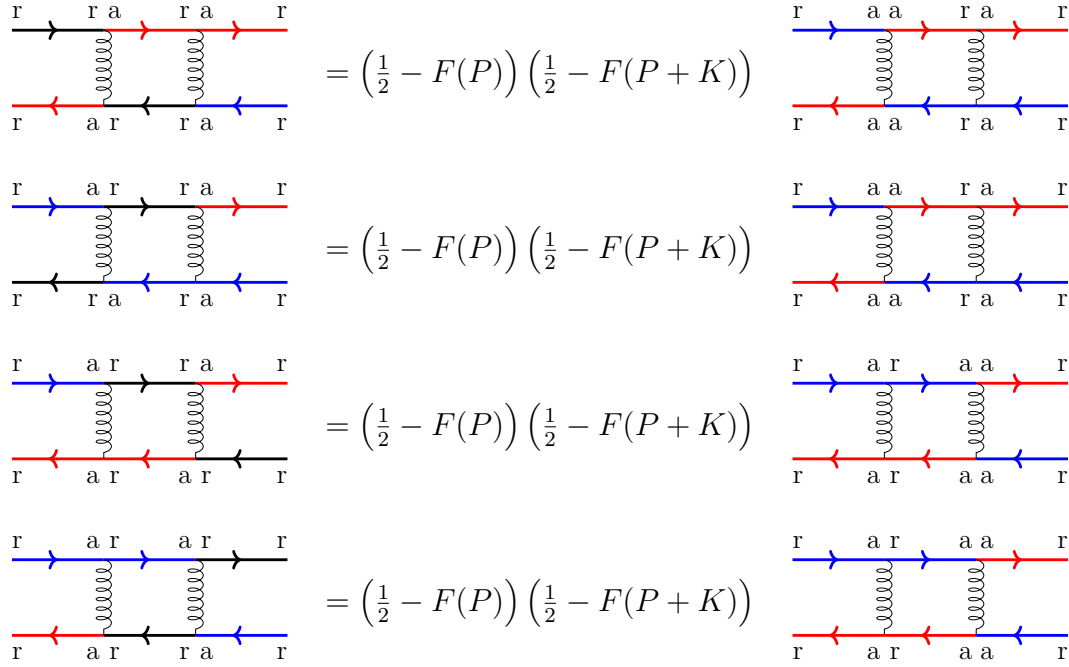


Figure 6.10: Leading order contributions to S_{rrrr} where the S_{rr} propagators are diagonal to each other.

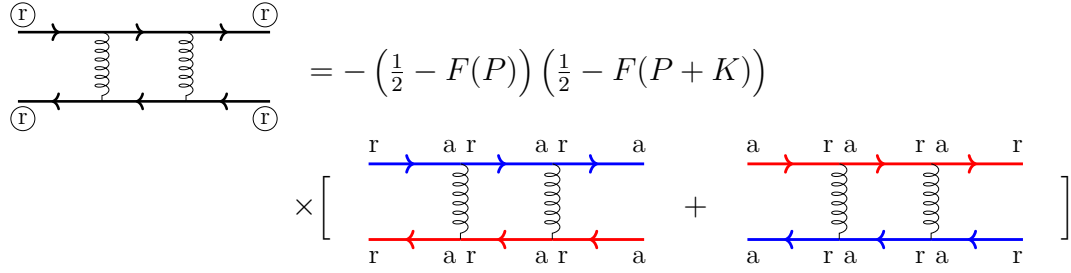


Figure 6.11: All leading order contributions to S_{rrrr} after simplification.

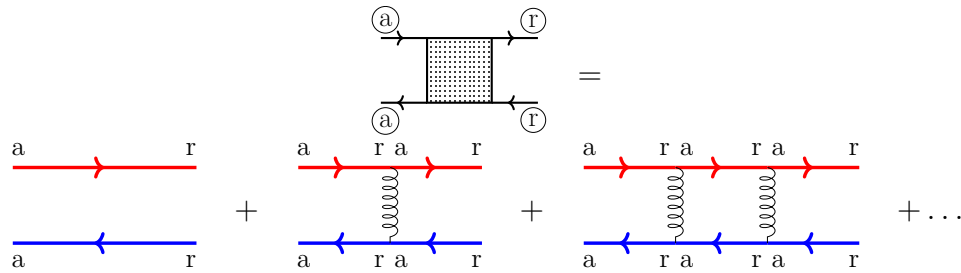


Figure 6.12: Leading order diagrams contributing to S_{aarr} .

6.2 Summing ladder diagrams

The only thing left is to evaluate S_{arr} by summing up the ladder diagrams in Fig. 6.12. The discussion will be brief because the derivation is almost the same as in thermal equilibrium [25]. We use the same notation which is taken from [76]. All equations are for the case of fermionic quarks.

In Chapter 5 we decomposed the retarded fermion propagator into a left-handed and right-handed part which do not interact. The right-handed part can be written as

$$S_{\text{ret}}^R(P) = \frac{i}{2p} \left[\frac{vv^\dagger}{p^0 - \Sigma^0 + p - \boldsymbol{\Sigma} \cdot \hat{\mathbf{p}}} + \frac{uu^\dagger}{p^0 - \Sigma^0 - p + \boldsymbol{\Sigma} \cdot \hat{\mathbf{p}}} \right]. \quad (6.17)$$

We are interested in the case of hard, on-shell quarks that are collinear with the photon. If the photon is travelling in the z direction, the quark momentum is $p^z \sim T$ and $\mathbf{p}_\perp \sim gT$ where $p_\perp = (p^x, p^y, 0)$. Furthermore $p^0 = p^z + \mathcal{O}(g^2T)$. We define the thermal mass of the quark as $m_\infty^2 = 2P \cdot \text{Re} \Sigma$ and the decay width by $p^0 \Gamma = -2P \cdot \text{Im} \Sigma$. They are both of order g^2T . A simple calculation shows that up to order $\mathcal{O}(g^2)$ in denominators we can write

$$S_{\text{ret}}^R(P) = \frac{i}{2p} \left[\frac{vv^\dagger}{p^0 + E_{\mathbf{p}} + i\Gamma_{\mathbf{p}}/2} + \frac{uu^\dagger}{p^0 - E_{\mathbf{p}} + i\Gamma_{\mathbf{p}}/2} \right] \quad (6.18)$$

where $E_{\mathbf{p}} = \sqrt{p_z^2 + \mathbf{p}_\perp^2 + m_\infty^2}$ is the energy of the quasiparticle. The first term corresponds to $p^0 \sim -p$ and the second one to $p^0 \sim p$.

We need an expression for the gluon vertices. We can consider the spinors u and v from the neighbouring propagators as part of the vertices. We use results from Appendix B. For terms with $p^0 \sim p$ we get

$$u^\dagger(\mathbf{p})\sigma^\mu u(\mathbf{p}) = 2(p, \mathbf{p}) \approx 2(p^0, \mathbf{p}) = 2P^\mu \quad (6.19)$$

and for terms with $p^0 \sim -p$ we get

$$v^\dagger(\mathbf{p})\sigma^\mu v(\mathbf{p}) = 2(p, -\mathbf{p}) = -2(p^0, \mathbf{p}) = -2P^\mu. \quad (6.20)$$

The minus sign is cancelled by minus signs from the other quark rail. Thus all vertices are of the form $2P^\mu$ which is the same as in scalar QCD. Furthermore $u^\dagger \sigma^\mu v = v^\dagger \sigma^\mu u = 0$ showing that the different modes do not interact. Similarly the photon vertices give a factor $2P^\mu + K^\mu$.

We must find the contribution from pinching poles by integrating over pairs of propagators as in Fig. 6.4. The integral

$$\mathcal{F}(P; K) = \int \frac{dp^0}{2\pi} S_{\text{adv}}^R(K + P) S_{\text{ret}}^R(P) \quad (6.21)$$

is easy to evaluate using eq. (6.18) and the corresponding equation

$$S_{\text{adv}}^R(P + K) = \frac{i}{2|\mathbf{p} + \mathbf{k}|} \left[\frac{vv^\dagger}{p^0 + k^0 + E_{\mathbf{p}+\mathbf{k}} - i\Gamma_{\mathbf{p}+\mathbf{k}}/2} + \frac{uu^\dagger}{p^0 + k^0 - E_{\mathbf{p}+\mathbf{k}} - i\Gamma_{\mathbf{p}+\mathbf{k}}/2} \right]. \quad (6.22)$$

The residue theorem gives that

$$\mathcal{F}(P; K) = \frac{1}{4p^z(p^z + k) \left[\frac{1}{2}(\Gamma_{\mathbf{p}} + \Gamma_{\mathbf{p}+\mathbf{k}}) + i\delta E \right]}. \quad (6.23)$$

where we omit the spinor structure and include it as part of the vertices. The denominator is the distance between poles from $S_{\text{adv}}^R(K + P)$ and $S_{\text{ret}}^R(P)$. δE is defined as

$$\delta E = k^0 + E_{\mathbf{p}} \text{sgn}(p^z) - E_{\mathbf{p}+\mathbf{k}} \text{sgn}(p^z + k). \quad (6.24)$$

It is of order g^2 for collinear quarks and photons.

We are now ready to evaluate the ladder diagrams in Fig. 6.13. The procedure is explained in Fig. 6.14. We get an integral equation for the effective vertex, \mathcal{D} , in terms of the bare photon vertex, \mathcal{I} , the gluon rung, \mathcal{M} , and pinching poles from quark propagators, \mathcal{F} . See Fig. 6.15 for the definition of these quantities.

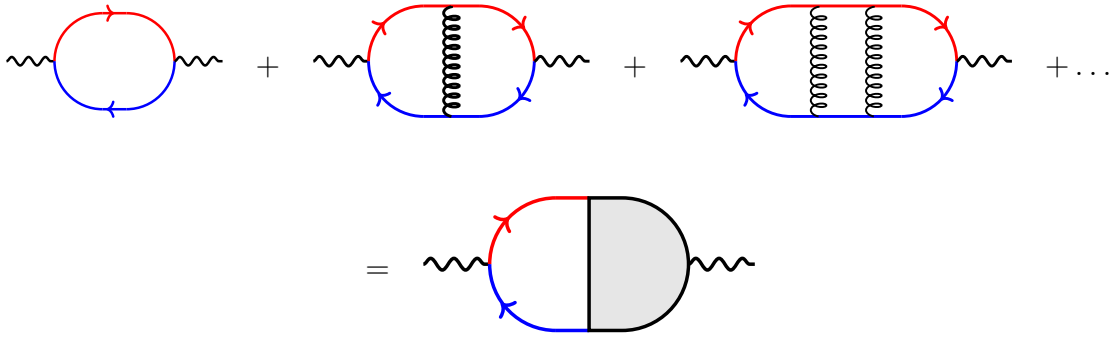


Figure 6.13: The diagrams that contribute at leading order to the photon polarization tensor Π_{12}^γ . Red propagators are S_{ar} and blue propagators are S_{ra} .

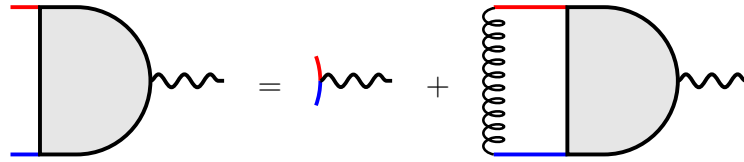


Figure 6.14: Procedure for summing up the diagrams in Fig. 6.13.

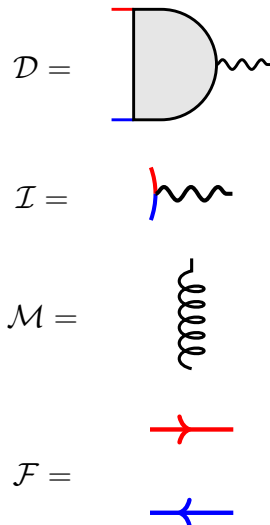


Figure 6.15: Definition of the quantities in eq. 6.25.

The integral equation is formally

$$\mathcal{D}^\mu = \mathcal{I}^\mu + \int \mathcal{M} \mathcal{F} \mathcal{D}^\mu. \quad (6.25)$$

It can be cast in a simple form by defining

$$f^\mu(\mathbf{p}) = -4p^z(p^z + k) \int \frac{dp^0}{2\pi} \mathcal{F} \mathcal{D}^\mu. \quad (6.26)$$

f is implicitly dependent on \mathbf{k} . In our case of fermionic quarks one gets that [25]

$$2P^\mu + K^\mu = \left(i\delta E + \frac{1}{2}(\Gamma_{\mathbf{p}} + \Gamma_{\mathbf{p}+\mathbf{k}}) \right) f^\mu(\mathbf{p}) - \int \frac{d^2q_\perp}{(2\pi)^2} \mathcal{C}(\mathbf{q}_\perp) f^\mu(\mathbf{p} + \mathbf{q}_\perp) \quad (6.27)$$

The term on the left-hand side comes from the photon vertex. The former term on the right-hand side is the effective photon vertex with δE and Γ coming from pinching poles. The last term is the integral in eq. (6.25). The collision kernel, \mathcal{C} , comes from the gluon rung and is defined by

$$\mathcal{C}(\mathbf{q}_\perp) = g^2 C_F \int \frac{dq^0 dq^z}{(2\pi)^2} 2\pi \delta(q^0 - q^z) G_{rr}(Q)^{\mu\nu} \hat{K}_\mu \hat{K}_\nu. \quad (6.28)$$

In Chapter 4 we evaluated it to be

$$\mathcal{C}(\mathbf{q}_\perp) = g^2 C_F \Omega T \left[\frac{1}{\mathbf{q}_\perp^2} - \frac{1}{\mathbf{q}_\perp^2 + m_D^2} \right]. \quad (6.29)$$

where Ω is the occupation density of soft gluons and m_D^2 is the Debye mass.

We have yet to find the decay width Γ . In Chapter 5 we showed that

$$\text{Im} \Sigma_{\text{ret}}(P) = -\pi g^2 C_F \text{sgn}(p^0) \gamma_\mu \not{P} \gamma_\nu \int \frac{d^4 Q}{(2\pi)^4} G_{rr}^{\mu\nu}(Q) \delta(2P \cdot Q). \quad (6.30)$$

Using that $G_{rr}^{\mu\nu}$ is a symmetric tensor and that

$$\frac{1}{2} \left(\gamma_\mu \not{P} \gamma_\nu + \gamma_\nu \not{P} \gamma_\mu \right) = P_\mu \gamma_\nu + P_\nu \gamma_\mu - \not{P} g_{\mu\nu} \quad (6.31)$$

we can write

$$2P \cdot \text{Im} \Sigma_{\text{ret}}(P) = -4\pi g^2 C_F \text{sgn}(p^0) P_\mu P_\nu \int \frac{d^4 Q}{(2\pi)^4} G_{rr}^{\mu\nu}(Q) \delta(2P \cdot Q). \quad (6.32)$$

for an on-shell momentum. A simple rewriting using $P^\mu/p^0 \approx \hat{K}^\mu$ then shows that

$$\Gamma = g^2 C_F \int \frac{d^4 Q}{(2\pi)^4} 2\pi \delta(q^0 - q^z) G_{rr}^{\mu\nu}(Q) \hat{K}_\mu \hat{K}_\nu. \quad (6.33)$$

We see that $\Gamma_{\mathbf{p}}$ is independent of the momentum \mathbf{p} at leading order. Furthermore

$$\Gamma = \int \frac{d^2 q_\perp}{(2\pi)^2} \mathcal{C}(\mathbf{q}_\perp) \quad (6.34)$$

This is an example of a more general result. Using the Ward identity, Gagnon and Jeon have shown that the collision kernel and decay width must be the same in ladder diagrams for evaluating transport coefficients [77, 78].

Using eq. (6.34) we can rewrite our integral equation as

$$2P^\mu + K^\mu = i\delta E f^\mu(\mathbf{p}) + \int \frac{d^2 q_\perp}{(2\pi)^2} \mathcal{C}(\mathbf{q}_\perp) [f^\mu(\mathbf{p}) - f^\mu(\mathbf{p} + \mathbf{q}_\perp)]. \quad (6.35)$$

This is a Boltzmann-like equation with an intuitive interpretation. $f^\mu(\mathbf{p}; \mathbf{k})$ is the distribution of quarks with momentum \mathbf{p} emitting a photon with momentum \mathbf{k} . $i\delta E f^\mu(\mathbf{p}; \mathbf{k})$ can be viewed as the time derivative of f in momentum space. It describes how the quark loses energy by emitting a photon. As the energy difference δE is greater the process is more rapid. The integral, on the other hand, describes how the quark changes its momentum through the exchange of soft gluons with the medium. There is a gain term coming from the gluon rungs and a loss term coming from the quark self-energy.

The only thing left is to express the photon production rate in terms of f^μ . The sum over all ladder diagrams is

$$W^{\mu\nu} = \int \frac{d^4 P}{(2\pi)^4} 2F(P+K) (1 - F(P)) \mathcal{I}^\mu \text{Re} [\mathcal{F}\mathcal{D}^\nu]. \quad (6.36)$$

Here we have used eq. (6.16) to relate S_{1122} and S_{aarr} . This can be conveniently written as

$$W^{\mu\nu} = \int \frac{d^3p}{(2\pi)^3} \frac{F(P+K)[1-F(P)]}{2p^z(k+p^z)} (2P^\mu + K^\mu) \text{Re } f^\nu(\mathbf{p}; \mathbf{k}) \quad (6.37)$$

where $p^0 = (-k^0 + E_{\mathbf{p}} \text{sgn}(p^z) + E_{\mathbf{p}+\mathbf{k}} \text{sgn}(p^z + k))/2$. This equation has been derived for fermionic quarks but it happens to be equally valid for scalar QCD. Finally one substitutes this in eq. (6.1). The final result for photon production through bremsstrahlung and pair-annihilation including the LPM effect is then

$$k \frac{dR}{d^3k} = \frac{3Q^2 \alpha_{EM}}{4\pi^2} \times \int \frac{d^3p}{(2\pi)^3} F(P+K)[1-F(P)] \frac{p^{z^2} + (p^z + k)^2}{2p^{z^2}(p^z + k)^2} 2\mathbf{p}_\perp \cdot \text{Re } \mathbf{f}(\mathbf{p}; \mathbf{k}) \quad (6.38)$$

The new factors in p^z and k come from summing over the physical polarization of the photon [25]. Q is defined by

$$Q^2 e^2 = \sum_{\text{flavour}} q^2 \quad (6.39)$$

where we sum over the charge squared of different flavours of quarks.

6.3 Summary of results

We summarize our results for a non-equilibrium QGP with an isotropic momentum distribution. We have shown that the photon production rate, R , through bremsstrahlung and pair-annihilation taking the LPM effect into account is given by

$$k \frac{dR}{d^3k} = \frac{3Q^2 \alpha_{EM}}{4\pi^2} \int \frac{d^3p}{(2\pi)^3} F(P+K)[1-F(P)] \frac{p^{z^2} + (p^z + k)^2}{2p^{z^2}(p^z + k)^2} 2\mathbf{p}_\perp \cdot \text{Re } \mathbf{f}(\mathbf{p}; \mathbf{k}) \quad (6.40)$$

where \mathbf{k} is the photon momentum. F is the momentum distribution of quarks with Fermi suppression of outgoing quarks taken into account,

$$F(P) = f_q(\mathbf{p})\theta(p^0) + (1 - f_q(\mathbf{p}))\theta(-p^0) \quad (6.41)$$

Here $p^0 = (-k^0 + E_{\mathbf{p}} \operatorname{sgn}(p^z) + E_{\mathbf{p}+\mathbf{k}} \operatorname{sgn}(p^z + k))/2$

To find the transversal components of \mathbf{f} one must solve the integral equation

$$2\mathbf{p}_\perp = i\delta E \mathbf{f}(\mathbf{p}) + \int \frac{d^2q_\perp}{(2\pi)^2} \mathcal{C}(\mathbf{q}_\perp) [\mathbf{f}(\mathbf{p}) - \mathbf{f}(\mathbf{p} + \mathbf{q}_\perp)]. \quad (6.42)$$

δE is given by

$$\delta E = k^0 + E_{\mathbf{p}} \operatorname{sgn}(p^z) - E_{\mathbf{p}+\mathbf{k}} \operatorname{sgn}(p^z + k). \quad (6.43)$$

where $E_{\mathbf{p}} = \sqrt{p^2 + m_\infty^2}$ and m_∞^2 is the non-equilibrium thermal mass of hard quarks. The collision kernel in the integral equation is simply

$$\mathcal{C}(\mathbf{q}_\perp) = g^2 C_F \Omega T \left[\frac{1}{\mathbf{q}_\perp^2} - \frac{1}{\mathbf{q}_\perp^2 + m_D^2} \right] \quad (6.44)$$

The results are quite simple. Apart from $F(P)$ the equations only depend on three constants, Ω , m_D^2 and m_∞^2 . Ω is the density of soft gluons sourced by hard quasi-particles. It is given by

$$\Omega = \frac{-\int_0^\infty dy y^2 \frac{d}{dy} [2N_f f_q + 2N_c f_g]}{\int_0^\infty dy y^2 [2N_f f_q(1 - f_q) + 2N_c f_g(1 + f_g)]} \quad (6.45)$$

where f_g is the gluon distribution function and $y = p/T$. In thermal equilibrium $\Omega = 1$ but in general it can have any positive value. m_D^2 is the non-equilibrium Debye mass which describes the screening of chromoelectric fields. It is given by

$$m_D^2 = \frac{g^2}{\pi^2} \int_0^\infty dp p [2N_f f_q(p) + 2N_c f_g(p)] \quad (6.46)$$

Finally, m_∞^2 is the non-equilibrium thermal mass of hard quarks. It is given by $m_\infty^2 = 2K \cdot \operatorname{Re} \Sigma_{\text{ret}}(K)$. By evaluating the full self-energy for hard quarks one gets

that

$$m_\infty^2 = \frac{g^2 C_F}{\pi^2} \int_0^\infty dp p [f_g(p) + f_q(p)]. \quad (6.47)$$

Conclusion and next steps

In this work we have investigated how a quark-gluon plasma (QGP) shines when it is not in thermal equilibrium. The final goal is to use photons to learn about non-equilibrium properties of the QGP formed in heavy-ion collisions. Specifically we would like to extract transport coefficients, like shear viscosity and bulk viscosity, from photonic observables.

There are two leading-order processes for photon emission in the QGP. One is two-to-two scattering with a photon in the final state. We evaluated corrections to this channel due to bulk viscosity, complementing a previous study of shear viscosity [39]. We simulated photons in heavy-ion collisions and checked the effect of the bulk viscous correction. The yield of photons was nearly unchanged but the elliptic flow was reduced.

The other process is photon emission through quark bremsstrahlung and annihilation of a quark and an antiquark. This thesis is the first study of these channels in a non-equilibrium QGP. They are more involved because of the Landau-Pomeranchuk-Migdal (LPM) effect which says that the quarks scatter off particles in the medium while emitting a photon. We derived an integral equation describing these channels without using the Kubo-Martin-Schwinger relation which is only valid in equilibrium. We assumed an isotropic momentum distribution of quarks and gluons. The integral equation is dependent on the screening length of chromoelectric fields, the thermal mass of hard quarks and the occupation density of soft gluons.

An immediate next step is to solve the integral equation for bulk viscous corrections. Our results should also be extended to non-isotropic momentum distributions.

This would allow us to evaluate shear viscous corrections to all leading order processes of photon production. Finally the LPM effect is not unique to photons. Jets propagating in a QGP lose energy and broaden in a process similar to that in this thesis. An interesting future direction is to analyze jets in a non-equilibrium medium, allowing us to learn about the transport coefficients of QGP through jets.

A

The Feynman rules of QCD

This appendix is a brief refresher on quantum chromodynamics (QCD). See [48, 74] for further details.

QCD is a gauge theory with a $SU(3)$ gauge group. The corresponding charge is called colour. The Lagrangian is

$$\mathcal{L} = -\frac{1}{4}F_{\mu\nu}^a F_a^{\mu\nu} + \bar{\psi} (i\not{D} - m) \psi. \quad (\text{A.1})$$

Here ψ are the quark fields which are spinors. They transform in the fundamental representation of $SU(3)$ and thus come in $N_c = 3$ colours. Furthermore

$$D_\mu = \partial^\mu - igA_\mu^a t^a \quad (\text{A.2})$$

is the covariant derivative with t^a being the eight generators of $SU(3)$ and A^a the gluon fields. a is a colour index for the gluon. The field strength is defined by

$$F_{\mu\nu}^a = \partial_\mu A_\nu^a - \partial_\nu A_\mu^a + gf^{abc} A_\mu^b A_\nu^c \quad (\text{A.3})$$

f^{abc} are the structure constants which are defined by

$$[t^a, t^b] = if^{abc} t^c. \quad (\text{A.4})$$

We see that gluons transform in the adjoint representation of $SU(3)$ and thus come in eight colours.

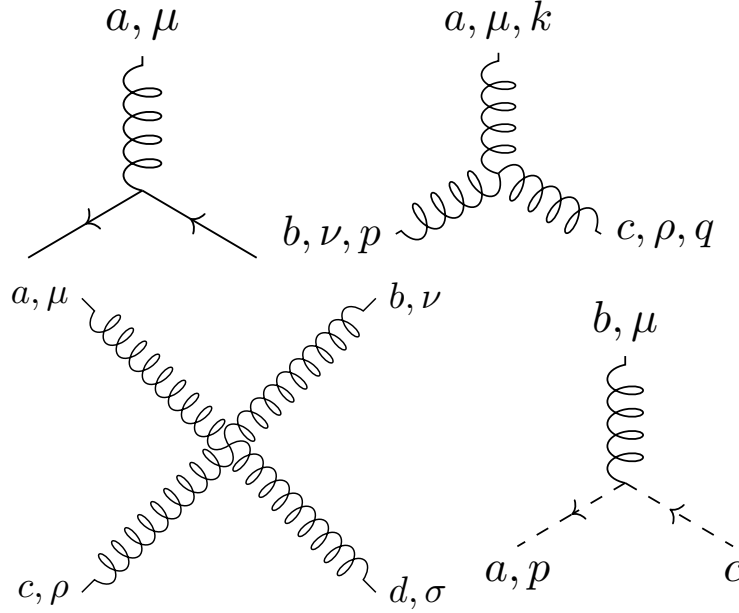


Figure A.1: Vertices in QCD. a, b, c, d are colour indices, μ, ν, ρ, σ are Lorentz indices and p, k, q are incoming momenta.

There are six flavours of quarks called up, down, strange, charm, bottom and top. The last three are too heavy to thermalize in heavy-ion collisions. We thus only consider up, down and possibly strange quarks all of which we approximate as massless.

When quantizing non-abelian gauge theories like QCD one must introduce fictional fields called Faddeev-Popov ghosts to preserve the gauge independence of physical results. In this thesis we work in the Feynman gauge. After gauge fixing the Lagrangian then becomes

$$\mathcal{L} = -\frac{1}{4}F_{\mu\nu}^a F_a^{\mu\nu} - \frac{1}{2}(\partial^\mu A_\mu^a)^2 + \bar{\psi}(i\not{D} - m)\psi + \bar{c}^a(-\partial^\mu D_\mu^{ac})c^c. \quad (\text{A.5})$$

where

$$D_\mu^{ac} = \delta^{ac}\partial_\mu + gf^{abc}A_\mu^b. \quad (\text{A.6})$$

Here c are the ghost fields which transform in the adjoint representation of $SU(3)$.

Staring at the Lagrangian in eq. (A.5) we see that there are four interaction terms,

see Fig. A.1. Using the notation from [48] the quark-gluon vertex is

$$ig\gamma^\mu t^a \quad (\text{A.7})$$

the three gluon vertex is

$$gf^{abc} [g^{\mu\nu}(k-p)^\rho + g^{\nu\rho}(p-q)^\mu + g^{\rho\mu}(q-k)^\nu] \quad (\text{A.8})$$

and the four gluon vertex is

$$\begin{aligned} & -ig^2 [f^{abe} f^{cde} (g^{\mu\rho} g^{\nu\sigma} - g^{\mu\sigma} g^{\nu\rho}) \\ & + f^{ace} f^{bde} (g^{\mu\nu} g^{\rho\sigma} - g^{\mu\sigma} g^{\nu\rho}) \\ & + f^{ade} f^{bce} (g^{\mu\nu} g^{\rho\sigma} - g^{\mu\rho} g^{\nu\sigma})]. \end{aligned} \quad (\text{A.9})$$

Finally there is a vertex with one gluon and two ghosts which has value

$$gf^{abc} p^\mu. \quad (\text{A.10})$$

To evaluate Feynman diagrams we need to be able to handle the generators t^a and structure constants f^{abc} of the gauge group. In this thesis we only need a few simple facts. The generators are usually normalized so that

$$\text{Tr}[t^A t^B] = t_{cd}^A t_{dc}^B = \frac{1}{2} \delta^{AB}. \quad (\text{A.11})$$

Here A and B label the generators (adjoint representation) and c and d label their matrix elements (fundamental representation). Using the Casimir operator one can then show that

$$t_{ab}^A t_{bc}^A = C_F \delta_{ac} \quad (\text{A.12})$$

where $C_F = (N_c^2 - 1)/2N_c = 4/3$. The corresponding formula in the adjoint representation is

$$f^{ACD} f^{BCD} = N_c \delta^{AB}. \quad (\text{A.13})$$

B

Spinors

In this appendix we derive some results about spinors used in the main part of the thesis. Spin 1/2 fields are represented by a four-component object, ψ , called a spinor. Under Lorentz transformations

$$\psi \rightarrow \exp\left(-\frac{i}{2}\omega_{\mu\nu}S^{\mu\nu}\right)\psi \quad (\text{B.1})$$

where e.g. ω_{12} is the rotation angle around the third axis and ω_{01} is the rapidity we boost with in the direction of the first axis [48].

In order to fulfill the commutation relations of Lorentz transformations we write

$$S^{\mu\nu} = \frac{i}{4} [\gamma^\mu, \gamma^\nu]. \quad (\text{B.2})$$

Here γ^μ is a collection of four 4×4 matrices that satisfy

$$\{\gamma^\mu, \gamma^\nu\} = 2g^{\mu\nu} \quad (\text{B.3})$$

where $g^{\mu\nu}$ is the usual Minkowski metric. A convenient convention for the gamma matrices is

$$\gamma^\mu = \begin{bmatrix} 0 & \sigma^\mu \\ \bar{\sigma}^\mu & 0 \end{bmatrix} \quad (\text{B.4})$$

where $\sigma^\mu = (1, \boldsymbol{\sigma})$, $\bar{\sigma}^\mu = (1, -\boldsymbol{\sigma})$. $\boldsymbol{\sigma}$ are the usual Pauli matrices

$$\sigma^1 = \begin{bmatrix} 0 & 1 \\ 1 & 0 \end{bmatrix}, \quad \sigma^2 = \begin{bmatrix} 0 & -i \\ i & 0 \end{bmatrix}, \quad \sigma^3 = \begin{bmatrix} 1 & 0 \\ 0 & -1 \end{bmatrix} \quad (\text{B.5})$$

that satisfy $[\sigma^i, \sigma^j] = 2i\epsilon^{ijk}\sigma^k$ and $\{\sigma^i, \sigma^j\} = 2\delta^{ij}$.

We define $u(\mathbf{p})$ and $v(\mathbf{p})$ as the eigenvectors of $\mathbf{p} \cdot \boldsymbol{\sigma}$ with eigenvalues $+1$ and -1 respectively. They correspond to states with spin parallel or anti-parallel to the particle's momentum, also known as right-handed or left-handed states or states with positive or negative helicity. For massless particles the helicity is invariant under Lorentz transformations. We define the states with normalization

$$u^\dagger u = v^\dagger v = 2p. \quad (\text{B.6})$$

It's easy to show that

$$uu^\dagger = \frac{1 + \hat{\mathbf{p}} \cdot \boldsymbol{\sigma}}{p} \quad (\text{B.7})$$

and

$$vv^\dagger = \frac{1 - \hat{\mathbf{p}} \cdot \boldsymbol{\sigma}}{p} \quad (\text{B.8})$$

by calculating the matrix elements on both sides in the orthogonal (u, v) basis.

In the main part of the text we need to evaluate expressions of the form $u^\dagger \sigma^\mu u$. This is trivial for $\mu = 0$. For the spatial indices we note that

$$\begin{aligned} \hat{\mathbf{p}} \cdot \boldsymbol{\sigma} \sigma^i \hat{\mathbf{p}} \cdot \boldsymbol{\sigma} &= \hat{p}^n \hat{p}^m \sigma^n \sigma^i \sigma^m \\ &= \hat{p}^n \hat{p}^m \left(-\sigma^i \sigma^n + 2\delta^{in} \right) \sigma^m \\ &= -\sigma^i + 2\hat{p}^i \hat{\mathbf{p}} \cdot \boldsymbol{\sigma} \end{aligned} \quad (\text{B.9})$$

where we used that $\hat{\mathbf{p}} \cdot \boldsymbol{\sigma} \hat{\mathbf{p}} \cdot \boldsymbol{\sigma} = 1$. Multiplying by u^\dagger on the left and u on the right we get that

$$u^\dagger \sigma^i u = 2p^i \quad (\text{B.10})$$

and similarly

$$v^\dagger \sigma^i v = -2p^i. \quad (\text{B.11})$$

Similar tricks give that $u^\dagger \sigma^i v = 0$ and $v^\dagger \sigma^i u = 0$.

To summarize

$$\begin{aligned} u^\dagger \sigma_\mu u &= 2p_\mu^+ \\ u^\dagger \bar{\sigma}_\mu u &= 2p_\mu^- \\ v^\dagger \sigma_\mu v &= 2p_\mu^- \\ v^\dagger \bar{\sigma}_\mu v &= 2p_\mu^+ \end{aligned} \quad (\text{B.12})$$

where $p^{+\mu} = (|\mathbf{p}|, \mathbf{p})$ and $p^{-\mu} = (|\mathbf{p}|, -\mathbf{p})$. All combinations with one u and one v vanish.

C

Final results from Chapter 3

C.1 Hard momentum loops

In this appendix we present final results for the bulk viscous correction to photon production through two-to-two scattering. We start with the hard loop part, see Chapter 3 for the notation. The bulk viscous correction to the u and t channels to first order in δf_{bulk} is

$$\begin{aligned}
\Gamma_{\text{bulk}} \Big|_{\text{hard}; t, u} &= -\frac{\mathcal{N}}{16(2\pi)^6 k} \int_{q_{\text{cut}}}^{\infty} dq \int_{\max\{q-2k, -q\}}^q d\omega \int_{(q-\omega)/2}^{\infty} dp' \\
&\left[\left(1 - \frac{2p'k(1 - \cos\theta_{kq} \cos\theta_{p'q})}{\omega^2 - q^2} \right) f_F(\omega + k) f_B(p') (1 - f_F(\omega + p')) \right. \\
&\quad \times \left\{ (1 - f_F(\omega + k)) \chi_F(\omega + k) + (1 + f_B(p')) \chi_B(p') \right. \\
&\quad \quad \left. \left. - f_F(\omega + p') \chi_F(\omega + p') \right\} \right. \\
&\quad - \frac{2p'k(1 - \cos\theta_{kq} \cos\theta_{p'q})}{\omega^2 - q^2} f_F(\omega + k) f_F(p') (1 + f_B(\omega + p')) \\
&\quad \times \left\{ (1 - f_F(\omega + k)) \chi_F(\omega + k) + (1 - f_F(p')) \chi_F(p') \right. \\
&\quad \quad \left. \left. + f_B(\omega + p') \chi_B(\omega + p') \right\} \right] \tag{C.1}
\end{aligned}$$

where

$$\cos\theta_{kq} = \frac{\omega^2 - q^2 + 2k\omega}{2kq} \tag{C.2}$$

and

$$\cos\theta_{p'q} = \frac{\omega^2 - q^2 + 2\omega p'}{2qp'}. \tag{C.3}$$

We have written

$$\delta f_{\text{bulk}} = -f_{\text{eq}} (1 \pm f_{\text{eq}}) \chi(p) \frac{\Pi}{15(\epsilon + \mathcal{P})(\frac{1}{3} - c_s^2)} \quad (\text{C.4})$$

so

$$\chi(p) = \left(\frac{m^2}{E} - E \right). \quad (\text{C.5})$$

F refers to fermions (quarks) and B refers to bosons.

We can write down a similar expression for the s channel, see [39] for a derivation.

$$\begin{aligned} \Gamma_{\text{bulk}} \Big|_{\text{hard}; s} &= -\frac{\mathcal{N}}{16(2\pi)^6 k} \int_k^\infty d\omega \int_{|2k-\omega|}^\omega dq \int_{(\omega-q)/2}^{(\omega+q)/2} dp' \\ &\left[\frac{2p'k(1 - \cos \theta_{kq} \cos \theta_{p'q})}{\omega^2 - q^2} f_B(\omega - p') f_F(p') (1 - f_F(\omega - k)) \right. \\ &\quad \times \left\{ (1 + f_B(\omega - p')) \chi_B(\omega - p') + (1 - f_F(p')) \chi_F(p') \right. \\ &\quad \left. \left. - f_F(\omega - k) \chi_F(\omega - k) \right\} \right] \quad (\text{C.6}) \end{aligned}$$

Note that there is no cutoff in the integrals because they are not infrared divergent.

Here

$$\cos \theta_{kq} = \frac{q^2 - \omega^2 + 2k\omega}{2kq} \quad (\text{C.7})$$

and

$$\cos \theta_{p'q} = \frac{q^2 - \omega^2 + 2\omega p'}{2qp'}. \quad (\text{C.8})$$

C.2 Soft momentum loops

In chapter 3 we showed that photon production from the soft loop part is

$$k \frac{dR}{d^3k} \Big|_{\text{soft}} = -\frac{8e^2 Q^2 N_C}{2(2\pi)^3} \frac{f_q(\mathbf{k})}{k} \int^{q_{\text{cut}}} \frac{d^3q}{(2\pi)^3} \text{Im} \frac{K \cdot (Q - \Sigma_{\text{ret}}(Q))}{(Q - \Sigma_{\text{ret}}(Q))^2} \Big|_{q^0=\mathbf{q}\cdot\hat{\mathbf{k}}} \quad (\text{C.9})$$

where

$$\Sigma_{\text{ret}}^\mu(Q) = C_F g^2 \int \frac{pdp}{2\pi^2} \frac{d\Omega_p}{4\pi} (f_q(\mathbf{p}) + f_g(\mathbf{p})) \frac{P^\mu}{P \cdot Q + i\epsilon} \Big|_{p^0=p}. \quad (\text{C.10})$$

We write the self-energy as

$$\Sigma_{\text{ret}}^\mu = \Sigma_{\text{eq}}^\mu - \frac{\Pi}{15(\epsilon + \mathcal{P})(\frac{1}{3} - c_s^2)} \Sigma_{\text{bulk}}^\mu. \quad (\text{C.11})$$

The equilibrium part contains the equilibrium distribution and the bulk viscous part contains δf_{bulk} .

A simple calculation shows that the equilibrium self-energy is

$$\Sigma_{\text{eq}}^\mu(Q) = \frac{g^2 T^2 C_F}{8q} [\alpha(z) Q^\mu / q + \beta(z) u^\mu] \quad (\text{C.12})$$

where $z = q^0/q$ and

$$\begin{aligned} \alpha(z) &= zQ_0(z) - 1 - iz\frac{\pi}{2} \\ \beta(z) &= (1 - z^2)Q_0(z) + z - i(1 - z^2)\frac{\pi}{2}. \end{aligned} \quad (\text{C.13})$$

Here

$$Q_0(z) = \frac{1}{2} \ln \frac{1+z}{1-z}. \quad (\text{C.14})$$

is a Legendre function of the second kind. Since the bulk viscous momentum distribution is isotropic the evaluation of Σ_{bulk} is almost identical. One gets that

$$\Sigma_{\text{bulk}}^\mu = \frac{g^2 T^2 C_F}{2\pi^2 q} [\alpha(z) Q^\mu / q + \beta(z) u^\mu] A_{\text{bulk}} \quad (\text{C.15})$$

where

$$A_{\text{bulk}} = \int_0^\infty dx x [f_F(x)(1 - f_F(x))\chi_F(x) + f_B(x)(1 + f_B(x))\chi_B(x)] \quad (\text{C.16})$$

with $x = q/T$.

The only thing left is to expand C.9 up to first order in δf_{bulk} . One gets that

$$\begin{aligned} \Gamma_{\text{bulk}}(k) \Big|_{\text{soft}} &= \frac{8e^2 Q^2 N_c f_F(k)}{2(2\pi)^3 k} \\ &\times \int^{q_{\text{cut}}} \frac{d^3 q}{(2\pi)^3} \left[-\text{Im} \left(\frac{K \cdot \Sigma_{\text{bulk}}}{Q_0^2} \right) + 2 \text{Im} \left(\frac{K \cdot Q_0}{Q_0^2} \frac{Q_0 \cdot \Sigma_{\text{bulk}}}{Q_0^2} \right) \right. \\ &\quad \left. + (1 - f_F(k))\chi_F(k) \text{Im} \left(\frac{K \cdot Q_0}{Q_0^2} \right) \right] \Big|_{q^0 = q \cos \theta} \end{aligned} \quad (\text{C.17})$$

Here we have defined

$$Q_0^\mu = Q^\mu - \Sigma_{\text{eq}}^\mu. \quad (\text{C.18})$$

This complicated integral must be done numerically.

Bibliography

- [1] M. A. Stephanov, “QCD phase diagram: An Overview,” *PoS*, vol. LAT2006, p. 024, 2006.
- [2] Z. Fodor and S. D. Katz, “The Phase diagram of quantum chromodynamics,” 2009. [arXiv:0908.3341].
- [3] A. Bazavov *et al.*, “Equation of state in (2+1)-flavor QCD,” *Phys. Rev.*, vol. D90, p. 094503, 2014.
- [4] S. Borsanyi, Z. Fodor, C. Hoelbling, S. D. Katz, S. Krieg, and K. K. Szabo, “Full result for the QCD equation of state with 2+1 flavors,” *Phys. Lett.*, vol. B730, pp. 99–104, 2014.
- [5] D. Tong, “Kinetic Theory.” <http://www.damtp.cam.ac.uk/user/tong/kinetic.html>, 2012.
- [6] N. Astrakhantsev, V. Braguta, and A. Kotov, “Temperature dependence of shear viscosity of $SU(3)$ -gluodynamics within lattice simulation,” 2017. [arXiv:1701.02266].
- [7] P. B. Arnold, G. D. Moore, and L. G. Yaffe, “Transport coefficients in high temperature gauge theories. 1. Leading log results,” *JHEP*, vol. 11, p. 001, 2000.
- [8] P. B. Arnold, G. D. Moore, and L. G. Yaffe, “Transport coefficients in high temperature gauge theories. 2. Beyond leading log,” *JHEP*, vol. 05, p. 051, 2003.
- [9] G. Policastro, D. T. Son, and A. O. Starinets, “The Shear viscosity of strongly coupled $N=4$ supersymmetric Yang-Mills plasma,” *Phys. Rev. Lett.*, vol. 87, p. 081601, 2001.

- [10] B. Schenke, P. Tribedy, and R. Venugopalan, “Fluctuating Glasma initial conditions and flow in heavy ion collisions,” *Phys. Rev. Lett.*, vol. 108, p. 252301, 2012.
- [11] B. Schenke, S. Jeon, and C. Gale, “(3+1)D hydrodynamic simulation of relativistic heavy-ion collisions,” *Phys. Rev.*, vol. C82, p. 014903, 2010.
- [12] F. Cooper and G. Frye, “Comment on the Single Particle Distribution in the Hydrodynamic and Statistical Thermodynamic Models of Multiparticle Production,” *Phys. Rev.*, vol. D10, p. 186, 1974.
- [13] S. A. Bass *et al.*, “Microscopic models for ultrarelativistic heavy ion collisions,” *Prog. Part. Nucl. Phys.*, vol. 41, pp. 255–369, 1998. [Prog. Part. Nucl. Phys.41,225(1998)].
- [14] W. A. Horowitz, *Probing the Frontiers of QCD*. PhD thesis, Columbia U., 2010.
- [15] P. Romatschke and U. Romatschke, “Viscosity Information from Relativistic Nuclear Collisions: How Perfect is the Fluid Observed at RHIC?,” *Phys. Rev. Lett.*, vol. 99, p. 172301, 2007.
- [16] P. Chakraborty and J. I. Kapusta, “Departure from Equilibrium of the Quasi-Particle Distribution Functions in High Energy Nuclear Collisions,” *Phys. Rev.*, vol. C95, no. 1, p. 014907, 2017.
- [17] R. D. Weller and P. Romatschke, “One fluid to rule them all: viscous hydrodynamic description of event-by-event central p+p, p+Pb and Pb+Pb collisions at $\sqrt{s} = 5.02$ TeV,” 2017.
- [18] S. Ryu, J. F. Paquet, C. Shen, G. S. Denicol, B. Schenke, S. Jeon, and C. Gale, “Importance of the Bulk Viscosity of QCD in Ultrarelativistic Heavy-Ion Collisions,” *Phys. Rev. Lett.*, vol. 115, no. 13, p. 132301, 2015.

- [19] C. Shen and U. Heinz, “The road to precision: Extraction of the specific shear viscosity of the quark-gluon plasma,” *Nucl. Phys. News*, vol. 25, no. 2, pp. 6–11, 2015.
- [20] J. E. Bernhard, J. S. Moreland, S. A. Bass, J. Liu, and U. Heinz, “Applying Bayesian parameter estimation to relativistic heavy-ion collisions: simultaneous characterization of the initial state and quark-gluon plasma medium,” *Phys. Rev.*, vol. C94, no. 2, p. 024907, 2016.
- [21] R. Baier, H. Nakkagawa, A. Niegawa, and K. Redlich, “Production rate of hard thermal photons and screening of quark mass singularity,” *Z. Phys.*, vol. C53, pp. 433–438, 1992.
- [22] J. I. Kapusta, P. Lichard, and D. Seibert, “High-energy photons from quark - gluon plasma versus hot hadronic gas,” *Phys. Rev.*, vol. D44, pp. 2774–2788, 1991. [Erratum: *Phys. Rev.*D47,4171(1993)].
- [23] P. Aurenche, F. Gelis, R. Kobes, and H. Zaraket, “Bremsstrahlung and photon production in thermal QCD,” *Phys. Rev.*, vol. D58, p. 085003, 1998.
- [24] P. Aurenche, F. Gelis, and H. Zaraket, “Landau-Pomeranchuk-Migdal effect in thermal field theory,” *Phys. Rev.*, vol. D62, p. 096012, 2000.
- [25] P. B. Arnold, G. D. Moore, and L. G. Yaffe, “Photon emission from ultrarelativistic plasmas,” *JHEP*, vol. 11, p. 057, 2001.
- [26] P. B. Arnold, G. D. Moore, and L. G. Yaffe, “Photon emission from quark gluon plasma: Complete leading order results,” *JHEP*, vol. 12, p. 009, 2001.
- [27] J. Ghiglieri, J. Hong, A. Kurkela, E. Lu, G. D. Moore, and D. Teaney, “Next-to-leading order thermal photon production in a weakly coupled quark-gluon plasma,” *JHEP*, vol. 05, p. 010, 2013.
- [28] S. Caron-Huot and G. D. Moore, “Heavy quark diffusion in perturbative QCD at next-to-leading order,” *Phys. Rev. Lett.*, vol. 100, p. 052301, 2008.

- [29] J. Ghiglieri and D. Teaney, “Parton energy loss and momentum broadening at NLO in high temperature QCD plasmas,” *Int. J. Mod. Phys.*, vol. E24, no. 11, p. 1530013, 2015. [,271(2016)].
- [30] J. Ghiglieri, O. Kaczmarek, M. Laine, and F. Meyer, “Lattice constraints on the thermal photon rate,” *Phys. Rev.*, vol. D94, no. 1, p. 016005, 2016.
- [31] K. Dusling, “Photons as a viscometer of heavy ion collisions,” *Nucl. Phys.*, vol. A839, pp. 70–77, 2010.
- [32] K. Dusling and T. Schäfer, “Bulk viscosity, particle spectra and flow in heavy-ion collisions,” *Phys. Rev.*, vol. C85, p. 044909, 2012.
- [33] M. Greif, F. Senzel, H. Kremer, K. Zhou, C. Greiner, and Z. Xu, “Nonequilibrium photon production in partonic transport simulations,” 2016. [arXiv:1612.05811].
- [34] J. Berges, K. Reygers, N. Tanji, and R. Venugopalan, “What shines brighter, Glasma or Quark-Gluon Plasma: a parametric estimate of photon production at early times in heavy-ion collisions,” 2017.
- [35] S. Turbide, C. Gale, E. Frodermann, and U. Heinz, “Electromagnetic radiation from nuclear collisions at RHIC energies,” *Phys. Rev.*, vol. C77, p. 024909, 2008.
- [36] C. Young and S. Pratt, “Electromagnetic recombination spectra at the quark-hadron phase transition,” *Phys. Rev.*, vol. C94, no. 4, p. 044916, 2016.
- [37] L. Adamczyk *et al.*, “Direct virtual photon production in Au+Au collisions at $\sqrt{s_{NN}} = 200$ GeV,” 2016. [arXiv:1607.01447].
- [38] J.-F. Paquet, C. Shen, G. S. Denicol, M. Luzum, B. Schenke, S. Jeon, and C. Gale, “Production of photons in relativistic heavy-ion collisions,” *Phys. Rev.*, vol. C93, no. 4, p. 044906, 2016.
- [39] C. Shen, J.-F. Paquet, U. Heinz, and C. Gale, “Photon Emission from a Momentum Anisotropic Quark-Gluon Plasma,” *Phys. Rev.*, vol. C91, no. 1, p. 014908, 2015.

- [40] M. Dion, J.-F. Paquet, B. Schenke, C. Young, S. Jeon, and C. Gale, “Viscous photons in relativistic heavy ion collisions,” *Phys. Rev.*, vol. C84, p. 064901, 2011.
- [41] R. Baier, M. Dirks, K. Redlich, and D. Schiff, “Thermal photon production rate from nonequilibrium quantum field theory,” *Phys. Rev.*, vol. D56, pp. 2548–2554, 1997.
- [42] B. Schenke and M. Strickland, “Fermionic Collective Modes of an Anisotropic Quark-Gluon Plasma,” *Phys. Rev.*, vol. D74, p. 065004, 2006.
- [43] B. Schenke and M. Strickland, “Photon production from an anisotropic quark-gluon plasma,” *Phys. Rev.*, vol. D76, p. 025023, 2007.
- [44] J. I. Kapusta and C. Gale, *Finite-temperature field theory: Principles and applications*. Cambridge University Press, 2011.
- [45] M. L. Bellac, *Thermal Field Theory*. Cambridge University Press, 2011.
- [46] N. P. Landsman and C. G. van Weert, “Real and Imaginary Time Field Theory at Finite Temperature and Density,” *Phys. Rept.*, vol. 145, p. 141, 1987.
- [47] K.-c. Chou, Z.-b. Su, B.-l. Hao, and L. Yu, “Equilibrium and Nonequilibrium Formalisms Made Unified,” *Phys. Rept.*, vol. 118, p. 1, 1985.
- [48] M. E. Peskin and D. V. Schroeder, *An Introduction to quantum field theory*. Westview Press, 1995.
- [49] F. Gelis, “The Effect of the vertical part of the path on the real time Feynman rules in finite temperature field theory,” *Z. Phys.*, vol. C70, pp. 321–331, 1996.
- [50] F. Gelis, “A New approach for the vertical part of the contour in thermal field theories,” *Phys. Lett.*, vol. B455, pp. 205–212, 1999.
- [51] L. V. Keldysh, “Diagram technique for nonequilibrium processes,” *Zh. Eksp. Teor. Fiz.*, vol. 47, pp. 1515–1527, 1964. [Sov. Phys. JETP20,1018(1965)].

- [52] J. Rammer, *Quantum field theory of non-equilibrium states*. Cambridge University Press, 2007.
- [53] E. Calzetta and B. L. Hu, “Nonequilibrium Quantum Fields: Closed Time Path Effective Action, Wigner Function and Boltzmann Equation,” *Phys. Rev.*, vol. D37, p. 2878, 1988.
- [54] J.-P. Blaizot and E. Iancu, “Kinetic theory and quantum electrodynamics at high temperature,” *Nucl. Phys.*, vol. B390, pp. 589–620, 1993.
- [55] H. Weigert and U. W. Heinz, “Kinetic Equations for the Quark - Gluon Plasma and Their Semiclassical Expansion,” *Z. Phys.*, vol. C50, pp. 195–204, 1991.
- [56] E. Braaten and R. D. Pisarski, “Soft Amplitudes in Hot Gauge Theories: A General Analysis,” *Nucl. Phys.*, vol. B337, pp. 569–634, 1990.
- [57] E. Braaten and R. D. Pisarski, “Deducing Hard Thermal Loops From Ward Identities,” *Nucl. Phys.*, vol. B339, pp. 310–324, 1990.
- [58] P. B. Arnold, G. D. Moore, and L. G. Yaffe, “Effective kinetic theory for high temperature gauge theories,” *JHEP*, vol. 01, p. 030, 2003.
- [59] C. Greiner and S. Leupold, “Interpretation and resolution of pinch singularities in nonequilibrium quantum field theory,” *Eur. Phys. J.*, vol. C8, pp. 517–522, 1999.
- [60] J. Serreau, “Out-of-equilibrium electromagnetic radiation,” *JHEP*, vol. 05, p. 078, 2004.
- [61] A. Majumder and C. Gale, “On the imaginary parts and infrared divergences of two loop vector boson selfenergies in thermal QCD,” *Phys. Rev.*, vol. C65, p. 055203, 2002.
- [62] S. Jeon and L. G. Yaffe, “From quantum field theory to hydrodynamics: Transport coefficients and effective kinetic theory,” *Phys. Rev.*, vol. D53, pp. 5799–5809, 1996.

- [63] S. Mrowczynski and M. H. Thoma, “Hard loop approach to anisotropic systems,” *Phys. Rev.*, vol. D62, p. 036011, 2000.
- [64] F. Karsch, D. Kharzeev, and K. Tuchin, “Universal properties of bulk viscosity near the QCD phase transition,” *Phys. Lett.*, vol. B663, pp. 217–221, 2008.
- [65] J. Noronha-Hostler, J. Noronha, and C. Greiner, “Transport Coefficients of Hadronic Matter near $T(c)$,” *Phys. Rev. Lett.*, vol. 103, p. 172302, 2009.
- [66] G. S. Denicol, S. Jeon, and C. Gale, “Transport Coefficients of Bulk Viscous Pressure in the 14-moment approximation,” *Phys. Rev.*, vol. C90, no. 2, p. 024912, 2014.
- [67] C. Shen, U. W. Heinz, J.-F. Paquet, and C. Gale, “Thermal photons as a quark-gluon plasma thermometer reexamined,” *Phys. Rev.*, vol. C89, no. 4, p. 044910, 2014.
- [68] A. Czajka and S. Mrowczynski, “Ghosts in Keldysh-Schwinger Formalism,” *Phys. Rev.*, vol. D89, no. 8, p. 085035, 2014.
- [69] P. Romatschke and M. Strickland, “Collective modes of an anisotropic quark gluon plasma,” *Phys. Rev.*, vol. D68, p. 036004, 2003.
- [70] P. Aurenche, F. Gelis, and H. Zaraket, “A Simple sum rule for the thermal gluon spectral function and applications,” *JHEP*, vol. 05, p. 043, 2002.
- [71] H. A. Weldon, “Covariant Calculations at Finite Temperature: The Relativistic Plasma,” *Phys. Rev.*, vol. D26, p. 1394, 1982.
- [72] K. A. Mamo and H.-U. Yee, “Spin polarized photons from an axially charged plasma at weak coupling: Complete leading order,” *Phys. Rev.*, vol. D93, no. 6, p. 065053, 2016.
- [73] H. A. Weldon, “Effective Fermion Masses of Order gT in High Temperature Gauge Theories with Exact Chiral Invariance,” *Phys. Rev.*, vol. D26, p. 2789, 1982.

-
- [74] M. D. Schwartz, *Quantum Field Theory and the Standard Model*. Cambridge University Press, 2014.
- [75] E. Wang and U. W. Heinz, “A Generalized fluctuation dissipation theorem for nonlinear response functions,” *Phys. Rev.*, vol. D66, p. 025008, 2002.
- [76] S. Jeon, “Hydrodynamic transport coefficients in relativistic scalar field theory,” *Phys. Rev.*, vol. D52, pp. 3591–3642, 1995.
- [77] J.-S. Gagnon and S. Jeon, “Leading order calculation of electric conductivity in hot quantum electrodynamics from diagrammatic methods,” *Phys. Rev.*, vol. D75, p. 025014, 2007. [Erratum: *Phys. Rev.*D76,089902(2007)].
- [78] J.-S. Gagnon and S. Jeon, “Leading Order Calculation of Shear Viscosity in Hot Quantum Electrodynamics from Diagrammatic Methods,” *Phys. Rev.*, vol. D76, p. 105019, 2007.